DISSERTATION

A General Solution to the Wrinkling Problem of Sandwiches

ausgeführt zum Zwecke der Erlangung des akademischen Grades eines Doktors der technischen Wissenschaften unter der Leitung von

o.Univ.Prof. Dipl.-Ing. Dr.techn. Franz G. Rammerstorfer
E317
Institut für Leichtbau und Flugzeugbau

eingereicht an der Technischen Universität Wien
Fakultät für Maschinenbau

von

Dipl.-Ing. Walter K. VONACH
Matr.Nr.: 9026650
Langstögergasse 17/7
A-3400 Klosterneuburg

Wien, im Mai 2001 *Walter K. Vonach*

Acknowledgments

This work was carried out in the course of my employment as "Universitätsassistent" at the Institute of Lightweight Structures and Aerospace Engineering (ILFB) at the Vienna University of Technology. I am deeply indebted to my thesis advisor, Prof. Dr. F.G. Rammerstorfer, head of the above Institute, who encouraged me to work in this field. Especially, I want to express my gratitude for the invaluable and highly motivating discussions on the current state and the possible developments of my research.

I also want to thank Prof. Dr. H. Troger from the Institute of Mechanics for acting as coadvisor for this thesis.

Last but not least, I would like to express my thanks to all colleagues at the ILFB, who have always been helpful and friendly. The resulting positive atmosphere at the ILFB has helped me during the scientific setbacks encountered from time to time and made my time at the ILFB an interesting, inspiring and joyful period.

Contents

Abstract

The aim of this work is to present a general analytical approach to the local instability failure mode of sandwich plates commonly referred to as wrinkling. The wrinkling problem is assumed to be a localized phenomenon and interaction with global buckling is not considered. Due to this assumption and the generality of the approach, it can also be used for automatic post processing of FE sandwich shell results. In this case, safety factors against wrinkling can be calculated on the basis of the FE stress results at integration point level of appropriate finite sandwich shell elements. This has not been generally possible up to now due to the lack of generality of the corresponding wrinkling models in terms of sandwich configuration and loading.

The new approach is much more general than existing ones focusing on wrinkling, since it takes into account unsymmetric sandwiches, arbitrary loading and orthotropic constituent materials. The Rayleigh Ritz method is employed, leading to a numerically efficient calculation scheme although the complexity of the problem is considerable and numerical optimization has to be used.

Within this study three different types of finite element verification models are formulated, including periodic unit-cell models. The advantages and drawbacks of the periodic unit-cell formulation as compared to classical models are evaluated. The FE verification models and the new analytical model generally show very good agreement. The deformation field which has been chosen for the Ritz ansatz was also verified by these FE calculations. Experimental verification is under progress, but not included in this work.

Apart from the analytical approach itself numerous results are presented which show the shortcomings of the commonly used wrinkling calculations and the resulting errors. It is demonstrated that even in the simplest case of a symmetric sandwich beam under compression, the commonly used wrinkling calculation schemes may lead to qualitatively and quantitatively wrong results. It is shown, that the type of core material used within the sandwich has a major influence on the applicability of the classical design formulas and on

the decision whether the sandwich is sufficiently thick for precluding face layer interaction. This is due to the fact that the in-plane core stiffness plays an important role concerning wrinkling. This new finding is of major importance to all existing wrinkling approaches because the influence of the in-plane core stiffness has generally been ignored in sandwich analysis up to now. The new approach presented in this work uses, in contrary to almost all other approaches, a core material description which is taking the in-plane core stiffness into account. Therefore it is applicable for all commonly used core materials.

Furthermore, results for pure bending of sandwich beams are presented which show, for the first time, the influence of the face layer which is under tension on the critical wrinkling load. The calculations show a significant influence for rather thin sandwiches.

Unsymmetric or orthotropic sandwich plates under general loading conditions, which are beyond the scope of the other currently used wrinkling models, have also been studied. The corresponding effects are evaluated using different example problems starting with rather simple cases and successively moving to more complex configurations. The corresponding results give valuable insight into the wrinkling behavior of these sandwich constructions.

Kurzfassung

Das Ziel dieser Arbeit ist die Entwicklung eines allgemeinen analytischen Modells zur Beschreibung des lokalen Instabilitätsversagens von Sandwichen, genannt "Wrinkling". Dabei wird davon ausgegangen, dass die Interaktion mit globalem Beulen oder Knicken des Sandwiches vernachlässigt werden kann. Ein Vorteil dieser rein lokalen Beschreibung und der sehr allgemeinen Formulierung ist, dass man das Modell auch in Verbindung mit Finite Elemente Berechnungen für ein automatisiertes Post-Processing einsetzen kann. In diesem Fall können Sicherheitsfaktoren gegen Wrinkling auf Integrationspunktebene ermittelt werden, ausgehend von den FE Spannungsergebnissen von passenden Sandwich Schalenelementen. Diese Vorgehensweise war zwar auch bisher prinzipiell möglich, aber wegen der sehr beschränkten Gültigkeitsbereiche bestehender Wrinkling-Algorithmen nicht praktikabel.

Das neue Wrinkling Modell ist wesentlich allgemeiner formuliert als die bestehenden Modelle, da es auch unsymmetrische Sandwiche, beliebige Membranlasten der Deckschichten und orthotrope Materialien inkludiert. Trotz der Kompliziertheit des Problems konnte zur Lösung der Differentialgleichungen ein passender und relativ einfacher Ritz Ansatz gefunden werden. Dadurch ist der Rechenaufwand eher gering, obwohl numerische Optimierungsalgorithmen eingesetzt werden müssen.

In dieser Arbeit werden neben dem analytischen Modell noch drei verschiedene Finite Elemente Modelle zur Wrinkling Berechnung formuliert, darunter auch Einheitszellenmodelle. Ein direkter Vergleich zeigt dabei die Vor- und Nachteile der verschiedenen FE Modelle. Die Lösungen des analytischen Modells und der FE Modelle zeigen in allen Aspekten eine sehr gute Übereinstimmung. Mit Hilfe der FE Modelle konnte auch das Deformationsfeld, das für den Ritz Ansatz verwendet wurde, verifiziert werden. Eine experimentelle Verifikation der Ergebnisse ist zur Zeit in Vorbereitung.

Abgesehen von der eigentlichen Herleitung des analytischen Modells werden eine Anzahl von Ergebnissen präsentiert, die die Mängel und Unzulänglichkeiten der bestehenden

Wrinkling Modelle aufzeigen. Dabei wird gezeigt, dass sogar im einfachsten Fall eines gedrückten symmetrischen Sandwichstabes die in der Literatur angeführten Wrinkling Berechnungen zu substantiellen qualitativen und quantitativen Fehlern führen können. Es zeigt sich, dass die Art des Kernmaterials (Schaum, Honigwaben) einen entscheidenden Einfluss auf die Anwendbarkeit der üblichen Wrinkling Berechnungen hat. Außerdem spielt die Art des Kernmaterials bei der Entscheidung, ob der Kern dick genug ist um eine Interaktion zwischen den beiden Deckschichten zu verhindern, eine wichtige Rolle. Diese Effekte sind darauf zurückzuführen, dass die Steifigkeit des Kerns in Plattenebene einen wichtigen Einfluss auf das Wrinkling-Verhalten hat. Diese Erkenntnis ist auch für die sinnvolle Verwendung der derzeit existierenden Wrinkling Modelle wichtig, da die Steifigkeit des Kerns in Plattenebene bisher bei der Berechnung von Sandwichkonstruktionen prinzipiell nicht berücksichtigt wurde. Das neue analytische Wrinkling Modell verwendet eine Kontinuumsbeschreibung für den Kern, die die Steifigkeit des Kerns in Plattenebene berücksichtigt, und kann deshalb für alle gängigen Kernmaterialien eingesetzt werden.

Das neue analytische Modell liefert auch interessante Ergebnisse für das Wrinkling von Sandwichstäben unter Biegung. Dabei wird, zum ersten Mal, quantifiziert in wie weit jene Deckschicht, die unter Zug steht, das Wrinkling-Verhalten unter Biegung beeinflusst. Die Resultate zeigen, dass bei dünnen Sandwichen ein signifikanter Einfluss vorhanden ist.

Im Rahmen dieser Studie werden zum ersten Mal auch unsymmetrische und orthotrope Sandwichplatten untersucht, die mit den derzeit existierenden Wrinkling Modellen nicht beschrieben werden können. Die dabei auftretenden Effekte werden an Hand von verschiedenen Sandwichkonfigurationen gezeigt. Die entsprechenden Ergebnisse geben einen guten Einblick in das Wrinkling-Verhalten dieser etwas komplexer aufgebauten Sandwichplatten.

Chapter 1

Introduction

1.1 Sandwiches

Sandwich plates and shells are usually defined as a three-layer type of construction, consisting of two thin sheets of high-stiffness, high-strength material, between which a thick layer of low average density, stiffness and strength is sandwiched. The resulting construction is superior in terms of global buckling loads, bending strength and bending stiffness, compared to a monolithic structure of the same weight consisting of one of the constituent materials. This so called 'sandwich effect' is due to the fact that the moment of inertia is substantially increased by separating the face layers. Since the separation is achieved by using low density core materials, the weight of the sandwich is only affected to a minor degree by the core mass. Thus, sandwiches can be seen as an analogy to an I-beam, where the face layers represent the two flanges, and the core acts as the web.

This concept can also be found in natural structures (leaves, bones, ... see e.g. Patzelt [1973]), and has been known since the 19th century. The boom in research and application of sandwich construction started around World War II, due to the needs of airplane and missile industry for lightweight high-stiffness panels with high local rigidity. This led to the extensive use of sandwich structures in airplanes. More exhaustive information on the history of sandwich construction can be found in the introductions of the standard literature on sandwich structures [Vinson, 1999; Zenkert, 1995; Plantema, 1966; Allen, 1969].

Motivated by aerospace industry driven improvements in the manufacturing processes, adhesives, core and face materials as well as in analysis techniques, sandwich construction

has entered a wide field of applications in all parts of lightweight design, e.g. :

- aerospace industry (fuselages, wings, flaps, radomes, flooring, satellite structures,...),
- naval engineering (hulls, deck,...),
- transportation industry (side panels and flooring of railway cars, containers, bus structures,...),
- sports industry (skis, snowboards, surfboards,...),
- ...

This list is by no means exhaustive. In contrary, it seems difficult to name fields of engineering where sandwich construction is not used, including civil engineering as well.

1.2 Motivation

Regarding the current state of sandwich construction, fiber reinforced materials such as GFRP, CFRP, etc. are widely used for the face layers due to their superior mechanical properties and the relative ease of three-dimensional shaping. It is also common practice to use face layers of different thickness and/or material. This is done, on the one hand, because of different environmental conditions and local strength and stiffness requirements on the two sides of the sandwich (e.g. in fuselage, hulls, flooring, ...). On the other hand, even a basic weight optimization of an isotropic sandwich beam under compressive and bending loads leads to face layers of different thickness. These considerations form, among others, the background for the increased use of orthotropic and unsymmetric sandwich plates and shells.

The global behavior of these complex sandwich structures is mainly studied via FE shell models, which are the common state of the art and satisfactory. The situation is different regarding the local, short wave buckling failure mode of wrinkling, which is not captured in a standard FE shell/beam analysis of a sandwich structure. The wrinkling calculations currently used are practically either restricted to isotropic symmetric sandwiches under pure compressive loading, or to very thick sandwiches. They are, therefore, used for engineering estimates, but not for the direct evaluation of the factor of safety against wrinkling failure of a specific design. In order to have an easily applicable solution to this

problem for the engineer, one needs a general calculation scheme, which is able to predict the onset of wrinkling failure for the orthotropic and unsymmetric sandwiches which are currently designed.

The need for efficiency is especially high regarding the possibility of using this routine in conjunction with FE sandwich shell results. The wrinkling algorithm can either be used as part of a non-linear shell material law [Starlinger and Rammerstorfer, 1992; Stiftinger and Rammerstorfer, 1997], or as a post-processing routine for FE results which calculates the safety against wrinkling *a posteriori*. In either case, the wrinkling calculation has to be done at the integration point level and, therefore, a very high number of calculations has to be performed. Moreover, the wrinkling calculation should allow for all the sandwich shell properties and loading types which are normally used in FE sandwich shell analysis. This causes the need for a general *and* efficient wrinkling calculation, which has the great advantage, that it can be used as a black box by the design engineer and still calculates reliable safety factors by including all major parameters of the problem.

It is the objective of this work to provide such a scheme and compare it to other approaches. However, investigating the corresponding non-linear effects such as the influence of imperfections, material non-linearities, post–wrinkling behavior, etc. falls out of the scope of the present study.

1.3 Sandwich design calculations

Sandwich construction leads to weight efficient design of structures, at least as far as bending strength and/or stiffness dominated design issues are concerned. This high efficiency is made possible by the heterogeneous structure of the sandwich, which combines high-stiffness, high-strength face layer materials with very soft core materials. This heterogeneity leads to more complex failure mechanisms and design calculations as compared to monolithic structures (e.g. shear deformability, local instabilities, ...).

1.3.1 Failure mechanisms

The main failure mechanisms, as stated in the standard literature on sandwich construction, are:

- global buckling,

- shear crimping,
- wrinkling,
- face dimpling,
- face/core yielding/fracture,
- core-face debonding,
- localized failure (load introduction, free edge effects, ...).

The present work concentrates on the topic of the wrinkling failure mechanism. However, the instability modes of global buckling and shear crimping are of certain interest to the problem, and the corresponding design formulas are briefly reviewed. Concerning the other failure modes, the reader is again referred to the standard literature on sandwich structures mentioned in the first part of this chapter.

Chapter 2

Literature review

The first section of this chapter very briefly introduces the fundamentals of global buckling and shear crimping of sandwiches and is meant to be the base for further discussions on the connection of wrinkling to these modes of instability. It is clearly not a review of the current research in this area. The second section is a review on the past and current research on wrinkling, mainly regarding linear approaches.

2.1 Global buckling and shear crimping

The problem of global buckling of sandwich beams is dealt with in the classical sandwich literature e.g. in Plantema [1966]. As shear deformation plays an important role in sandwich construction, the common Euler buckling formulas overestimate the buckling loads considerably. Starting from the differential equation of a Timoshenko (shear deformable) beam, a simple formula can be derived for the global buckling load P^{G}:

$$\frac{1}{P^{\mathrm{G}}} = \frac{1}{P^{\mathrm{E}}} + \frac{1}{P^{\mathrm{S}}}, \tag{2.1}$$

where P^{E} denotes the Euler buckling load and P^{S} the shear crimping load of the beam, which is equal to the shear stiffness of the beam

$$P^{\mathrm{S}} = G\, b\, c. \tag{2.2}$$

Here G denotes the transverse core shear modulus, and b and c denote the core width and thickness, respectively.

This approach is only valid under certain conditions (similarity of shear and bending deformation patterns) and is widely used due to its simplicity. Essentially, eq. 2.1 splits the buckling load into a bending part and a shear part, and this approach is therefore also named 'method of split rigidities'. In the case of infinite shear stiffness, the problem reduces to the classical Euler buckling problem. In the case of infinite global beam bending stiffness, the problem reduces to pure shear crimping. In this case, buckling is only determined by the shear stiffness of the beam and is independent of the face layers. The face layers are not strained at all.

This shows the problems of the approach in conjunction with an extremely shear dominated sandwich, since a sandwich beam can not be deformed by shear in the core without a deformation of the individual face layers. This deformation of the individual face layers has been neglected, because the deformation only leads to bending of the individual face layer, and not to bending of the whole beam. Thus plain beam theory (Kirchhoff or Timoshenko beam kinematics) is not appropriate any more and has to be extended, as shown in unified approaches (e.g. Hegedüs and Kollàr [1989]). These approaches include bending of the individual faces. In this regime, it has to be judged very carefully which theory is appropriate and whether continuum mechanics has to be used instead of structural mechanics based on kinematic constraints.

Thus, the shear crimping load should not blindly be used as a failure criteria of its own, but rather as an input to further calculations of global stability failure (via eq. 2.1 or, if the bending stiffness of the individual face layer starts to be of influence, a refined approach as sketched above). Shear crimping alone is a conservative estimate of a local buckling load, since the energy needed to strain the face layers is disregarded, which is only justified in certain cases. These basic aspects can naturally be transferred to sandwich plates as well.

It can be shown, that eq. 2.2, along with all its assumptions, also holds for the case of combined compression and bending, as long as P^{S} is taken to be the total axial compressive section force of the beam. Thus, in the case of pure bending or a combination of bending and tension, shear crimping can not occur.

2.2 Wrinkling

Wrinkling (i.e. short wavelength buckling of the face layers) is a common local stability problem of sandwich plates and shells under compressive or bending loads, leading to a loss in stiffness of the structure. The literature usually divides the wrinkling problem into

two different mode shapes, namely the symmetrical mode (ideal "hourglass mode") and the antimetrical mode (ideal "snake mode"), which can be seen in fig. 2.1. It is clear, that the symmetrical and antimetrical mode are limited to the case of symmetrical sandwiches under pure global compressive loading (i.e. a symmetrical problem with respect to its middle surface). In the case of unsymmetry, bending, etc. the terms "snake mode" and "hourglass mode" are used to describe the mode shape qualitatively. These patterns are local short wavelength patterns consisting of a large number of similar waves.

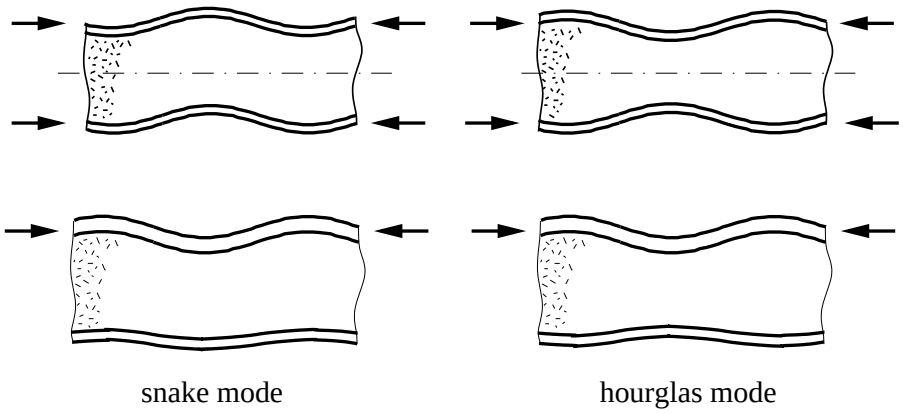

Figure 2.1: Snake and hourglass mode (upper row: ideal mode shapes)

The problem is characterized by the interaction between the sandwich core and the face layers, which are bonded to the core. As a result, the critical forces leading to wrinkling of the face layers are a function of the stiffness parameters of the face layers and the core, the geometry of the problem and the bonding and loading conditions.

In the following, section 2.2.1 lists the general assumptions which are the basis the for further discussion of wrinkling. Sections 2.2.2 to 2.2.4 review the state of the art for wrinkling approaches of sandwiches having isotropic faces, and sections 2.2.5 to 2.2.8 deal with more general approaches currently used (for orthotropic sandwiches, post–wrinkling, etc. . .).

2.2.1 General assumptions

Concerning this work (as well as the standard sandwich literature), some general assumptions are made in order to derive the fundamental equations describing the sandwich behavior. These assumptions, which are commonly used in sandwich construction, are not

questioned in detail in this work. The following list is therefore also meant to indicate the scope of this work (and this literature review):

- the constituent materials show ideal elastic behavior
  (elastoplastic face layers can always be described in an approximate manner by using the plastic effective modulus instead of the elastic modulus as described e.g. in Plantema [1966]),
- the bonding between core and face is perfect,
- the thickness of the face layers $t^{\mathrm{u}}, t^{\mathrm{l}}$ is substantially lower than the thickness of the core c,
- the sandwich is absolutely smooth, imperfections are not taken into account
- global bending and membrane loads of the sandwich plate are carried by the face layers only. The contribution of the core in this respect is neglected due to the low stiffness of the core as compared to the face layers.

2.2.2 Classical design formulas: thin cores

The classical sandwich theory divides the wrinkling problem into two different cases. The first case is the "thick sandwich" case [Gough et al., 1940; Hoff and Mautner, 1945, ...], where it is assumed that the thickness of the sandwich is big enough to preclude interaction between the two face layers. The second case is the "thin sandwich" case, where interaction between the face layers is included. Both cases have been compared and discussed more closely in Yusuff [1955] and are used in the standard sandwich literature (see e.g. Plantema [1966]; Allen [1969]; Zenkert [1995]). Due to their practical importance in sandwich design, these cases are now discussed in detail.

Both models are sandwich beam rather than sandwich plate models, and the justification of this approach is discussed at the end of this section. The models can either be derived by using the energy method, or a differential equation approach. Since the results are equivalent and the differential equation approach is extensively used by the author, it is also employed in the following.

The models are derived using the equation for the isotropic plate on an elastic founda-

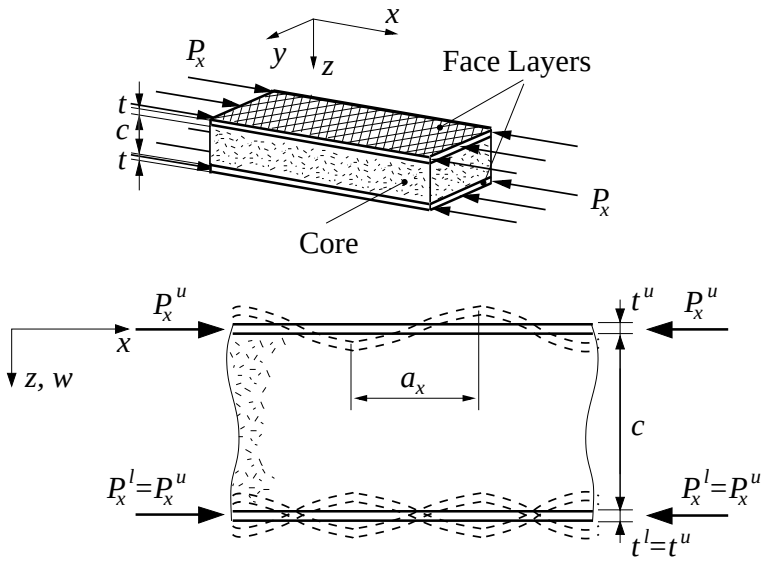

Figure 2.2: 3D and 2D sketch of the wrinkling model for symmetrical isotropic beams

tion specialized for unidirectional loading in x-direction P_x^{u} (see fig. 2.2):

$$B^{\mathrm{u}}\frac{\partial^4 w^{\mathrm{u}}}{\partial x^4} + P_x^{\mathrm{u}}\frac{\partial^2 w^{\mathrm{u}}}{\partial x^2} + k w^{\mathrm{u}} = 0\,, \tag{2.3}$$

where B^{u} denotes the plate bending stiffness of the upper face layer and P_x^{u} the compressive membrane force per unit width of the upper face layer in x–direction. w^{u} is the deflection of the upper face layer, and k the foundation's stiffness. The foundation is made up of the core and the lower face layer. It is of no importance which of the face layers is denoted as upper face layer and as lower face layer. These terms are introduced at this stage in order to be consistent with the following chapters. The superscripts ^{u}, ^{l} and ^{c} refer to the upper and the lower face layer and the core, respectively.

The wrinkling pattern (in z-direction) of the upper face layer, and therefore also for the core surface which is perfectly bonded to it, is taken to be a sine pattern:

$$w^{\mathrm{u}} = w^{\mathrm{c}}(z{=}0) = w^{\mathrm{u}*}\sin\left(\frac{\pi x}{a_x}\right)\,. \tag{2.4}$$

Using eq. 2.4 as a Rayleigh-Ritz ansatz (including the *a priori* unknown wave-length a_x) in eq. 2.3, the problem is fully defined apart from the foundation stiffness k, which has to be specified. The differences between the analytical approaches to this problem lie in the determination of k, which is a function of the properties of the core and the lower face layer.

In the model for thin cores, the continuous elastic medium of the core is modeled as a set of parallel closely set elastic springs (Winkler foundation). Therefore, this model takes only the transverse core stiffness E_z^{c} into account, and neglects the shear stiffness as well as the in-plane stiffness of the core. These simplifications are meant to lead only to useful results if the core thickness is relatively small. However, a further regime where this approach can be used is described in section 4.4.

By presupposing that the sandwich is symmetric (i.e. upper and lower face are identical) and symmetrically loaded (i.e. global compression), the face layers are *a priori* assumed to undergo symmetrical buckling in the hourglass mode. The fact that an antimetrical (snake) buckling mode may also exist and may lead to lower critical loads is not taken into account. Considering a symmetrical buckling pattern, the mid surface of the sandwich remains undeformed during buckling:

$$w^{\mathrm{c}}(z = c/2) = 0. \tag{2.5}$$

Using this boundary condition, the foundation stiffness corresponding to this "old" model for thin cores $k^{\mathrm{thin,old}}$ can be calculated (compare e.g. Allen [1969]; Yusuff [1955]):

$$k^{\mathrm{thin,old}} = E_z^{\mathrm{c}} \frac{2}{c} \,. \tag{2.6}$$

Inserting this result into eq. 2.3 and using eq. 2.4, P_x^{u} is obtained as a function of the wavelength a_x. The minimization of P_x^{u} with respect to the wavelength a_x (for nontrivial solutions of w^{u}) leads to the critical compressive force per unit width in the face layer $P^{\mathrm{cr,thin,old}}$:

$$P^{\mathrm{cr,thin,old}} = 2\sqrt{k^{\mathrm{thin,old}} B^{\mathrm{u}}} = 2t^{\mathrm{u}} \sqrt{\frac{E^{\mathrm{u}} E_z^{\mathrm{c}} t^{\mathrm{u}}}{6c(1-(\nu^{\mathrm{u}})^2)}} \,. \tag{2.7}$$

2.2.3 Classical design formulas: thick cores

In the case of very thick cores it is assumed that the two face layers do not influence each other. This asymptotic approach uncouples the upper and lower face layers, and each face layer is treated as a thin plate on an infinitely thick elastic foundation. This assumption drastically simplifies the analytical derivation. However, it is not clear which core thickness is really needed to satisfy this assumption. In the literature (see e.g. Plantema [1966]; Hertel [1960]), it is assumed that a ratio of core thickness c to face layer thickness t^{u} exceeding some value (around 50) justifies the 'thick core' assumption. However, this value of about 50 has been judged from experiments dating back to 1945 which included, naturally, only

a very limited number of sandwich designs. This rule does not seem to be very reliable regarding other sandwich designs (especially different materials). Moreover, a c/t^{u} ratio exceeding 50 is not very common in structural sandwich components. A highly improved insight into the applicability of the 'thick core' assumption is given in section 4.4.

Taking only global uniaxial compression of the face layer into account, the deformation of the core is considered as orthotropic plane stress problem (in x-z direction). This is a slightly conservative assumption, since the core is rather in a state of plane strain than plane stress. The face layer, which is orders of magnitude stiffer than the core, is generally assumed to lead to $\varepsilon_x^{\mathrm{c}}(z=0) = 0$ in the core-face layer interface.

In the differential equation approach (see e.g. Wiedemann [1986]), this boundary condition is simplified by taking the core stiffness in loading direction E_x^{c} to be infinity. This leads to $\varepsilon_x^{\mathrm{c}} = 0$ in the whole core. On the other hand, the core stiffness in loading direction can be very small in reality (e.g. honeycomb cores). Therefore, the assumption of an infinitely high stiffness seems to be questionable. However, this simplification appears to be based on the assumption that the influence of in-plane core action can generally be neglected in this problem.

The majority of authors [Gough et al., 1940; Hoff and Mautner, 1945; Yusuff, 1955; Plantema, 1966; Zenkert, 1995, etc...] used an energy approach to this problem, and assumed the in-plane displacements u (in x direction) to be zero. This is essentially the same assumption as mentioned above. The results are also practically the same as in the differential equation approach cited above.

Using these simplifications, the foundation stiffness corresponding to this "old" model for thick cores $k^{\mathrm{thick,old}}$ can be calculated in an asymptotic sense, i.e. no interaction between upper and lower face:

$$k^{\mathrm{thick,old}} = \frac{\pi}{a_x}\sqrt{E_z^{\mathrm{c}} G_{xz}^{\mathrm{c}}}\,, \tag{2.8}$$

Inserting this result into eq. 2.3, using eq. 2.4 and minimizing with respect to the wavelength a_x, the critical force per unit width per face layer $P^{\mathrm{cr,thick,old}}$ can be derived:

$$P^{\mathrm{cr,thick,old}} = 1.89\sqrt[3]{B^{\mathrm{u}} E_z^{\mathrm{c}} G_{xz}^{\mathrm{c}}} \quad \overset{\nu^{\mathrm{u}}=0.3}{\Longrightarrow} \quad 0.85\, t^{\mathrm{u}}\sqrt[3]{E^{\mathrm{u}} E_z^{\mathrm{c}} G_{xz}^{\mathrm{c}}}\,. \tag{2.9}$$

Depending on the exact method of derivation, the constant factor in eq. 2.9 varies in the range of 0.78 to 0.91.

From experimental investigations on sandwiches with *isotropic* cores by Hoff and Mautner [1945], the scatter was observed to be rather high, and the following formula was

recommended for practical design:

$$P^{\mathrm{cr,thick,old}} = 0.5\, t^{\mathrm{u}} \sqrt[3]{E^{\mathrm{u}} E_z^{\mathrm{c}} G_{xz}^{\mathrm{c}}}\,. \tag{2.10}$$

This formula is widely used in sandwich design and already includes a safety margin, since it was fitted in a conservative manner to experimental results.

This approach originates from the early 40's, when orthotropy was not considered in a rigorous manner. In fact, the first authors did not mention orthotropy of the core at all. However, in the standard sandwich literature, this solution is also recommended for orthotropic cores, such as honeycomb, in the form given in eqs. 2.9 and 2.10. This is clearly not recommended by the author and further discussed in section 4.4.

2.2.4 Extension from beams to plates

Using a three-dimensional approach in analogy to the thick sandwich approach given above, Plantema [1966] showed that the critical wrinkling load as well as the wave form under *biaxial* compressive load is solely determined by the major compressive membrane force in the face layer. This statement is limited to sandwiches having isotropic face layers and a transversely isotropic core ($G_{xz}^{\mathrm{c}} = G_{yz}^{\mathrm{c}}$). Therefore, the three-dimensional wrinkling problem of the sandwich plate can, in these cases, easily be reduced to a two-dimensional (sandwich beam) problem. This is done by defining the x-direction used in the derivations above as the direction of the major compressive membrane force in the face layer, which also holds for the thin core solution given above in the case of for symmetric sandwiches under symmetrical loading.

Essentially, this means that in the cases mentioned above, the direction of wrinkling (the direction in which the sinusoidal buckling pattern is forming) is *a priori* known. Therefore, the plate problem can be reduced to a beam model which is oriented in the direction of wrinkling.

2.2.5 Sandwiches with anisotropic face layers

The use of orthotropic face layers poses the problem that the direction of wrinkling is generally unknown *a priori*. Only in the case of a single compressive force acting directly in the direction of one of the material axes of the orthotropic face layer, it is possible to state that wrinkling will occur also in this direction. In these cases, the approaches given in

the last section can be applied, simply by using the appropriate orthotropic plate bending stiffness instead of the isotropic plate bending stiffness. However, this method incorporates such a large number of restrictions (loading direction, symmetry or very thick cores, only a single compressive membrane force, ...) that it can be used for engineering estimates, but not for the prediction of wrinkling in sandwich structures used in practice.

2.2.6 Approaches of higher generality

There have been some advanced approaches to the wrinkling problem of sandwiches having anisotropic face layers. Yusuff [1960] considered the effect of initial irregularities by including them into the geometrical model and, therefore, transforming the wrinkling instability problem into a stress problem. This approach mainly addresses the transverse core strength as a limiting factor for the load carrying capacity.

Webber et al. [1976] and Gutierrez and Webber [1980] extended the wrinkling calculations of symmetric sandwich columns to general laminated face layers by including the stiffness coupling matrix B. They assumed that the material axis of the face layers coincides with the beam axis (loading direction) and did not tackle the plate problem.

The interesting semi–analytical solution by Starlinger and Rammerstorfer [1992], which was later extended by Stiftinger and Rammerstorfer [1997], is the first solution of the 3D core problem that includs the in-plane core stiffness ($E_x^{c\prime}$, $E_y^{c\prime}$) into the continuum model of the core. The effects of the in-plane core stiffness on the wrinkling behavior have, however, not been studied by these authors. Their approach is limited to symmetrical sandwich plates with orthotropic face layers and, again, loading is only permissible in the directions of the material axes. The buckling pattern used in this approach differs from the usually employed sine pattern (eq. 2.4), and is the product of two orthogonal sine waves. The implications of this are discussed in the results chapter (section 5.2). The model includes wrinkling due to bending, by assuming that the face layer under tension remains perfectly flat, while the face layer under compression buckles. This assumption has also been used by other authors (e.g. Gutierrez and Webber [1980]), however, it overestimates the stiffness of the system in the case of rather thin cores. Another interesting feature of this approach is, that the critical wrinkling load in the transition regime between pure bending and pure compression is approximated by an interpolation in core stiffness proposed by Stamm and Witte [1974]. The problems arising from the latter two assumptions are discussed in detail in section 4.6. Since a FORTRAN implementation of this approach was readily available to the author, this model is often used for comparison in the following chapters. The author

also used this model and its theoretical background as a starting point for his own research presented here.

Another interesting approach originates from continuum mechanics by regarding a sandwich as a stack of different 3D continua having highly different stiffness parameters. This approach was chosen by Bufler and Kennerknecht [1983]. The approach is not based on symmetry, different transversely isotropic face layers are allowed for. The effects of unsymmetry have, unfortunately, not been studied. Due to the very general formulation, this approach is at the present stage limited to beam problems (where the beam axis and one of the material axes coincide), or to face layers which are isotropic. This general method could be extended to orthotropic face layers, but even at the present stage it is leading to very expensive calculations. Due to this high computational effort and due to the complexity of the model (which is clearly not necessary for studying wrinkling only), the author chose to use a different and much more efficient approach.

Regarding the topic of wrinkling under combined loads, the findings of Hegedüs and Kollàr [1989] are very interesting. They are able to give a simple closed form solution to the problem of a sandwich beam under a combination of compressive and bending loads. These results are, however, again restricted to symmetric sandwiches with isotropic faces and cores which show a special type of orthotropy (antiplane cores).

2.2.7 Interaction effects and unified models

There exist several works on the interaction between global buckling (including transverse shear effects) and wrinkling, [Benson and Mayers, 1967; Leotoing et al., 2000; Niu and Talreja, 1999] and the excellent work by Hegedüs and Kollàr [1989]. These models are able to predict the critical load leading to buckling (local or global) as a function of the wavelength. In this sense these models can be seen as unified approaches covering local and global buckling. These formulations only regard isotropic face layers and beam problems so that closed form results can be derived.

As far as global buckling is concerned, the interaction approach is an extension in the sense that the transverse core flexibility is included. A simple formula to approximate this effect is given in Hegedüs and Kollàr [1989].

The first unified solution to the sandwich plate problem with isotropic face layers has been derived by Benson and Mayers [1967] and has been extended by a number of authors, e.g. Hadi and Matthews [2000]. The approach has been generalised within numerous

publications by Frostig [e.g. Frostig, 1998; Frostig and Baruch, 1993, ...], by including laminated plates and other refinements. The face layers are modeled using thin plate kinematics, and the core by using linear continuum mechanics. The continuity conditions between face and core are taking the face layer thickness into account, which is another refinement as compared to classical sandwich theory. Using a variational principle, a set of differential equations is obtained that has to be solved using appropriate boundary conditions. This approach is not using a Ritz ansatz type derivation and, therefore, the calculations are numerically expensive since the deformation fields have to be integrated numerically. Within this model it is possible to define different boundary conditions for each layer of the sandwich, thus simulating local load introduction effects. A drawback of this approach is that, despite its generality, the in-plane core stiffness is set to zero i.e. the in-plane core strains are omitted in the calculation of the strain energy. As shown in section 4.4, this has far reaching consequences and limits the applicability of this model for the calculations of local effects such as wrinkling or load introduction problems severely. Considering the global behaviour of sandwich plates, the in-plane stiffness is of very limited importance and this method can be applied to different plate geometries by appropriate choice of boundary conditions, including the effects of transverse and shear stiffness of the core. It seems to be quite possible to include the in-plane strains correctly into this framework without severe alterations of the concept. This would be highly recommendable, since it would lead to a very powerful (and complex) unified tool for the calculation of global and local stress and stability problems of sandwich constructions including coupling effects.

Since the difference in length scale between wrinkling and global buckling is rather large, the interaction effects seem not to be very pronounced, and the calculation of wrinkling by an uncoupled model as described in the last sections remains valid. Despite the number of unified models in the literature, no study was found which is focussing on the absolute value of the errors induced by calculating wrinkling failure with a model which is uncoupled from global buckling. The other problem connected to this issue, namely the calculation of the errors induced by calculating the global buckling via an uncoupled model has received far more attention.

2.2.8 Post–wrinkling behavior

The initial elastic post buckling behavior after the occurrence of wrinkling seems to be stable [Stiftinger and Rammerstorfer, 1997], like the post buckling behavior of an elastic plate on an elastic foundation. However, interaction with global buckling, large deforma-

tions and load introduction effects can lead to localization and to a globally unstable post buckling behavior, even in the case of elastic constituent materials. These effects have been investigated, for example in Wadee and Hunt [1998]; Hunt et al. [1988] and Kühhorn [1991].

The post–wrinkling behavior in typical practically used sandwich constructions is highly unstable [Stiftinger and Rammerstorfer, 1997; Martikainen and Hassinen, 1996; Stockinger, 1996], leading to an abrupt loss of stiffness in the affected region. This is likely to be due to the fact that wrinkling is only observed at relatively high stress levels and the additional stresses caused by the short wave deformation lead (almost immediately) to stresses beyond the elastic limits of the commonly used constituent materials. This behavior was observed in numerous experiments. The failed specimens generally show a single fold (caused by plastic deformation of the faces or crushing of the core or by fracture) which indicates localization in the post–wrinklinging regime. An example of this behavior is shown in fig. 2.3. This experimentally observed post–wrinkling behavior can currently not be described by analytical means, since the combination of geometrical and material nonlinearities, interaction with global buckling and localisation forms a very complex problem.

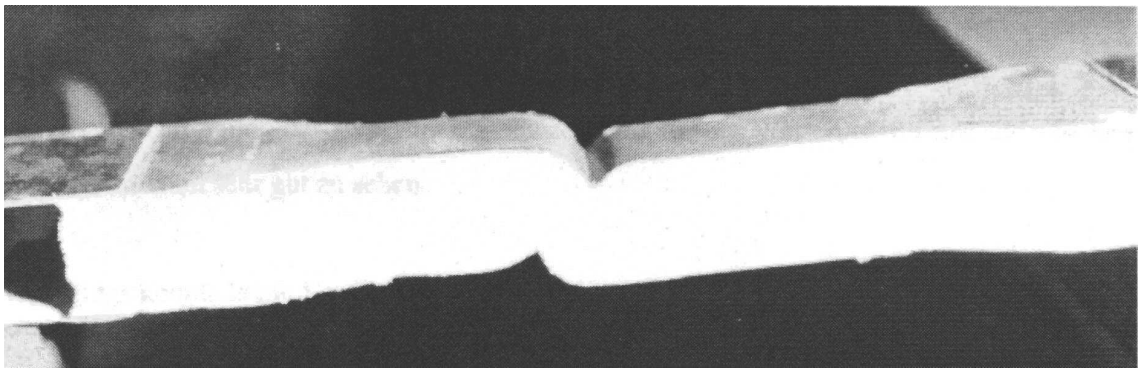

Figure 2.3: Sandwich beam after wrinkling failure [Stockinger, 1996]

Regarding the use of linear wrinkling calculations (such as derived in this work) within FE sandwich shell elements at the integration point level, it becomes clear that their use within a non linear material law trying to describe the post–wrinkling regime as well (as in Starlinger and Rammerstorfer [1992]) is highly questionable. It makes much more sense and is more efficient to perform the wrinkling calculations in a post processing routine, due to several reasons:

- the post–wrinkling regime can currently not be described properly. Therfore, the

occurence of wrinkling has to be put on a level with the total failure of the affected region, which will in practically all cases lead to the failure of the sandwich.

- It is numerically more efficient, since the wrinkling calculations have to be performed only once, as compared to numerous times when doing a non-linear FE analysis.
- localized stress concentrations which are due to FE modelling issues and stress results at the edges of panels, where the wrinkling theory is not valid, can be judged seperately by the engineer. Declaring these regions as totally failed regions during the FE analysis, because the wrinkling calculation is incorporated into the material law, is clearly not practical.
- in practical sandwich construction, wrinkling is only one of the possible failure modes and not the most common one. It is, therefore, sensible for the engineer to include wrinkling on the basis that it is checked for, but it is not the core part of the design evolution and evaluation.

2.2.9 Conclusions

The wrinkling instability of sandwiches has conceived considerable attention over the last decades. The simple formulas which are mainly used in the design process are subject to numerous limitations (isotropy, thick cores or symmetry,...) the effects of which are difficult to estimate. However, they are useful design tools that are very easy to handle. Even the refined approaches do not overcome these restrictions in a general way.

As soon as orthotropic face layers are concerned, the available wrinkling approaches are restricted to rather special conditions:

- loading solely in the direction of the axis of orthotropy of the faces.
- in the very important case of thin cores:
  - symmetric sandwiches (identical face layers),
  - symmetric loading conditions (no bending allowed),

Moreover, it is not clear, which sandwich configurations have to be assessed via the thin core approaches. Another drawback is, that the influence of the in–plane core stiffness is disregarded in the literature on sandwich structures. The effects of all these restrictions

have not been quantified yet. It is the aim of this work to derive an efficient full solution for the critical wrinkling load of an orthotropic unsymmetric sandwich under general loading conditions, and to investigate the results in terms of new effects and the applicability of simplified approaches.

Chapter 3

Analytical approach

3.1 Overview

In this section a refined approach to the wrinkling of sandwich plates is presented, which takes into acount arbitrary and different orthotropic face layers, finite core thickness and orthotropic core material. The analytical derivation is conducted for this most general case, and simplified formulae are given for the cases of thick cores and isotropic face layers. These three cases were published in [Vonach and Rammerstorfer, 2001, 2000b,a], respectively.

3.2 Derivation

The basics of the analytical approach are similar to the classical model for thick cores (section 2.2.3), i.e. the sandwich is split into the upper face layer and a foundation which represents the mechanical behavior of the core and the lower face layer. The problem is also solved via a Rayleigh-Ritz ansatz. The Ritz approach is, of course, much more efficient as compared to a general solution of the elasticity problem which incorporates the (numerical) intergation of the strains in order to derive the displacement fields. The validity of the Ritz ansatz is verified via FE calculations in section 5.5. The assumptions listed in section 2.2.1 are assumed to be valid.

3.2.1 Upper face layer, Ritz ansatz

The upper face layer is supported by the core and, via the core, by the lower face layer. The buckling deformation pattern of the upper face layer w^{u} is assumed to be sinusoidal in r–direction and constant in s–direction (see fig. 3.1):

$$w^{\mathrm{u}} = w^{\mathrm{u}*} \sin\left(\frac{\pi r}{a_r}\right) = w^{\mathrm{u}*} \sin\left(\frac{\pi(x\cos\varphi + y\sin\varphi)}{a_r}\right) . \tag{3.1}$$

The superscript $^{\mathrm{u}}$ refers to the upper face layer, $^{\mathrm{c}}$ to the core, $^{\mathrm{l}}$ to the lower face layer, and * to amplitude values. Eq. 3.1 is a Rayleigh-Ritz ansatz for the wrinkling pattern with two free variables, namely the half-wavelength a_r and the direction of the buckling pattern φ. Both of these variables are *a priori* unknown. This is a considerable extension to eq. 2.4. The geometry of the problem is shown in fig. 3.1. The xyz coordinate system denotes the global coordinate system defined by the material axes of the upper face layer, and the rsz system is defined by the angle of the sine wave φ.

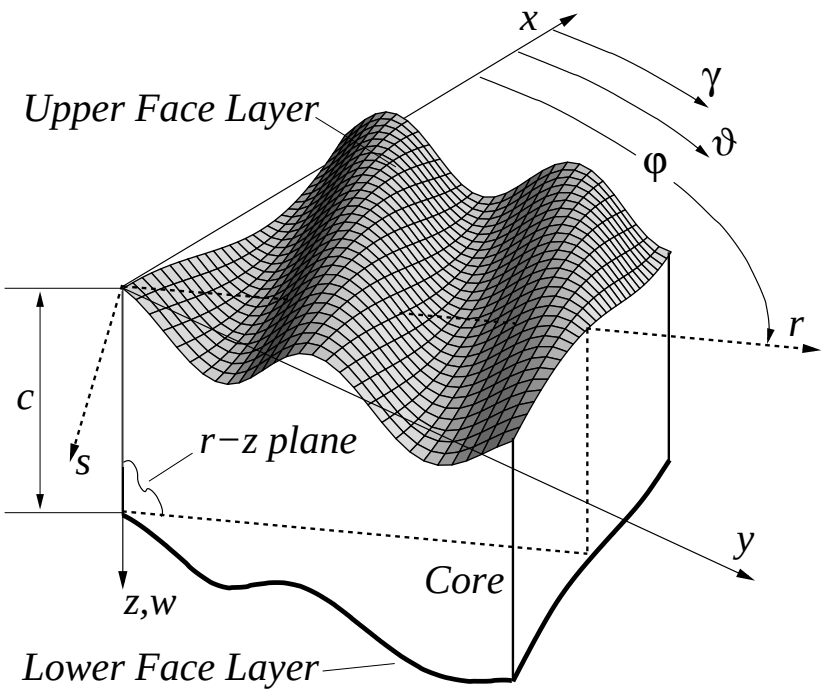

Figure 3.1: Geometry of the buckling pattern

The orthotropic upper face layer is described using the differential equation of a thin

elastic orthotropic plate on an elastic foundation

$$B_x^{\mathrm{u}}\frac{\partial^4 w^{\mathrm{u}}}{\partial x^4} + 2B_{xy}^{\mathrm{u}}\frac{\partial^4 w^{\mathrm{u}}}{\partial x^2 \partial y^2} + B_y^{\mathrm{u}}\frac{\partial^4 w^{\mathrm{u}}}{\partial y^4} + P_x^{\mathrm{u}}\frac{\partial^2 w^{\mathrm{u}}}{\partial x^2} + 2P_{xy}^{\mathrm{u}}\frac{\partial^2 w^{\mathrm{u}}}{\partial x \partial y} + P_y^{\mathrm{u}}\frac{\partial^2 w^{\mathrm{u}}}{\partial y^2} + w^{\mathrm{u}} k^{\mathrm{thin}} = 0 \quad (3.2)$$

where the individual B's are the plate bending stiffness terms and the P's are the compressive membrane forces. k^{thin} denotes the stiffness of the elastic foundation, which depends on the core material, lower face layer material and lower face layer loading.

Using the deformation pattern in eq. 3.1, the plate equation can be reduced to the equation of a beam (in r–direction) of unit-width on an elastic foundation:

$$B_r^{\mathrm{u}}(\varphi)\frac{\partial^4 w^{\mathrm{u}}}{\partial r^4} + P_r^{\mathrm{u}}(\varphi)\frac{\partial^2 w^{\mathrm{u}}}{\partial r^2} + w^{\mathrm{u}} k^{\mathrm{thin}} = 0\ . \quad (3.3)$$

The beam bending stiffness B_r^{u} and section force P_r^{u} are formulated in r–direction which makes them dependent on the angle φ. The loading is defined by ρ^{u}, ξ^{u} and ζ^{u} relative to the global load level P.

$$\begin{aligned} B_r^{\mathrm{u}}(\varphi) &= B_x^{\mathrm{u}}\cos^4(\varphi) + 2B_{xy}^{\mathrm{u}}\sin^2(\varphi)\cos^2(\varphi) + B_y^{\mathrm{u}}\sin^4(\varphi)\ , \\ P_r^{\mathrm{u}}(\varphi) &= P\left(\rho^{\mathrm{u}}\cos^2(\varphi) + 2\zeta^{\mathrm{u}}\sin(\varphi)\cos(\varphi) + \xi^{\mathrm{u}}\sin^2(\varphi)\right)\ , \\ \rho^{\mathrm{u}} &= P_x^{\mathrm{u}}/P,\ \ \xi^{\mathrm{u}} = P_y^{\mathrm{u}}/P \ \text{ and } \ \zeta^{\mathrm{u}} = P_{xy}^{\mathrm{u}}/P \end{aligned} \quad (3.4)$$

Inserting eq. 3.1 into eq. 3.3 yields

$$B_r^{\mathrm{u}}(\varphi)\left(\frac{\pi}{a_r}\right)^4 - P_r^{\mathrm{u}}(\varphi)\frac{\pi}{a_r}^2 + k^{\mathrm{thin}} = 0 \quad (3.5)$$

Apart from the two free variables a_r and φ, the only remaining unknown in this equation is the foundation (spring) stiffness k^{thin} which is derived in the following section.

3.2.2 Foundation stiffness

The foundation stiffness k^{thin} is defined as

$$k^{\mathrm{thin}} = \frac{-\sigma_z^{\mathrm{u}}}{w^{\mathrm{u}}} \quad (3.6)$$

where σ_z^{u} is the stress in z–direction and w^{u} is the deflection in z–direction, both at the perfectly bonded interface between the core and the upper face layer.

The deflection w^{u} is defined in eq. 3.1. It can be shown, that this sinusoidal deflection leads to a sinusoidal distribution of the normal stresses in z–direction, σ_z^{u}, at the interface. To derive the foundation stiffness according to eq. 3.6, the core and the lower face layer, which is bonded to the core, are loaded by this (self equilibrating) sinusoidal stress distribution:

$$\sigma_z^{\mathrm{u}} = \sigma_z^{\mathrm{c}}(z=0) = \sigma_z^{\mathrm{u}*} \sin\left(\frac{\pi r}{a_r}\right). \tag{3.7}$$

The amplitude of this load $\sigma_z^{\mathrm{u}*}$ is arbitrary, since a linear elastic response is expected. The deflections $w^{\mathrm{u}} = w^{\mathrm{c}}_{z=0}$ of the core which result from this loading are calculated using linear elasticity and thus k^{thin} can be determined from eq. 3.6. This calculation will now be discussed in detail.

In order to allow for an efficient analytical solution it is assumed, that the deformation w of the core and the lower face layer is also a single sine wave, having the same wavelength a_r and wave direction φ as the upper face layer, but an amplitude $w^*(z)$ that depends on z:

$$\begin{gathered} w^{\mathrm{c}}(z) = w^{\mathrm{c}*}(z) \sin\left(\frac{\pi r}{a_r}\right) \;=\; w^{\mathrm{c}*}(z) \sin\left(\frac{\pi(x\cos\varphi + y\sin\varphi)}{a_r}\right), \\ \text{with } w^{\mathrm{u}} = w^{\mathrm{c}}(z=0) \text{ and } w^{\mathrm{l}} = w^{\mathrm{c}}(z=c)\,. \end{gathered} \tag{3.8}$$

This assumption is the key to the further derivations and is, therefore, discussed in more detail in section 5.5.

3.2.2.1 Core

Regarding the deformation pattern in eq. 3.8 it can be stated that the deformations are constant in s–direction (see fig. 3.1). Therefore, it is sufficient to regard the core and the lower face layer as a 2D plane strain problem in the r-z plane as sketched in fig. 3.2. The deformation mode indicated in fig. 3.2 is leading to a snake mode. In the case of an hourglass mode, the deflection of the lower face layer is reversed, leading to a negative $w^{\mathrm{l}*}$.

The elastic behaviour of the core is modeled using Airy's stress function in the r-z plane

$$\begin{gathered} \frac{1}{D_z^{\mathrm{c}}}\frac{\partial^4 F}{\partial r^4} + \frac{2}{D_{rz}^{\mathrm{c}}}\frac{\partial^4 F}{\partial r^2 \partial z^2} + \frac{1}{D_r^{\mathrm{c}}}\frac{\partial^4 F}{\partial z^4} = 0\,, \\ \sigma_r^{\mathrm{c}} = \frac{\partial^2 F}{\partial z^2}, \quad \sigma_z^{\mathrm{c}} = \frac{\partial^2 F}{\partial r^2}, \quad \sigma_{rz}^{\mathrm{c}} = \frac{\partial^2 F}{\partial r \partial z}\,, \end{gathered} \tag{3.9}$$

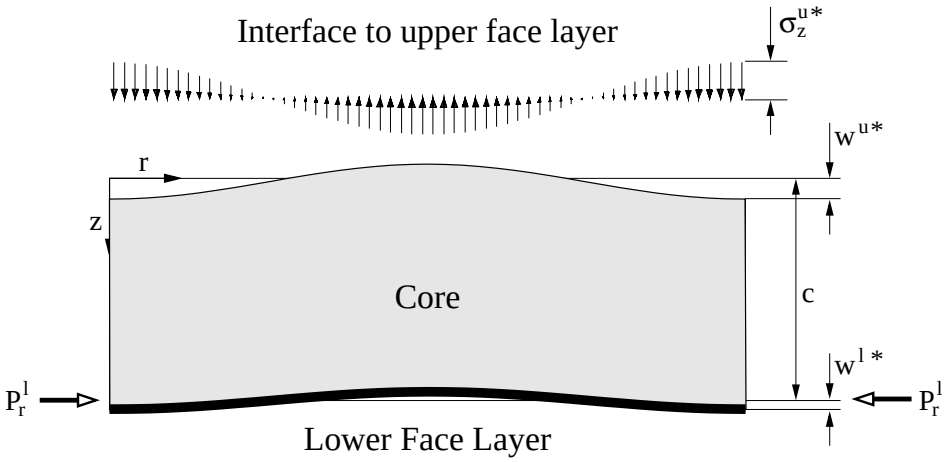

Figure 3.2: Loading and deflection of the foundation model

with the membrane stiffness terms:

$$D_r^c = E_r^{c\prime} \ , \quad D_{rz}^c = \frac{2E_r^{c\prime}G_{rz}^c}{-2\nu_{rz}^{c\prime}G_{rz}^c + E_r^{c\prime}} \ , \quad D_z^c = E_z^{c\prime} \ . \tag{3.10}$$

Using Airy's stress function the full 2D plane strain problem is solved, and the influence of the in-plane core stiffness $E_r^{c\prime}$ is included (in contrast to all other approaches, except Stiftinger and Rammerstorfer [1997]). This is of high importance when strongly orthotropic core materials, such as honeycombs, as well as isotropic cores are to be described in a unified theory. This topic is discussed in detail in section 4.4.

Airy's stress function is normally used to solve plane stress problems. In order to transform Airy's stress function equations from plane stress to plane strain, modified stiffness values (see e.g. Timoshenko and Goodier [1988]) may be used. These modified stiffness values of the core are marked with $'$ in eq. 3.10.

Core stiffness parameters

In sandwich construction, the z–axis is generally a material axis of the core which is also assumed here. The orientation of the material axes of the core in the xy-plane is defined by the angle ϑ (fig. 3.1) which is used together with φ to evaluate the core stiffness parameters ($E_r^{c\prime}$, $E_z^{c\prime}$, $\nu_{rz}^{c\prime}$, G_{rz}^c) which are needed in the rsz-coordinate frame. Starting from a fully

orthotropic core material law in its main coordinate frame

$$\begin{pmatrix} \varepsilon_{11} \\ \varepsilon_{22} \\ \varepsilon_{33} \\ \gamma_{12} \\ \gamma_{13} \\ \gamma_{23} \end{pmatrix} = \begin{pmatrix} C_{11} & C_{12} & C_{13} & 0 & 0 & 0 \\ C_{12} & C_{22} & C_{23} & 0 & 0 & 0 \\ C_{13} & C_{23} & C_{33} & 0 & 0 & 0 \\ 0 & 0 & 0 & C_{44} & 0 & 0 \\ 0 & 0 & 0 & 0 & C_{55} & 0 \\ 0 & 0 & 0 & 0 & 0 & C_{66} \end{pmatrix} \begin{pmatrix} \sigma_{11} \\ \sigma_{22} \\ \sigma_{33} \\ \sigma_{12} \\ \sigma_{13} \\ \sigma_{23} \end{pmatrix}, \tag{3.11}$$

a rotation of $\bar{\vartheta} = \varphi - \vartheta$ about the z–axis (3–axis) leads to the following material law in the rsz-coordinate frame:

$$\begin{pmatrix} \varepsilon_{rr} \\ \varepsilon_{ss} \\ \varepsilon_{zz} \\ \gamma_{rs} \\ \gamma_{rz} \\ \gamma_{sz} \end{pmatrix} = \begin{pmatrix} C_{rrrr}(\bar{\vartheta}) & C_{rrss}(\bar{\vartheta}) & C_{rrzz}(\bar{\vartheta}) & C_{rrrs}(\bar{\vartheta}) & 0 & 0 \\ C_{rrss}(\bar{\vartheta}) & C_{ssss}(\bar{\vartheta}) & C_{sszz}(\bar{\vartheta}) & C_{ssrs}(\bar{\vartheta}) & 0 & 0 \\ C_{rrzz}(\bar{\vartheta}) & C_{sszz}(\bar{\vartheta}) & C_{zzzz} & C_{zzrs}(\vartheta) & 0 & 0 \\ C_{rrrs}(\bar{\vartheta}) & C_{ssrs}(\bar{\vartheta}) & C_{zzrs}(\bar{\vartheta}) & C_{rsrs}(\bar{\vartheta}) & 0 & 0 \\ 0 & 0 & 0 & 0 & C_{rzrz}(\bar{\vartheta}) & C_{rzsz}(\bar{\vartheta}) \\ 0 & 0 & 0 & 0 & C_{rzsz}(\bar{\vartheta}) & C_{szsz}(\bar{\vartheta}) \end{pmatrix} \begin{pmatrix} \sigma_{rr} \\ \sigma_{ss} \\ \sigma_{zz} \\ \sigma_{rs} \\ \sigma_{rz} \\ \sigma_{sz} \end{pmatrix} \tag{3.12}$$

The wrinkling pattern is assumed to be constant in s–direction, leading to the kinematic plane strain conditions:

$$\gamma_{rs} = \gamma_{sz} = 0 \, . \tag{3.13}$$

The rotation of the orthotropic material law leads to the additional coupling terms $C_{rrrs}(\bar{\vartheta})$, $C_{ssrs}(\bar{\vartheta})$, $C_{zzrs}(\bar{\vartheta})$ and $C_{rzsz}(\bar{\vartheta})$ in eq. 3.12. Therefore, the use of the plane strain condition in combination with eq. 3.12 leads to additional stresses σ_{rs} and σ_{sz}. Within the framework of this theory (plane strain in the core), these stresses cannot be accounted for.

Equation eq. 3.12 shows that the material law can be split up into two uncoupled parts. The first four lines contain the new coupling terms $C_{rrrs}(\bar{\vartheta})$, $C_{ssrs}(\bar{\vartheta})$ and $C_{zzrs}(\bar{\vartheta})$ which originate from $C_{11} \neq C_{22}$ and $C_{13} \neq C_{23}$. The last two lines contain the new coupling term $C_{rzsz}(\varphi)$ which originates from $C_{55} \neq C_{66}$.

Thus, in the case of a transversely isotropic core material (xy–plane = 12–plane = plane of isotropy), the coupling terms vanish, and no error or inaccuracy is introduced into the calculation. A more general core material law than transversely isotropic induces systematic errors into the calculation presented here. It is not possible to estimate the magnitude of this error in a straightforward way, but the inaccuracy of the corresponding results can be shown to be small for common sandwich core materials (see section 5.4)

Thus, the derivation of the core stiffness parameters entering Airy's stress function (eq. 3.9) is defined. In order to solve eq. 3.9 the proper boundary conditions have to be defined.

Boundary conditions

Using the sinusoidal stress distribution given in eq. 3.7, the full solution of eq. 3.9 is

$$F = \sum_{i=1}^{4} C_i \left(\frac{a_r}{\pi}\right)^2 \exp\left(\frac{\mu_i \pi z}{a_r}\sqrt[4]{\frac{D_r^{\mathrm{c}}}{D_z^{\mathrm{c}}}}\right) \sin\left(\frac{\pi r}{a_r}\right) \tag{3.14}$$

with the following four coefficients

$$\mu_{1,3} = \pm\sqrt{\xi + \sqrt{\xi^2 - 1}}\,, \quad \mu_{2,4} = \pm\sqrt{\xi - \sqrt{\xi^2 - 1}}\,, \qquad \xi = \frac{\sqrt{D_r^{\mathrm{c}} D_z^{\mathrm{c}}}}{D_{rz}^{\mathrm{c}}}\,. \tag{3.15}$$

In order to calculate the four constants C_i, four boundary conditions have to be used. Two boundary conditions are imposed at the interface to the upper face layer ($z = 0$), one of which is defined in eq. 3.7. The second one is derived from the common sandwich approximation that the strains in the core in r–direction are set to zero. This assumption is based on the fact that the facing material is much stiffer than the core material, thus restraining core deformation. This leads to the second boundary condition:

$$\varepsilon_r^{\mathrm{c}} = \frac{1}{E_r^{\mathrm{c}\prime}}\left(\sigma_r^{\mathrm{c}} - \nu_{rz}^{\mathrm{c}\prime}\sigma_z^{\mathrm{c}}\right) = 0 \quad \text{at } z{=}0. \tag{3.16}$$

The remaining two boundary conditions are defined analogously at the interface between the lower face layer and the core which is located at $z{=}c$:

$$\sigma_z^{\mathrm{l}} = \sigma_z^{\mathrm{c}}(z{=}c) = \sigma_z^{\mathrm{l}*} \sin\left(\frac{\pi r}{a_r}\right)\,, \tag{3.17}$$

$$\varepsilon_r^{\mathrm{c}} = \frac{1}{E_r^{\mathrm{c}\prime}}\left(\sigma_r^{\mathrm{c}} - \nu_{rz}^{\mathrm{c}\prime}\sigma_z^{\mathrm{c}}\right) = 0 \quad \text{at } z{=}c. \tag{3.18}$$

These four boundary conditions lead to the four constants C_i:

$$\begin{aligned} C_1 &= \frac{\left(\mathcal{A}\,\sigma_z^{\mathrm{l}*} - \sigma_z^{\mathrm{u}*}\right) X_3}{-1 + \mathcal{A}^2} & C_3 &= \frac{\mathcal{A}\left(-\sigma_z^{\mathrm{l}*} + \mathcal{B}\,\sigma_z^{\mathrm{u}*}\right) X_3}{-1 + \mathcal{A}^2} \\ C_2 &= -\frac{\left(\mathcal{B}\,\sigma_z^{\mathrm{l}*} - \sigma_z^{\mathrm{u}*}\right) X_4}{-1 + \mathcal{B}^2} & C_4 &= -\frac{\mathcal{B}\left(-\sigma_z^{\mathrm{l}*} + \mathcal{B}\,\sigma_z^{\mathrm{u}*}\right) X_4}{-1 + \mathcal{B}^2} \end{aligned} \tag{3.19}$$

with

$$X_3 = \frac{\mu_2^2 + \nu_{rz}^{c\prime}\sqrt{\frac{D_z^c}{D_r^c}}}{\mu_1^2 - \mu_2^2} \qquad X_4 = \frac{\mu_1^2 + \nu_{rz}^{c\prime}\sqrt{\frac{D_z^c}{D_r^c}}}{\mu_1^2 - \mu_2^2}$$
$$\mathcal{A} = \exp\left(\frac{c}{a}\mu_1\pi\sqrt[4]{\frac{D_r^c}{D_z^c}}\right) \qquad \mathcal{B} = \exp\left(\frac{c}{a}\mu_2\pi\sqrt[4]{\frac{D_r^c}{D_z^c}}\right) \tag{3.20}$$

At this stage, the stress and strain fields in the core are known as functions of a_r, φ, the upper interface stress amplitude σ_z^{u*}, and the lower interface stress amplitude σ_z^{l*}. The upper interface stress amplitude represents the loading at which the deflections have to be calculated to solve eq. 3.6. The lower interface stress amplitude leads to a deformation of the lower face layer. This is calculated using the constitutive equation for the lower face layer.

3.2.2.2 Lower face layer

The lower face layer is modeled exactly the same way as the upper face layer, i.e. using the differential equation of a thin elastic plate on an elastic foundation, which is again reduced to the form equivalent to eq. 3.3:

$$B_r^l(\varphi,\gamma)\frac{\partial^4 w^l}{\partial r^4} + P_r^l(\varphi)\frac{\partial^2 w^l}{\partial r^2} + \sigma_z^{l*}\sin\left(\frac{\pi r}{a_r}\right) = 0\ . \tag{3.21}$$

The orientation of the material axes of the lower face layer with respect to the xyz–coordinate frame is defined by the angle γ (fig. 3.1) which is used together with φ to calculate the beam bending stiffness in r–direction (B_r^l). The loading $P_r^l(\varphi)$ is formulated relative to the same global loading parameter P as in the case of the upper face layer (analogous to eq. 3.4).

3.2.2.3 Foundation stiffness

The stresses and strains in the core and the lower face layer are now defined in dependence on a_r, φ, σ_z^{u*}, and σ_z^{l*}. However, given a_r, φ and σ_z^{u*}, i.e. a given load distribution, will always results in a certain σ_z^{l*}, which is nothing but a stress value in the interior of the foundation. Thus, σ_z^{l*} can be calculated by minimizing the strain energy of the foundation (i.e. core and lower face layer).

The calculation and minimization of the strain energy of the core and the lower face layer with respect to σ_z^{l*} is a basic but arduous procedure. Since the results are long and

cumbersome equations, they will not be given here. The minimization of the strain energy leads to σ_z^{l*}, which is proportional to σ_z^{u*} and depends on the free parameters a_r and φ as well as on the geometric, material and load input parameters of the core and the lower face layer.

Using this result, the strains in the core in z–direction can be calculated and integrated over the core thickness, which gives the deflection of the core. Together with the resulting deflection of the lower face layer w^l (calculated from eq. 3.21), the total deflection of the foundation under a given load σ_z^{u*} is derived as (see fig. 3.2)

$$w^u = \int_c^0 \varepsilon_z^c \, dz \; + \; w^l = -\sigma_z^u \, H(a_r, \varphi) = -\sigma_z^{u*} \, H(a_r, \varphi) \, \sin\left(\frac{\pi r}{a_r}\right) \; . \tag{3.22}$$

Regarding eq. 3.6, the foundation stiffness k^{thin} is equal to the lengthy but simple explicit function $1/H(a_r, \varphi)$, which also depends on the material, geometry and loading parameters of the core and the lower face.

3.2.3 Wrinkling load

Inserting the result for k^{thin} into eq. 3.5, and solving the resulting equation for a non-trivial equilibrium ($w^u \neq 0$) leads to a quadratic equation for the critical load level P as a function of a_r and φ. Thus, for each combination of wavelength a_r and wave angle φ two load levels $P_{1,2}$ are calculated, the smaller one being decisive.

The reason for the two results for P is, that the load level enters the model in the equation for the upper and the lower face layer (via eq. 3.5 and k^{thin}, respectively). Regarding very thick sandwiches, where the upper and the lower face layer are uncoupled, it is obvious that there have to be two possible load levels P with the same wavelength a_r and wave angle φ, one corresponding to the buckling of each face layer. These two solutions have different deformation patterns in the sense that the amplitude of the deformation $w^*(z)$ varies differently throughout the core thickness while a_r and φ are identical. In the case of thin cores, the two solutions have been observed to correspond to an hourglass mode and a snake mode solution, respectively, at a given a_r and φ. However, this is not always the case.

It is an important aspect of this solution that the resulting load levels are independent of the choice which of the two face layers is taken as the upper face layer. Regarding the derivation it becomes clear that, although the "face layer on a foundation" approach is used, both face layers are modeled the same way using equivalent boundary conditions.

Therefore, the solution is symmetric in the sense that the solution is independent of whether a given face layer is the upper or the lower face.

In order to calculate the critical load level P^{cr} at which wrinkling will occur, $P(a_r, \varphi)$ has to be minimized with respect to a_r and φ. This minimization has to be done numerically.

3.2.4 Numerical minimization

Two different methods have been employed to minimize $P(a_r, \varphi)$ with respect to a_r and φ. In the rather simple case of isotropic symmetric sandwiches it is sufficient to use a local search algorithm. In this case, only two local minima of $P(a_r, \varphi)$ exist and both of them are easily found by calculating estimates for the starting points and using a sequential quadratic programming algorithm. Fig. 3.3 shows the value of P as a function of a_r and φ in this simple case.

However, in the case of orthotropic sandwiches with different loading and material parameters for the two face layers, the situation is more complex. Fig. 3.4 shows the value of P as a function of a_r and φ in such a case. There are several local minima of $P(a_r, \varphi)$ in vicinity of each other. Although considerable effort was put into the calculation of appropriate starting values for different local search algorithms, it was not possible to obtain all local minima by this method, and thus the global minimum was not always found using this approach.

An example of these results is displayed in fig. 3.5 which shows the critical load level as a function of the core thickness for an unsymmetric orthotropic sandwich. The dashed line represents the results of the local search algorithm and the saw teeth show that the local algorithm is sometimes not able to find the global minimum.

Consequently, a stochastic global optimization code based on Boender et al. [1982] and Csendes [1988] is employed. This routine calculates the value of $P(a_r, \varphi)$ at a number of different stochastic values of a_r and φ and starts a local search algorithm from the lowest values of P found so far. This global and local search is repeated until no new local minimum is found. Moreover a clustering algorithm prevents the code from evaluating the same minimum too often. Using a logarithmic scale for a_r (as in fig. 3.4), the use of this algorithm for finding all local minima and thus the global minimum of $P(a_r, \varphi)$ proved to be robust and reliable. The computational effort is kept to about 1000 evaluations of the explicit function $P(a_r, \varphi)$ to find all minima. Correspondingly, the computing time needed is relatively low. Besides, the different local minima found by this code can all be

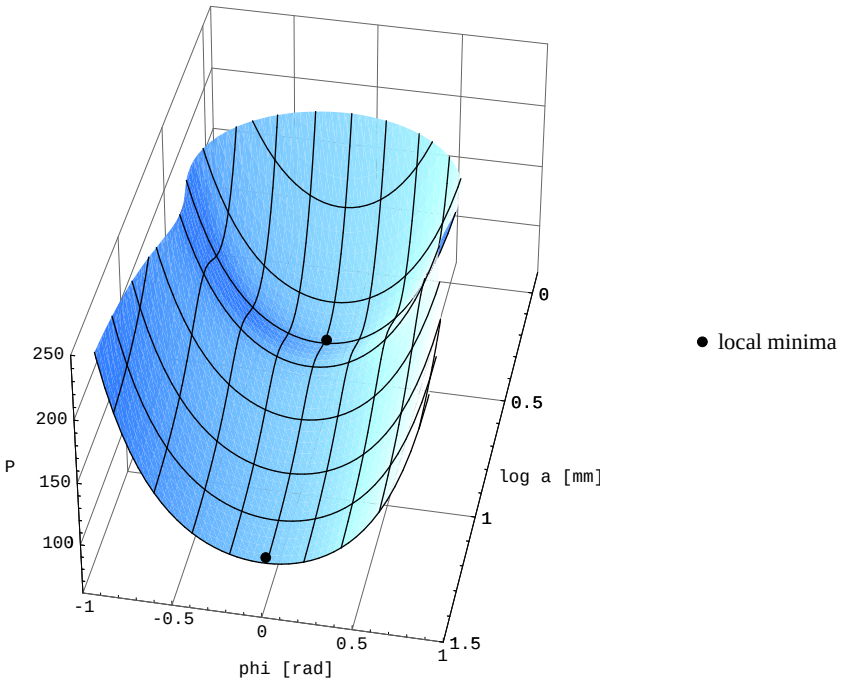

Figure 3.3: Load level P as a function of a_r and φ, symmetric isotropic sandwich

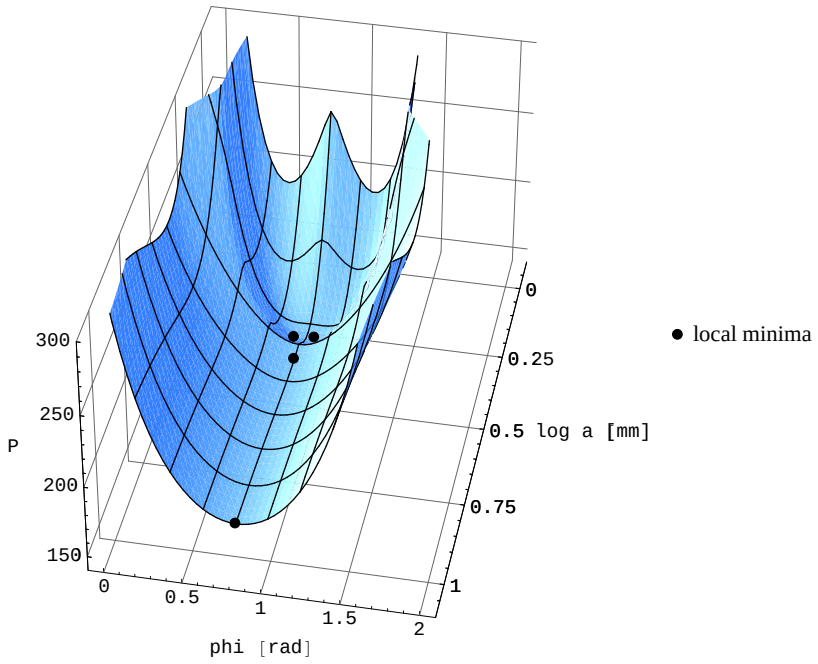

Figure 3.4: Load level P as a function of a_r and φ, unsymmetric orthotropic sandwich

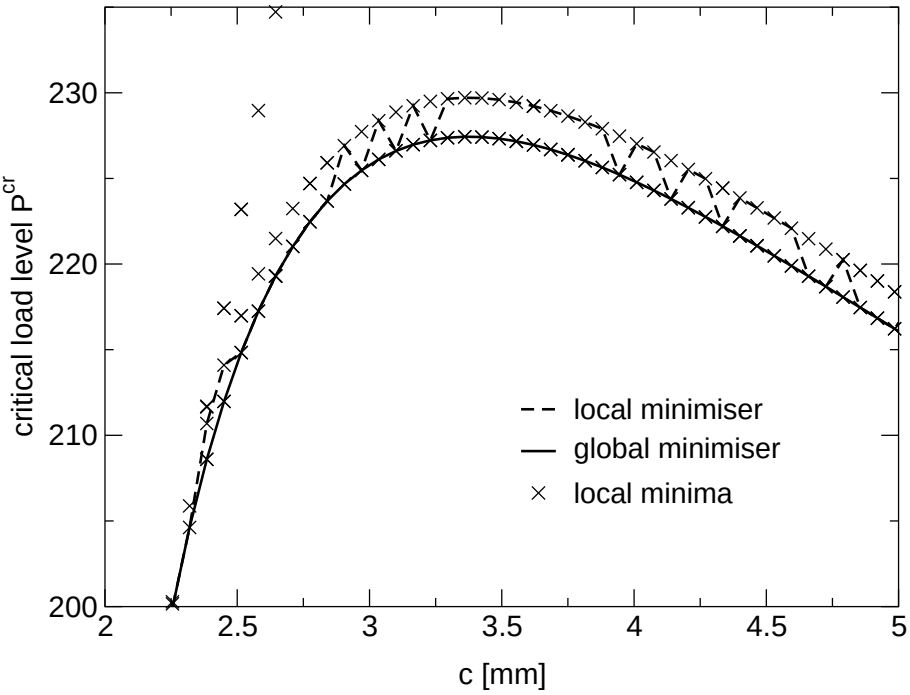

Figure 3.5: Global and local optimization results

related to buckling patterns such as an hourglass mode, a snake mode and shear crimping in different directions (see e.g. section 5.5).

It is interesting to note that the result of $P(a_r \to \infty)$, which is not a minimum in the strict sense but an asymptotic point, corresponds to the shear crimping load given in eq. 2.2. This coincidence cannot be explained mechanically. Since this approach has been set up to investigate the local phenomenon of wrinkling under the assumption that the wavelength a_r is much smaller than the overall dimensions of the sandwich, a result for an infinite wavelength a_r is not within the scope of this approach. However, from the mathematical point of view it can be stated that the strain energy due to bending of the faces and the core vanishes compared to the strain energy due to shear deformation of the core as a_r approaches infinity. Since the shear crimping load is independent of the wavelength a_r and the buckling shape, the case $a_r \to \infty$ represents the case of pure shear crimping of the core. This shear crimping load is regarded as a conservative estimate for a *local* failure load, since $a_r < \infty$ leads to a higher critical load. It is obvious, that for a *global* failure mode the interaction with Euler buckling has to be considered (see section 2.1), but this is not within the scope of this contribution. It is assumed, that the global

failure modes are checked separately (e.g. by FE sandwich shell analysis).

3.3 Simplifications

By making use of the "thick core" assumption (which is very limiting), the analytical derivation is simplified markedly. The resulting formulas for the critical wrinkling load are much easier to use and are given in the following. The simplification in handling the formulas is mainly due to the fact that the numerical optimization is strongly simplified or eliminated.

3.3.1 Thick transversely isotropic core, orthotropic face

In the case of thick transversely isotropic cores and orthotropic face layers, the derivation is identical to the general one up to eq. 3.16, but the other two boundary conditions for the core are that all core stresses vanish as the core thickness c approaches infinity. These conditions immediately lead to $C_1 = C_2 = 0$. The remaining constants can be split into the boundary stress amplitude σ_z^{u*} and the dimensionless factors X_3 and X_4 defined in eq. 3.20

$$C_3 = \sigma_z^{u*} X_3, \quad C_4 = -\sigma_z^{u*} X_4 \; . \tag{3.23}$$

The stresses in the core are now fully determined, the lower face layer being of no influence. The strains in the core and, therefore, the amplitude of the transverse displacements w^{u*} at the interface can be calculated:

$$w^{u*} = \int_{\infty}^{0} \varepsilon_z^c \, \mathrm{d}z = -\sigma_z^{u*} \frac{a_r}{\pi} \left[\left(\frac{X_3}{\mu_1} - \frac{X_4}{\mu_2} \right) + \nu_{zr}^{c\prime} \left(X_3 \mu_1 - X_4 \mu_2 \right) \sqrt{\frac{E_x^{c\prime}}{E_z^{c\prime}}} \right] \frac{1}{E_z^{c\prime}} \sqrt[4]{\frac{E_z^{c\prime}}{E_x^{c\prime}}}$$

$$\stackrel{\text{eq.3.6}}{=} -\sigma_z^{u*} (k^{\text{thick}})^{-1} \tag{3.24}$$

This equation defines the foundation stiffness for thick cores k^{thick} depending on the wavelength a_r. The core stiffness k^{thick} is now split into $\bar{k}^{\text{thick}}$, which is independent of a_r, and (a_r/π)

$$k^{\text{thick}} = \frac{\pi}{a_r} \bar{k}^{\text{thick}} \; . \tag{3.25}$$

Since the core is taken to be transversely isotropic, the core stiffness is independent of the wave angle φ, and only the constant core stiffness $E_x^{c\prime} = E_y^{c\prime} = E_r^{c\prime}$ enters k^{thick} (and not $E_r^{c\prime}(\varphi)$, as in the case of orthotropic cores). k^{thick} is, analogous to k^{thin} in the previous

section, inserted into eq. 3.5. The load level P^{thick} depending on a_r and φ can now be calculated in the global coordinate system:

$$P^{\text{thick}}(a_r,\varphi) = \frac{\left(\frac{\pi}{a_r}\right)^2 \left(B_x^{\text{u}} \cos^4\varphi + 2B_{xy}^{\text{u}} \cos^2\varphi \sin^2\varphi + B_y^{\text{u}} \sin^4\varphi\right) + \frac{a_r}{\pi}\bar{k}^{\text{thick}}}{\rho^{\text{u}} \cos^2\varphi + 2\zeta^{\text{u}} \sin\varphi\cos\varphi + \xi^{\text{u}} \sin^2\varphi} = \frac{U}{V} \quad (3.26)$$

To derive the critical load level, P^{thick} has to be minimized with respect to the two unknown variables a_r and φ. The minimization is done analytically and leads to the following two equations:

$$a_r^3 = \frac{2\pi^3}{\bar{k}^{\text{thick}}} \left(B_x^{\text{u}} \cos^4\varphi + 2B_{xy}^{\text{u}} \cos^2\varphi \sin^2\varphi + B_y^{\text{u}} \sin^4\varphi\right) \ , \quad (3.27)$$

$$\frac{\left(\frac{\pi}{a_r}\right)^2 4\sin\varphi\cos\varphi \left[-B_x^{\text{u}} \cos^2\varphi + B_{xy}^{\text{u}} \cos(2\varphi) + B_y^{\text{u}} \sin^2\varphi\right] V}{\left(\rho^{\text{u}} \cos^2\varphi + 2\zeta \sin\varphi\cos\varphi + \xi \sin^2\varphi\right)^2} -$$

$$\frac{\left(-\rho^{\text{u}} \sin\varphi\cos\varphi + \zeta\cos(2\varphi) + \xi \sin\varphi\cos\varphi\right) U}{\left(\rho^{\text{u}} \cos^2\varphi + 2\zeta \sin\varphi\cos\varphi + \xi \sin^2\varphi\right)^2} = 0 \ . \quad (3.28)$$

Inserting eq. 3.27 into eq. 3.28, a single implicit equation for φ as a function of the stiffness and loading parameters is derived, which has to be solved numerically. However, the numerical effort is very low, since $0 \leq \varphi < 180°$, and an accuracy in φ of about $1°$ tends to lead to sufficiently accurate solutions.

Inserting φ back into eq. 3.27 and eq. 3.26, a_r and the critical load level $P^{\text{cr,thick}}$ leading to wrinkling failure are easily calculated. In contrast to the approaches mentioned in the literature chapter, this method includes the influence of the in-plane core stiffness $E_x^{\text{c}\prime}$ as well as face layer orthotropy and general loading.

3.3.2 Thick core, isotropic faces

Simplifying the problem further by assuming isotropic face layers, wrinkling will always take place in the direction of the major compressive membrane force in the face layer (i.e. in the direction φ which leads to a maximum of $P_r(\varphi)$). Since the wrinkling direction is known *a priori*, φ is eliminated from the problem. The r–direction is now defined as the direction of the major compressive membrane force in the face layer P_r.

Simplifying eqs. 3.26 and 3.27 an explicit formula for the critical wavelength a_r^{cr} and the critical compressive section force $P_r^{\mathrm{cr,thick}}$ leading to wrinkling is obtained:

$$a_r^{cr} = \sqrt[3]{2\,B^{\mathrm{u}}\,\frac{\pi^3}{\bar{k}^{\mathrm{thick}}}}\,, \tag{3.29}$$

$$P_r^{\mathrm{cr,thick}} = \left(\sqrt[3]{2} + \sqrt[3]{\frac{1}{4}}\right)\sqrt[3]{B^{\mathrm{u}}\left(\bar{k}^{\mathrm{thick}}\right)^2} \quad \overset{\nu^{\mathrm{u}}=0.3}{\Longrightarrow} \quad 0.85\,t^{\mathrm{u}}\,\sqrt[3]{E^{\mathrm{u}}\left(\bar{k}^{\mathrm{thick}}\right)^2}\,. \tag{3.30}$$

This equation is similar to the classical approach for thick cores (eq. 2.9), but includes the influence of the in-plane core stiffness, which is disregarded in the classical approach.

3.4 Computer implementation

The three new approaches for the critical load level leading to wrinkling derived in this chapter have been coded in double precision FORTRAN and implemented together with the approach of Stiftinger and Rammerstorfer [1997] and the classical wrinkling and buckling formulas into the program 'wrinklwizard'. This program is able to calculate the critical load level of sandwich configurations for all the approaches mentioned above. The new approaches are formulated for plane stress in the core (i.e. the modification of the stiffness values mentioned in section 3.2.2 is not performed), since the classical approaches are also formulated for plane stress. This leads to comparable results, and plain strain in the core can simply be achieved by modifying the core stiffness values in the input file, which leads to plane strain in the new as well as in the classical models.

The implementation of the model is rather simple when using an optimisation code which is already available. However, the numerical problems encountered are described in the following.

Considering the formulation of the model, it can be shown that the case of $P_r^{\mathrm{l}} = 0$ or $P_r^{\mathrm{u}} = 0$ and the case of an isotropic core lead to numerical problems in the sense that certain terms (e.g. X_3 and X_4) are infinite and the results depend on a subtraction or a division of these terms. Therefore, in these cases a small perturbation is introduced. This procedure proved to lead to accurate and reliable results.

If the new model for thin cores is used with rising core thickness values, the result converges to the result of the new model for thick cores, as expected. However, if the core thickness input value c is very large, another numerical problem, similar to the above, is encountered. Namely, two large almost identical numbers are subtraced from each other,

the resulting number being decisive for the calculation of the critical load level. This problem was circumvented by checking for the size of the involved numbers and, in the case of a critical constellation, an alteration of the core thickness to a smaller value will be performed. This problem has only been encountered at core thickness values which are beyond the core thickness which is leading to two uncoupled problems which have already converged to the valid result for thick cores. Nevertheless, an additional routine is implemented which checks this convergence. In the case of a single precision implementation this behavior might lead to more severe problems.

Chapter 4

Results for sandwich beams

This chapter presents findings and numerical results which have been obtained in the course of studying sandwich beam problems. These problems are only two dimensional, and thus the direction of wrinkling (r-direction) is known *a priori* to be the x-direction. Even in these simple cases it is shown that the existing models may lead to severe errors because they disregard the in-plane core stiffness on the one hand and interaction effects in bending on the other hand.

The results are derived from the analytical models described in chapter 3 and additionally the results from different verification models are displayed. For the sake of convenience, the deformation patterns displayed within this chapter are mostly taken from FE models. It is emphasized here, that these deformation patterns have been checked to be practically identical to the deformation patterns obtained by the analytical model, unless stated otherwise. The reason for using the FE results for deformation plots is simply the readily available visualization software.

4.1 Verification models

The new analytical approach has been verified by different analytical and FE models. In the following, these different verification models are introduced.

4.1.1 Analytical models

For verification purposes, the new approach has been compared to the classical analytical approaches shown in section 2.2.2 and 2.2.3 and to the model of Stiftinger and Rammerstorfer [1997], which is in the following refered to as "Stiftinger model". When compensating for the fact that the classical models assume plane stress in the core and the Stiftinger model uses a full 3D core solution which is rather equivalent to plane strain in the core, the different models show good agreement. Naturally, this is limited to the regions of applicability of the different models. Unfortunately, it turns out, that these regions of applicability often cannot be determined *a priori*. Only the new model and the Stiftinger model use a core material law which takes the in-plane core stiffness explicitly into account, all other analytical models assume either an infinite or a zero in-plane core stiffness.

4.1.2 2D FE foundation model

In order to verify the stress distribution in the core and the foundation behavior, 2D FE models are used. The FE method has also been employed by other authors [e.g. Hadi, 2001; Stiftinger and Rammerstorfer, 1997], but these authors have modeled the whole sandwich beam and extracted the corresponding buckling modes and eigenvalues. In contrast to this, only the foundation (i.e. the core and the lower face layer) is modeled here, corresponding to the mechanical model shown in fig. 3.2. The core is represented by 2D plain strain elements and the lower face by planar beams. The upper face layer is not modeled, but the appropriate boundary condition (eq. 3.16) is enforced and the model is loaded by the sinusoidal interface stress distribution originating from the upper face layer (eq. 3.7). Just like fig. 3.2, the model consists of one wavelength in the direction of the beam axis. The edges at $z = 0$ and $z = c$ are restrained from movement in x-direction (symmetry condition). To be able to capture the effect of loading of the lower face layer on the foundation stiffness, the analysis has to be performed non-linearily. The results of the FE calculations agree very well with the analytical results in all cases that have been studied, which was to be expected due to the similarity of the models.

4.2 Foundation behavior

4.2.1 Influence of loading

It has proven to give insight into the mechanics of wrinkling to analyze the foundation behavior alone, which is a static stress problem, at a first stage before dealing with the stability problem of wrinkling. This is mainly due to the fact that the new analytical model uses a refined foundation formulation as compared to other existing analytical models, whereas the face layer description is – in the case of sandwich beams – identical to the other analytical models available. The main difference to other foundation approaches in different fields of mechanics is that the foundation is of finite thickness and includes a second part, namely the lower face layer, which is carrying an external load. The influence of this external load P_x^{l} on the foundation behavior is now investigated. The corresponding results are shown in fig. 4.1 for a sandwich beam at fixed wavelength ($a_x = 12.83\mathrm{mm}$) having a moderately orthotropic core ($E_x^{\mathrm{c}} = 20\mathrm{N/mm}^2$, $E_z^{\mathrm{c}} = 120\mathrm{N/mm}^2$, $G_{xz}^{\mathrm{c}} = 43\mathrm{N/mm}^2$, $\nu_{xz}^{\mathrm{c}} = 0.395$) with aluminium face layers ($E = 70000\mathrm{N/mm}^2$, $\nu = 0.3$) and the geometric values $c = 5\mathrm{mm}$ and $t = 1\mathrm{mm}$. The wavelength corresponds to the critical wavelength of the corresponding symmetric sandwich beam under pure compression ($P_x^{\mathrm{l}} = P_x^{\mathrm{u}}$).

The foundation stiffness $k^{\mathrm{thin}}(P_x^{\mathrm{l}})$ has been normalized with the foundation stiffness at an unloaded face layer $k^{\mathrm{thin}}(P_x^{\mathrm{l}} = 0)$ and the normal stress at the lower core–face layer interface is given as a fraction of the normal stress at the upper core–face layer interface (which is the loading of the foundation model). The configuration has been chosen in such a way that a snake mode is active.

It is shown in fig. 4.1, that the foundation stiffness decreases as the compressive force in the lower face layer is rising. This was to be expected due to the destabilizing effect of compressive forces on the global foundation behavior. At a certain value of the compressive force (marked by Y), the foundation stiffness is zero. This marks the critical compressive force in the lower face layer which leads to the instability of the foundation itself, i.e. if no upper face layer is present, the foundation itself buckles due to the force P_r^{l} acting on the lower face layer. At compressive loads exceeding Y, the foundation stiffness turns negative which means that these regions can only be reached if the foundation is stiffened (supported) by the upper face layer. A further increase of P_r^{l} eventually leads to the point where the foundation stiffness approaches minus infinity. This is the value of P_r^{l} which leads to wrinkling even in the case of a rigid upper face layer. Results beyond this point are obviously of no further interest.

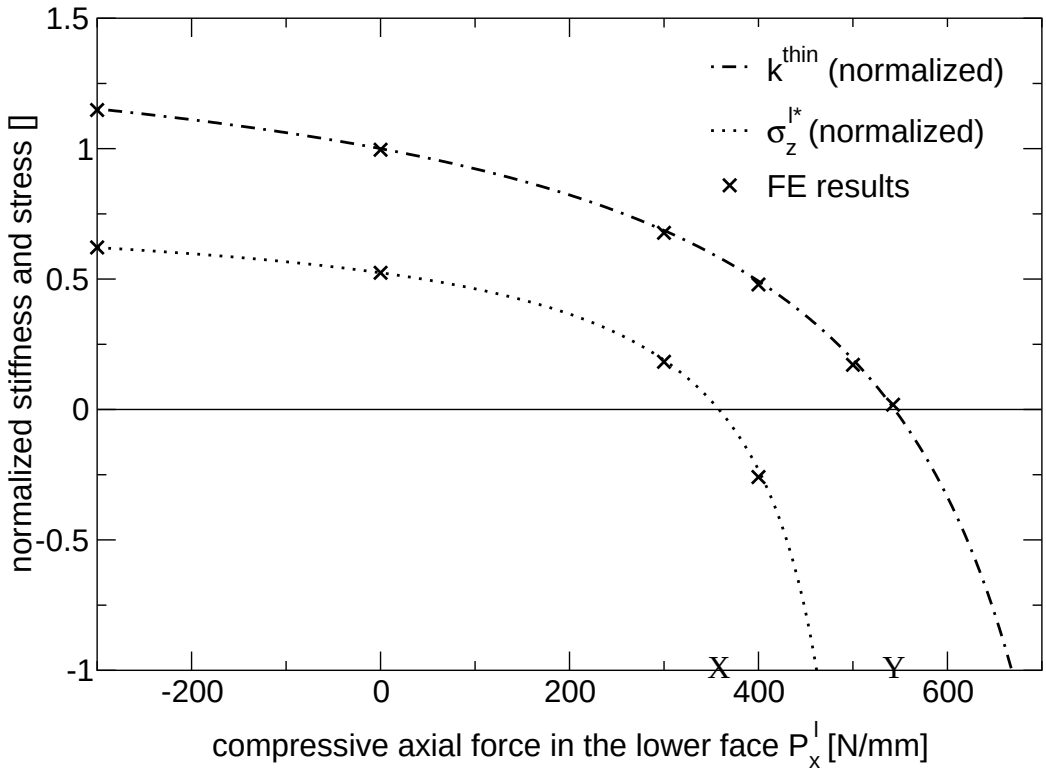

Figure 4.1: Foundation stiffness and stresses, snake mode

In order to capture the influence of the lower face layer alone, the stress amplitude at the lower core–face layer interface σ_z^{l*} is also displayed. Qualitatively, the results are very similar to the results for the foundation stiffness described above. If the lower face layer is not loaded, it is supporting the core via the stresses at the lower interface. These stresses, which are stiffening the system, vanish as the compressive force reaches a certain level (marked with X). At this point the lower face layer is loaded with a compressive force which is exactly the buckling load of the unsupported lower face layer at the given wavelength a_x. Therefore, the lower face layer has zero transversal stiffness in this state leading to zero stresses in the interface (analogous to the point Y regarding the whole foundation). If the compressive loading is further increased, the buckling load of the lower face layer is exceeded and the lower face layer is not deformation driven any more, but driving the deformations, thus softening the foundation. Therefore, the interface stresses have changed sign. The whole foundation is still stable, since the core is stiff enough to support the lower face layer (region between X and Y). As the load reaches the instability point of the foundation itself (Y), the interface stresses approach infinity. This is due to

the foundation stiffness being zero as explained above. Beyond Y, the interface stresses have changed sign and are finite again.

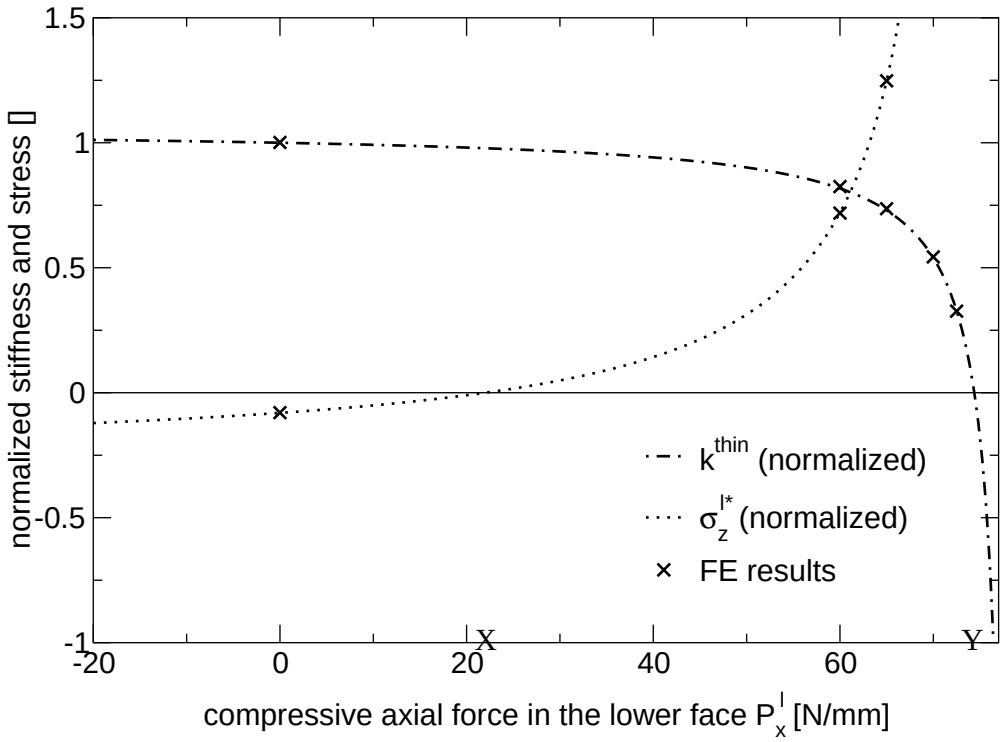

Figure 4.2: Foundation stiffness and stresses, hourglass mode

In the case of a sandwich configuration which is wrinkling in hourglass mode, the results look similar, but the sign of the lower interface stresses is reversed due to the reversed mode shape of the lower face layer. A corresponding result is shown in fig. 4.2 ($E_x^c = 1\text{N/mm}^2$, $E_z^c = 310\text{N/mm}^2$, $G_{xz}^c = 110\text{N/mm}^2$, $\nu_{xz}^c = 0$) at fixed wavelength ($a_x = 1.7\text{mm}$) with aluminium face layers ($E = 70000\text{N/mm}^2$, $\nu = 0.3$) and the geometric values $c = 6\text{mm}$ and $t = 0.1\text{mm}$.

It is again emphasized, that the wrinkling concept presented here, which is based on this foundation approach, is independent of the choice which of the face layers is taken to be the upper or the lower face layer. This is due to the fact that the foundation results are valid in the whole parameter range even for values of P_x^l beyond Y. The agreement between the analytical model and 2D FE results is excellent.

4.2.2 Core stress distribution

The analytically and numerically (2D FE model) calculated stress fields in the core are compared in fig. 4.3. The stress values are normalized for a deformation amplitude $w^{u*} = 1\text{mm}$ at the interface to the upper face layer. Therefore, the absolute values are not of any relevance. In the case presented, a very thick sandwich with aluminium face layers ($t = 0.1\text{mm}$) and a transversely isotropic honeycomb core ($E_x^c = 1\text{N/mm}^2$, $E_z^c = 41\text{N/mm}^2$, $G_{xz}^c = 10.3\text{N/mm}^2$, $\nu_{xz}^c = 0$) was analyzed.

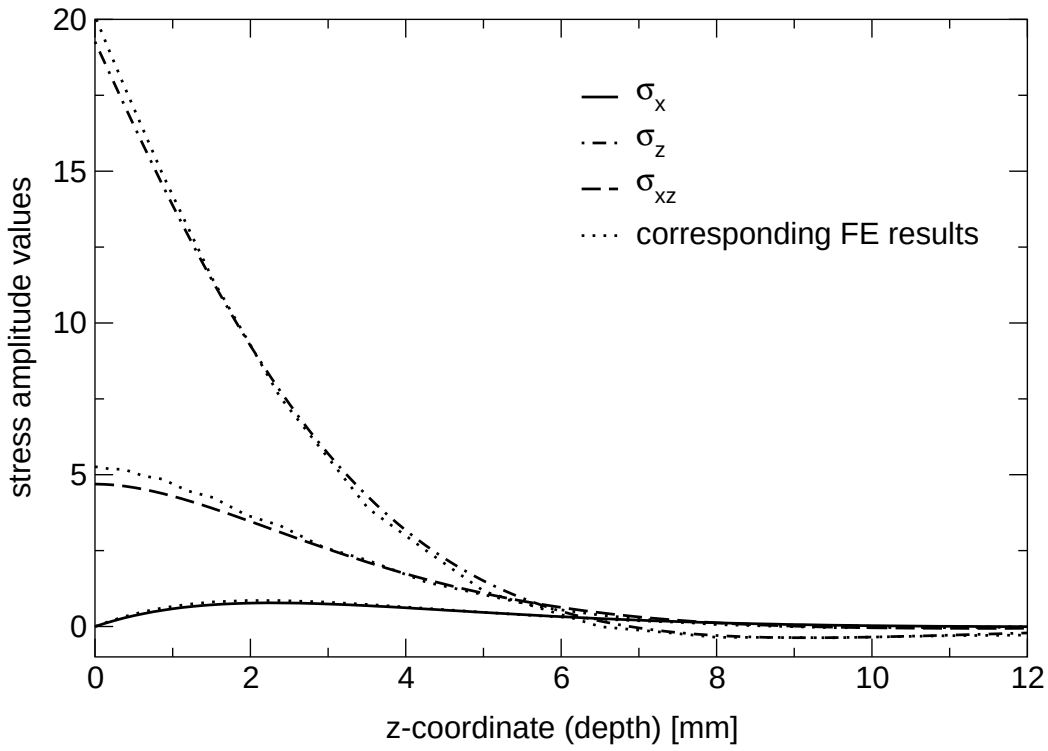

Figure 4.3: Core stresses: analytical and FE results

The analytically and numerically calculated core stresses agree very well, which was also found in the case of the limited number of other configurations investigated, including isotropic core materials.

4.3 Compression of symmetric sandwich beams

The simplest sandwich configurations which lead to wrinkling are symmetric sandwich beams under pure compressive loading. However, when looking more closely at the results even these simple configurations give rise to phenomena which have not been sufficiently investigated yet.

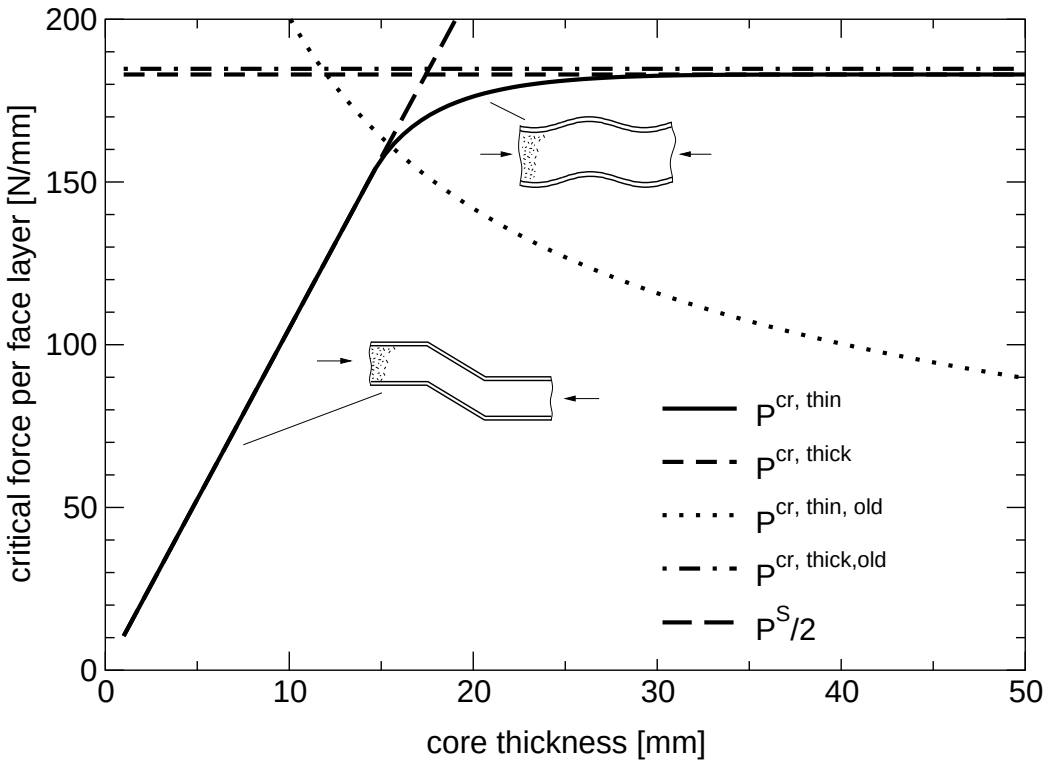

Figure 4.4: Critical load over core thickness, isotropic core

Fig. 4.4 shows the wrinkling load of a sandwich beam with aluminium face layers ($E = 70000\text{N/mm}^2$, $\nu = 0.3$, $t = 0.5\text{mm}$) and a nearly isotropic foam core (AIREX R63.80: $E = 56\text{N/mm}^2$, $\nu = 0.33$, $G = 21\text{N/mm}^2$) over the core thickness. At low core thickness values, the critical load corresponds to the shear crimping load $P^{\text{S}}/2$ as explained in section 3.2.4. Since P^{S} is defined as a beam section force (eq. 2.2) and the wrinkling loads are defined as section forces in the individual face layer, $P^{\text{S}}/2$ has to be compared to them in this case of equal section forces in both face layers. After a relatively short intermediate regime of the core thickness, the thickness is sufficiently high to preclude interaction between the two face layers and the critical load is independent of the core

thickness. This behavior can easily be recalculated via the two basic formulas of the "old" model for thick cores and the shear crimping formula, both of which agree very well with the new models (apart from the interaction region). The only mode change taking place in fig. 4.4 is the one from shear crimping to a snake mode. It has been observed within this study that isotropic cores always lead to a snake mode, and never to an hourglass mode. The "old" model for thin cores, which is based on an hourglass mode, therefore does not lead to satisfactory results - a fact which is unfortunately not communicated in the standard literature on sandwich construction.

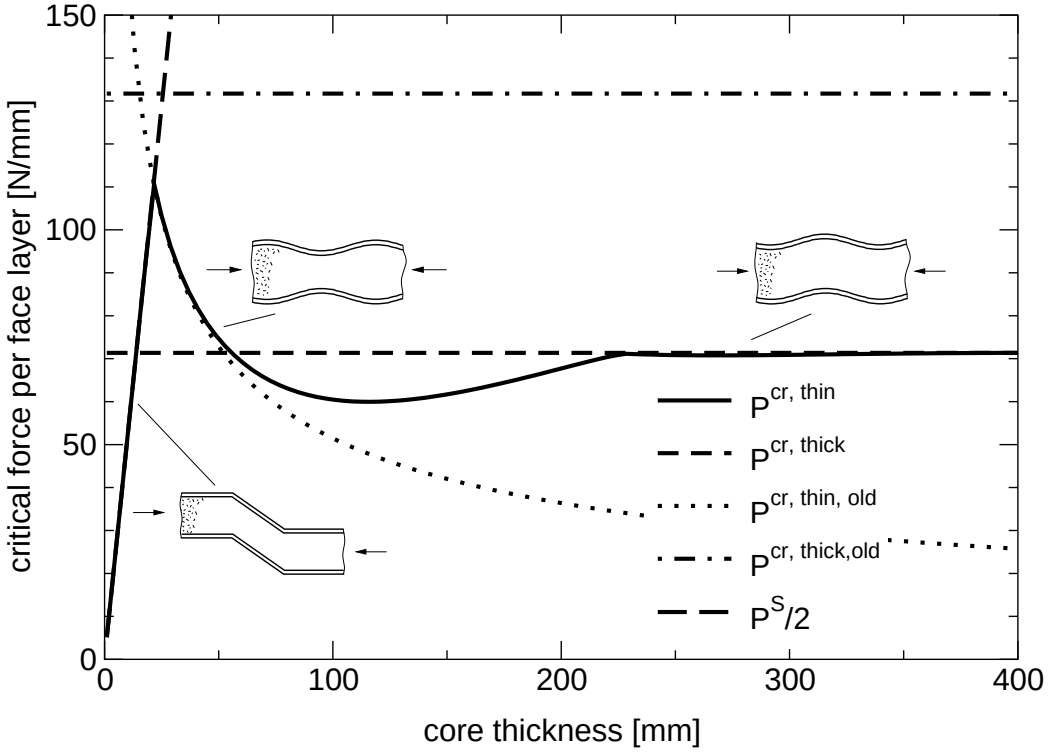

Figure 4.5: Critical load over core thickness, NOMEX honeycomb core

The situation is quite different if the same sandwich beam is studied with an highly orthotropic core (HEXCEL NOMEX HRH-10-3/16-1.5: $E_z^c = 41.3\text{N/mm}^2$, $E_x^c = 0.02\text{N/mm}^2$, $G_{xz}^c = 10.3\text{N/mm}^2$, $\nu_{xz}^c = 0$), see fig. 4.5. In this case, both snake and hourglass modes are observed (as also reported in Stiftinger and Rammerstorfer [1997]). Starting from low core thickness values, where shear crimping is always critical, the critical deformation pattern switches at first to an hourglass mode, then to a snake mode, and finally at very high core thickness values the interaction between the face layers vanishes and the hourglass and

snake modes are equivalent. In this case, the "old" model for thin cores gives a good estimate of the critical load within a certain range of the core thickness c, as it is based on the correct mode type. This agreement is excellent in the case of thin cores (shear crimping has to be checked for separately). With rising core thickness, the agreement deteriorates. The "old" model for thick cores does not lead to acceptable results in any part of the parameter range investigated here. Even in the case of very thick cores, this classical approach fails for this simple sandwich configuration.

It is now, of course, of interest what the reasons for this fundamentally different behavior of the two sandwich beams having an isotropic and a highly orthotropic core are. Phenomenologically, the difference is based on the different in-plane core stiffness value E_x^c. A thorough investigation into the effects taking place is given in the following section.

4.4 Influence of in-plane core stiffness

4.4.1 Mode shapes

Whether a snake or an hourglass modes are going to form in a certain sandwich configuration is mainly determined by the core behavior. Regarding the foundation problem only (as shown in fig. 3.2) it seems obvious, that the deformations of the upper and the lower face layer are both oriented in the same direction, leading to a snake mode. This is true as far as isotropic cores are concerned. The deformations of the corresponding 2D FE foundation model are shown in fig. 4.6 for an isotropic core.

The situation is different when highly orthotropic cores, such as honeycombs, are used. In this case, there is a parameter region, where the deformations of the upper and the lower face layer are oriented in different directions as shown in fig. 4.7, leading to an hourglass mode. This deformation mode is somewhat unexpected, bearing in mind that the foundation model is only loaded by a sinusoidal pressure distribution at the interface to the upper face layer. This effect is possible due to the very small in-plane core stiffness of honeycombs as compared to the transverse and shear stiffness. Therefore, the deformation pattern shows very large in-plane deformations of the core. Hourglass modes have been observed to be the critical wrinkling modes only within a certain range of the core thickness, loading and stiffness parameters involved. Within other ranges, snake modes are critical also in the case of honeycomb cores (as shown in fig. 4.5). In these cases, snake modes are also dominated by in-plane deformations, especially in the case of rather thick cores.

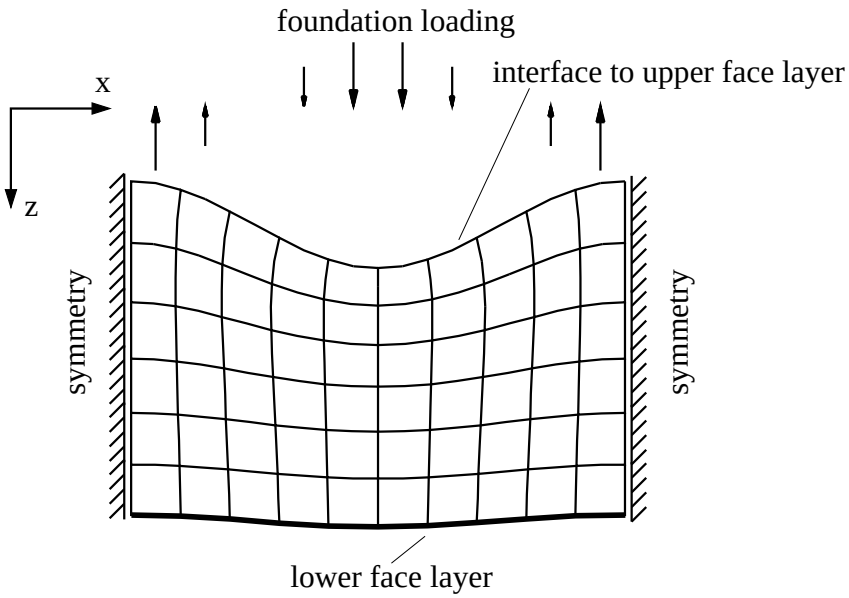

Figure 4.6: Foundation deformation, isotropic core, snake mode

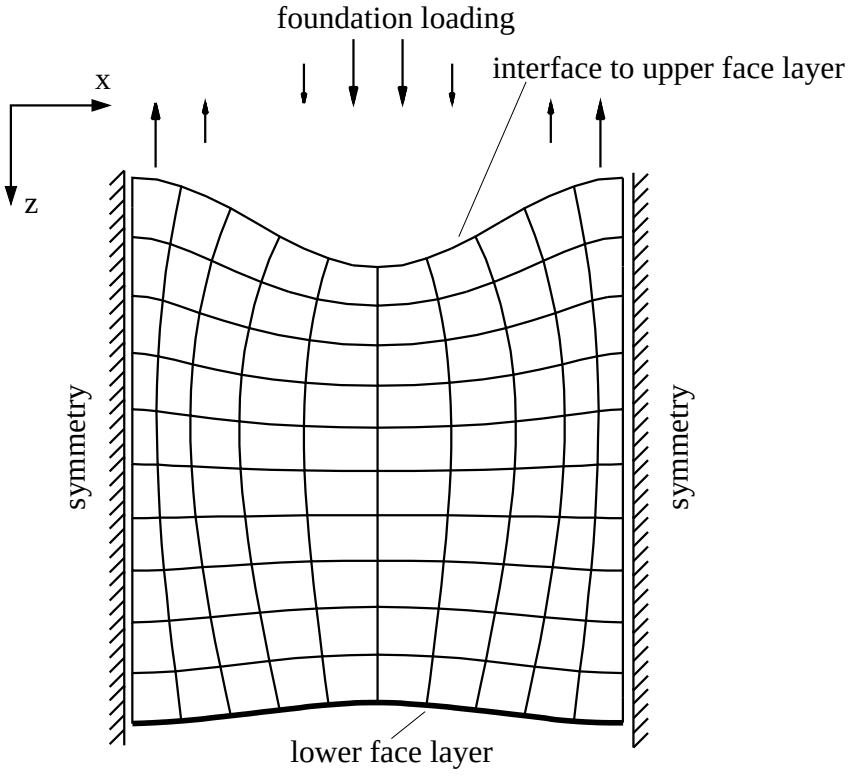

Figure 4.7: Foundation deformation, orthotropic core, hourglass mode

An example of a snake mode shape of a honeycomb core is given in fig. 4.8. Comparing this mode shape to fig. 4.6, it is observed, that the face layers deform similar, but the core deformation mode is quite different.

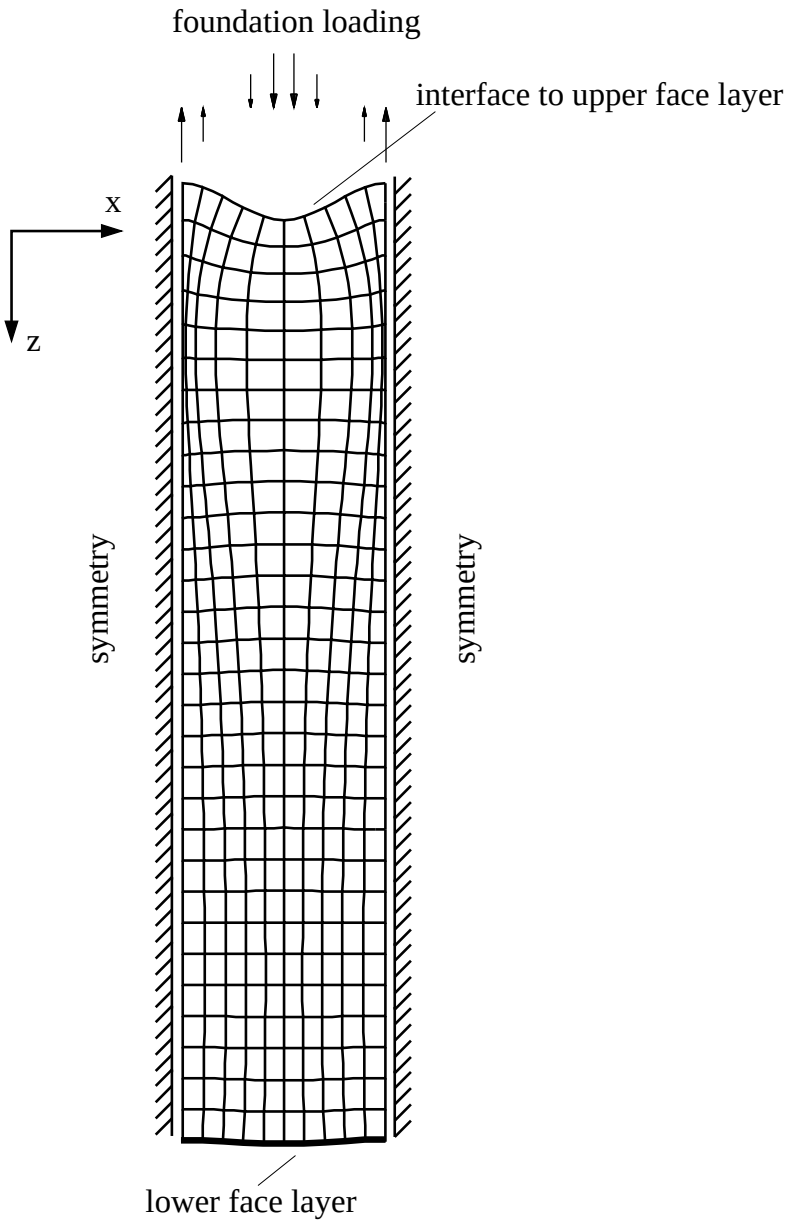

Figure 4.8: Foundation deformation, orthotropic core, snake mode

4.4.2 Critical load

It has been shown above that the in-plane core stiffness E_x^c is one of the important factors which determines which deformation mode is critical in a given sandwich configuration. This, of course, leads to the question to which extent the critical load is influenced by this in-plane core stiffness which has been disregarded in sandwich design calculations up to now.

4.4.2.1 Infinite core thickness

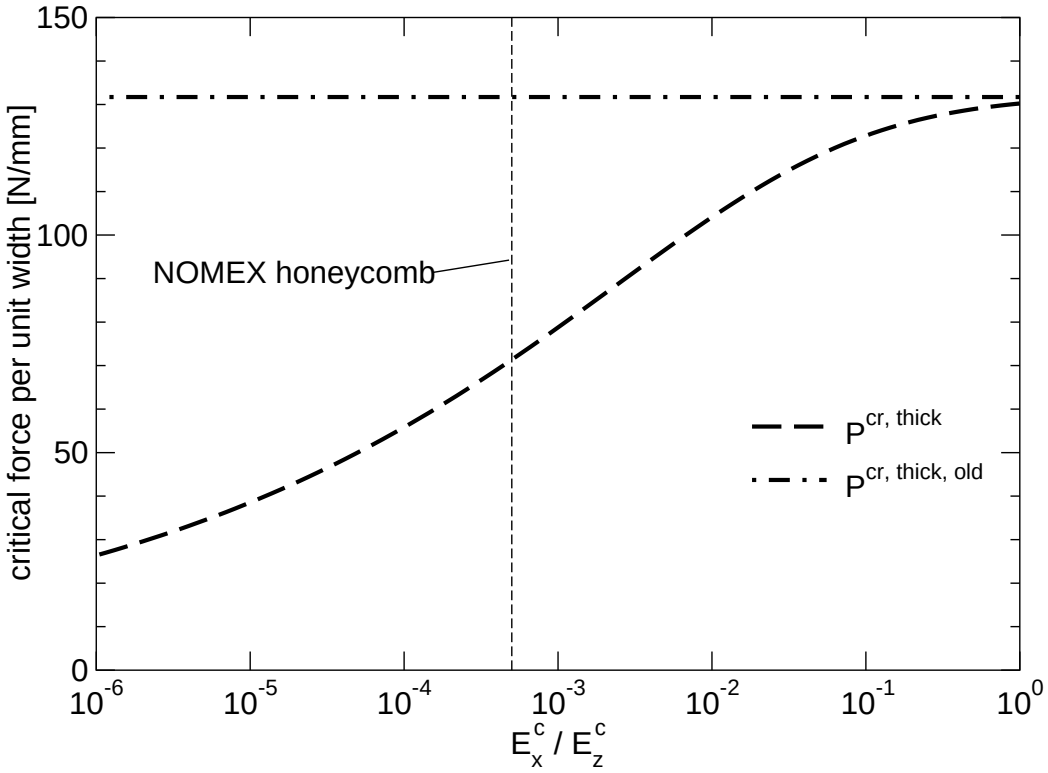

Figure 4.9: Critical load over in-plane core stiffness, infinitely thick core

In fig. 4.9 the critical load magnitude is plotted over the ratio of E_x^c/E_z^c on a logarithmic scale for the same sandwich beam configuration used in fig. 4.5. In order to simplify the explanation, the core is taken to be infinitely thick, thus interaction effects are eliminated, and the sandwich is again loaded by uni-axial compression. The result of the classical design formula for thick cores (see eq. 2.9) is denoted by $P^{cr,thick,old}$ and does not account

for the parameter E_x^c. On the right hand side of fig. 4.9, the ratio of E_x^c/E_z^c is 1, leading to a practically isotropic core behavior. In this region, the classical design formula for thick cores is quite close to the results of the new model. Thus, the fact that the classical model is based on $E_x^c = \infty$ leads to a slight overestimation of the critical force as compared to $E_x^c = E_z^c$. Towards the left side of the chart, as E_x^c is reduced, the critical load magnitude $P^{cr,thick}$ decreases and, therefore, the classical design formula for thick cores severely overestimates the critical load. This effect becomes pronounced when the ratio of E_x^c/E_z^c is below 0.1. In the case of commercial honeycombs, the ratio of E_x^c/E_z^c is about 1/2000 [Gibson and Ashby, 1997] which is marked by a vertical dashed line in the plot. Within this parameter range, the error of the classical model is definitely too large to be neglected.

The effect that the critical load decreases as E_x^c gets smaller has recently been reported for the first time by Hwang [1998] who used a numerical model, but no explanation was given. He concluded that E_x^c has an influence only if the ratio of face layer stiffness to transverse core stiffness is not too high, which practically excluded the usual application of structural sandwiches from this effect. However, apart from the honeycomb shown in fig. 4.9, numerous other honeycomb materials were investigated in the present study, and although the stiffness ratio mentioned above has been well over thousand, it was always obvious, that the influence of E_x^c must not be disregarded. This discrepancy to Hwang's considerations can be explained by the limited and different parameter range Hwang investigated, which did not include the high degree of orthotropy that is found in the homogenized honeycomb material values.

To gain a proper explanation for the decrease of the critical wrinkling force, the core deformation patterns are again to be considered. The core deformation pattern is a sine wave on the surface and has to decrease to an undeformed state with increasing distance from the surface. The classical model for thick cores assumes, that the only existing strains are shear and transverse strains. Therefore, the deformation pattern of the core is forced to look like fig. 4.10, the vertical grid lines being straight. This deformation pattern corresponds roughly to the deformation mode for an isotropic core calculated by th FE method shown in fig. 4.6. However, the classical model overestimates the critical load slightly since the vertical grid lines are not exactly straight in fig. 4.6.

The new approach also accounts for strains in the in-plane, i.e. x-direction. For the case of very small ratios of E_x^c/E_z^c the analytically calculated deformation pattern is shown in fig. 4.11. The strains in longitudinal direction must obviously not be neglected in this

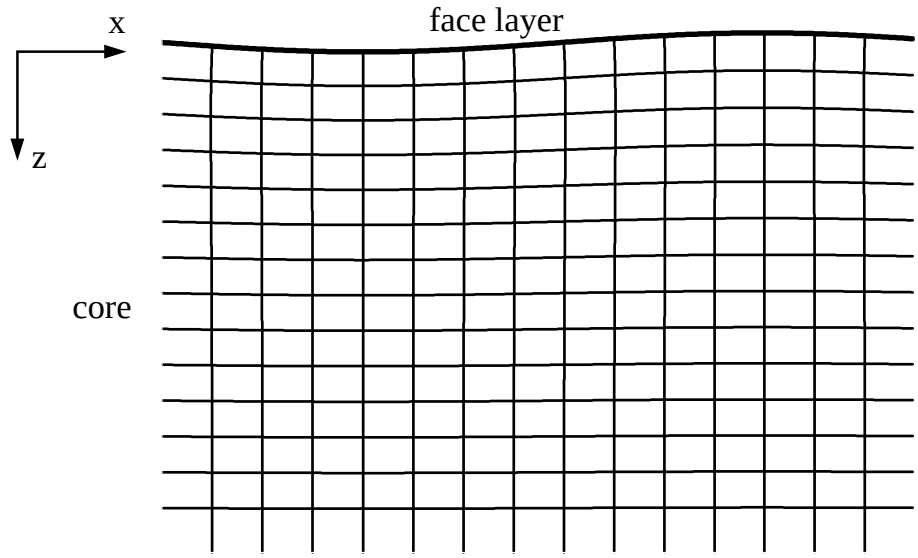

Figure 4.10: Deformation pattern, classical model for thick cores

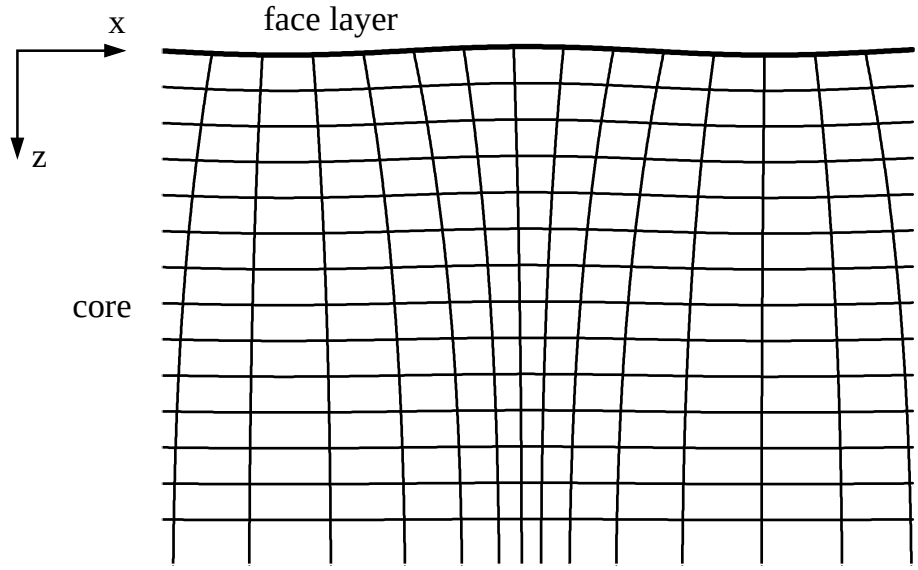

Figure 4.11: Deformation pattern for infinitely thick cores, new model at $E_x^c/E_z^c = 10^{-4}$

case. This is also noticed regarding the FE results for highly orthotropic cores shown in figs. 4.7 and 4.8. The new analytical model and the FE results agree in this respect. It is clear that the classical model for thick cores is thus not applicable in these cases and leads to severe errors.

The kinematics of deformation show that in-plane strains may take over the role of shear strains within the core. This can be seen when comparing the angles between the grid lines in figs. 4.10 and 4.11. In fig. 4.11, the grid lines are almost normal with respect to each other, leading to lower shear strains as compared to fig. 4.10. Whether the deformation pattern exhibits predominantly shear or in-plane strains (apart from the transverse strains) depends on the energy stored in these two modes and, therefore, on the moduli G^{c}_{xz} and E^{c}_{x}. In the case of isotropy, shear strains are dominant, but in the case of a very low in-plane stiffness of the core, in-plane strains are dominant. For $E^{\mathrm{c}}_{x} \to 0$ it is even possible to obtain deformation patterns without any shear strains. These are the reasons why the classical design formula for thick cores fails to predict the correct critical load in fig. 4.5 even for very high core thickness values.

It is interesting to note, that for $E^{\mathrm{c}}_{x} \to 0$ and $c \to \infty$ (to the left side of fig. 4.9), the critical load approaches zero. This can be explained by regarding the energy stored in the core: The strain energy due to transverse strains approach zero since the core thickness is infinite (just as in the case of the classical thin core solution based on a Winkler foundation). The strain energy due to in-plane strains is zero due to the zero in-plane stiffness, and shear strains are not present, also due the zero in-plane stiffness. The strain energy of the faces approaches zero as well because the wavelength of the critical pattern is growing very large. This configuration itself is rather of academic interest, but it shows the tendency that is followed when decreasing the in-plane core stiffness.

It is also worth noting that the region of the core which exhibits high deformations is much thicker for small ratios of $E^{\mathrm{c}}_{x}/E^{\mathrm{c}}_{z}$ than for high ones. This finding is in accordance with those of numerous other authors (e.g. [Stronge and Kashtalyan, 1997; Horgan, 1998]) who observed, that a higher grade of material anisotropy leads to a longer St. Venant decay length. This effect is also observed when comparing fig. 4.4 and fig. 4.5: Although the stiffness values of the constituent materials differ noticeably only in terms of the in-plane core stiffness, the core thickness range that leads to interaction between the face layers is very different. The effects of this are now examined more closely by investigating sandwiches having a finite core thickness.

4.4.2.2 Finite core thickness

The effect of the in-plane stiffness on the wrinkling load can be seen in fig. 4.12, which is based on a core thickness of $c = 50\mathrm{mm}$ (leading to a c/t ratio of 100). The sandwich configuration and the notation are identical to the infinite core model shown in fig. 4.9, and

additionally $P^{cr,thin,old}$ (classical design formula for thin cores, eq. 2.7) is also displayed. The section marked with the dashed line (material value of NOMEX honeycomb) corresponds exactly to fig. 4.5 at a core thickness c of 50mm.

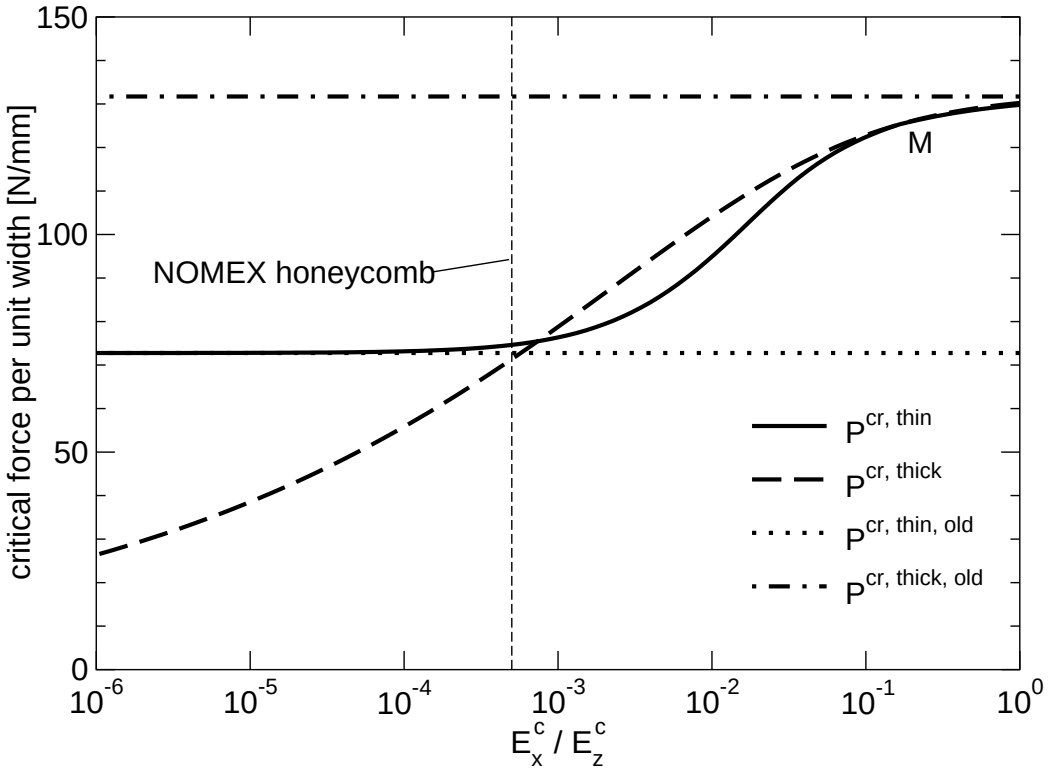

Figure 4.12: Critical load over in-plane core stiffness, $c = 50\text{mm} \Longrightarrow c/t = 100$

Regarding $P^{cr,thin}$ and $P^{cr,thick}$ it is observed, that the thin and the thick core solutions coincide in the range of isotropic and moderately orthotropic cores. This shows, that the c/t ratio of 100 defines a sufficiently thick core so that interaction effects between the face layers are not pronounced. Therefore, the simplified analytical solution derived within this work for thick cores gives a good approximation of the critical wrinkling load.

For a higher grade of orthotropy of the core material, the decrease of E_x^c/E_z^c at some point leads to a pronounced interaction between the face layers, and, therefore, the results for the thin core $P^{cr,thin}$ and the thick core $P^{cr,thick}$ calculated by the new analytical model do not match anymore. This point is marked with an M in fig. 4.12. In the parameter region beyond M, the assumption of an infinitely thick core is not appropriate anymore. It is noteworthy that this effect is also observed at a very high ratio of c/t (100 in the case of fig. 4.12, even 300 in the case of fig. 4.13) for realistic material values of honeycomb core

materials.

Regarding the mode shapes it is found that snake modes are the critical mode shapes for rather isotropic cores (to the right of M). The results for snake and hourglass modes do not differ very much in this regime, since there is hardly any interaction between the face layers. At the point M, the critical mode switches to an hourglass mode. Therefore, the $P^{\mathrm{cr,thin}}$ line shows a slight kink at the point M. This kink is barely visible in fig. 4.12, but more pronounced in fig. 4.13. To the left of M, the difference in results for snake and hourglass modes grows quickly due to face layer interaction, the hourglass mode having the lower critical load.

For a very low $E_x^{\mathrm{c}}/E_z^{\mathrm{c}}$ ratio, the critical wrinkling force approaches the classical design formula for thin cores $P^{\mathrm{cr,thin,old}}$. This design formula itself considers only the transverse strains, and no in-plane or shear strains. At the low ratios of $E_x^{\mathrm{c}}/E_z^{\mathrm{c}}$, where the new model and the classical thin solution coincide, there are no shear strains present anymore and the in-plane strains contain practically no energy due to the low longitudinal stiffness of the core, but a strong interaction between the two face layers exists. Therefore, the classical design formula for thin cores given in eq. 2.7 ($P^{\mathrm{cr,thin,old}}$) can be used to calculate critical wrinkling stresses also for rather thick cores, if the core material exhibits a sufficiently low ratio of $E_x^{\mathrm{c}}/E_z^{\mathrm{c}}$. Moreover, considering the stresses regarded within the different models, it becomes clear, that the classical design formula for thin cores gives a lower bound to the critical wrinkling load, if wrinkling occurs in the ideal hourglass mode (in the case of a snake mode, the situation is clearly different). This can also be seen in fig. 4.5 which shows the identical configuration at fixed E_x^{c} and variable c. The classical design formula for thin cores is an excellent estimate to the critical load in a certain parameter range (in this case up to $c = 50\mathrm{mm}$), and at higher core thickness values it is a lower bound to the critical wrinkling load.

Fig. 4.13 shows the same situation as fig. 4.12, but at a core thickness c of 150mm, thus also corresponding to fig. 4.5 at $c = 150\mathrm{mm}$. In this case, $P^{\mathrm{cr,thin,old}}$ is only appropriate at levels of core orthotropy which exceed usual honeycomb material values. The kink in the $P^{\mathrm{cr,thin}}$ line at the point M caused by the mode change is clearly visible. Considering the information given in figs. 4.5, 4.12 and 4.13, the wrinkling of a simple compressed sandwich beam is described as a function of the thickness and the in-plane stiffness of the core. These two parameters interact and mainly determine, which model can be used to describe wrinkling properly, the new model being always appropriate.

The decrease of the critical load with falling E_x^{c} described above gets more pronounced

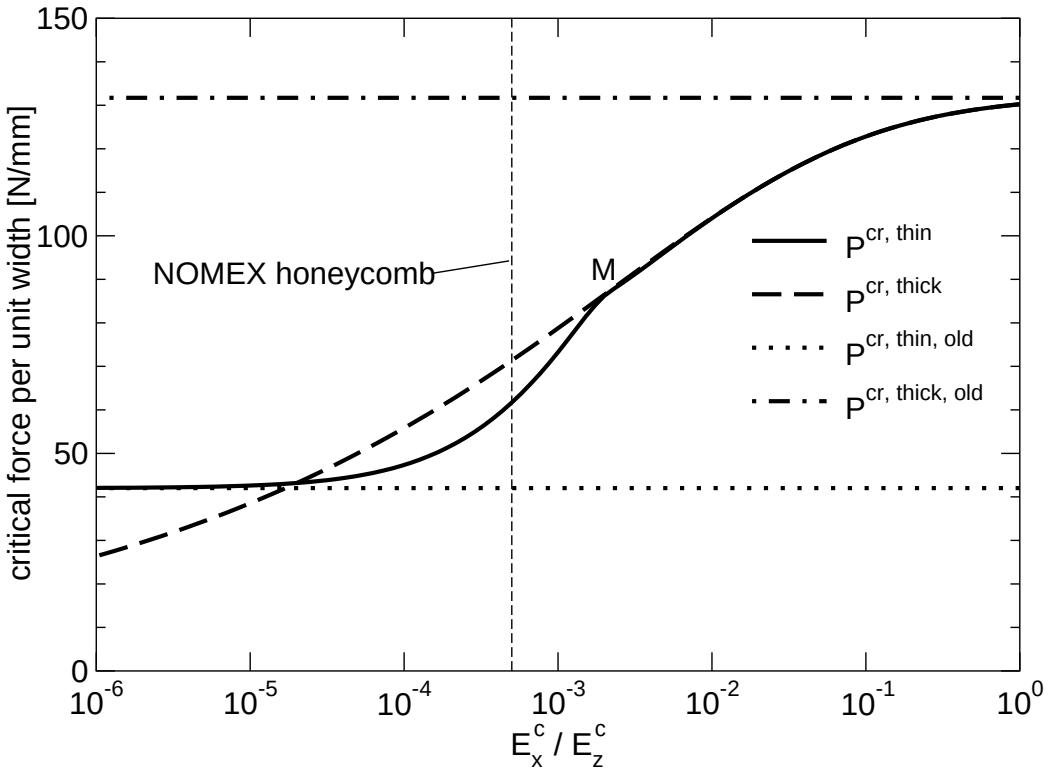

Figure 4.13: Critical load over in-plane core stiffness, $c = 150\text{mm} \Longrightarrow c/t = 300$

for higher ratios of G^c_{xz}/E^c_z, since a larger amount of strain energy is contained by the shear strains in the isotropic case and can be "released" by lowering E^c_x.

For deciding whether or not the core of a sandwich is thick enough to prevent face layer interaction, it is not sufficient to consider the c/t ratio only as e.g. in [Plantema, 1966; Zenkert, 1995; Rammerstorfer, 1992; Starlinger and Rammerstorfer, 1992; Wiedemann, 1986], the ratios E^c_x/E^c_z and G^c_{xz}/E^c_z have also to be considered. Therefore, it poses a complex problem to determine whether a sandwich can be considered as being thick. The c/t ratio of around 50 proposed in the literature seems to be based on isotropic cores only. In the case of honeycomb cores, the corresponding ratio is much larger and tends towards infinity as the in-plane core stiffness goes down to zero. Commonly used configurations of honeycomb sandwiches (which hardly exceed a c/t ratio of 100) cannot be described properly using the thick core assumption. In the case shown in fig. 4.12, the use of the classical model for thick cores (which is proposed in the literature) leads to an overestimation of the critical load of more than 70%!

The fundamentally different behavior of isotropic and highly orthotropic cores described above has been the reason for differences between the present work and the work of Frostig [1998]. Since some simplified models are based on the assumption that the in-plane stiffness of the core is negligible and, therefore, taken to be zero, these models always assume highly orthotropic cores (although this was not intended by the authors). This leads to the hourglass mode even if isotropic cores are the subject of investigation (e.g. [Frostig, 1998] or the classical design formula for thin cores), thus producing considerable errors in terms of critical load and mode shape when used in conjunction with isotropic cores. The corresponding authors report the hourglass mode to be always critical. Other simplified models are based on the assumption that the in-plane core deformation is neglible and, therefore, zero. In this case, the in-plane core stiffness is overestimated, which – artificially – prevents an hourglass deformation. These models (e.g. the classical model for thick cores and its different extensions) are also proposed to be used with honeycomb cores, which again leads to considerable errors. Both approaches are not suitable to calculate the real critical mode shape (and load) for both isotropic and honeycomb cores, since the absolute value of the in-plane core stiffness is not included in these calculations.

4.5 Compression of unsymmetric sandwich beams

The sandwich beams discussed up to now are symmetric. The new model presented here is capable of calculating the critical load levels for sandwich beams which are not symmetric as well. A corresponding result is presented in fig. 4.14. The solid line shows the critical load for the symmetrical sandwich beam used in fig. 4.5 ($t^{\mathrm{u}} = t^{\mathrm{l}} = 0.5\mathrm{mm}$, $\rho^{\mathrm{u}} = \rho^{\mathrm{l}} = 1\mathrm{N/mm}$). Additionally, the result for the same sandwich beam under pure compressive loading is displayed, where the thickness and section force of the upper face layer have been doubled ($t^{\mathrm{u}} = 1.0\mathrm{mm}$, $t^{\mathrm{l}} = 0.5\mathrm{mm}$, $\rho^{\mathrm{u}} = 2\mathrm{N/mm}$, $\rho^{\mathrm{l}} = 1\mathrm{N/mm}$). Thus, both face layers of both sandwich beams are loaded to the same *stress* level at a certain load level P. The loading of the unsymmetric sandwich beam represents pure compressive loading in the bending axis (main axis of the moment of inertia) of the beam. Thus the beam remains straight during loading.

The results show that the critical load level for the symmetrical and the unsymmetrical beams differ significantly. This is especially true for core thickness values up to 100mm, which is the region of most technical applications. The classical model for thin cores – which shows some agreement in the case of symmetrical sandwiches – fails to predict

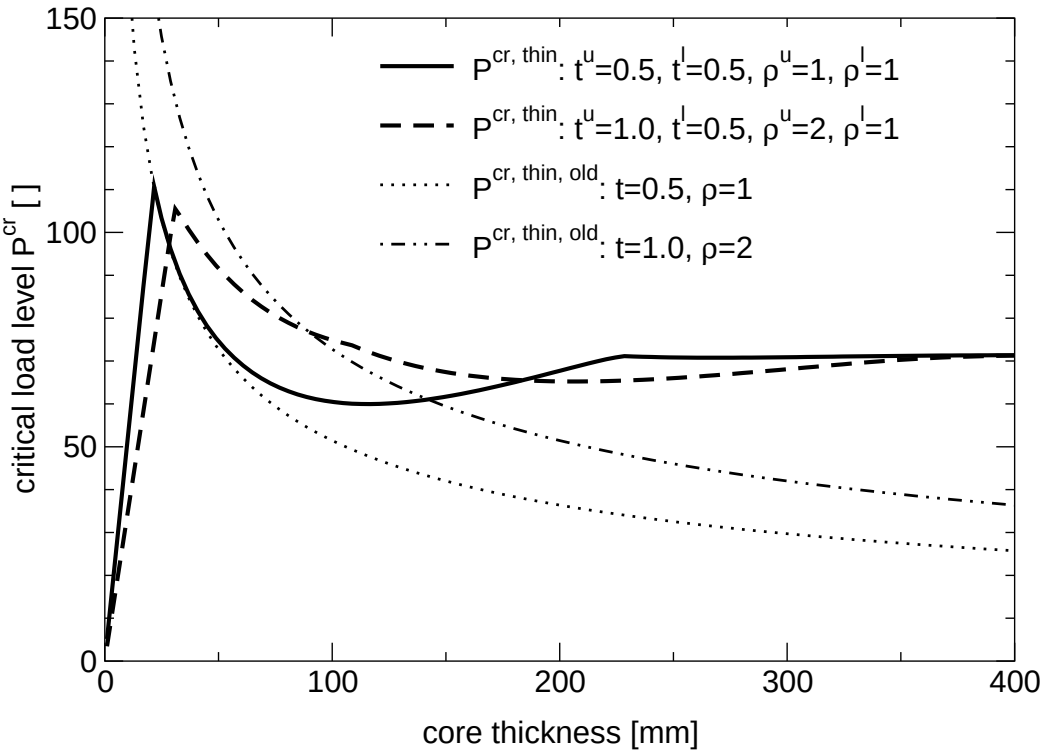

Figure 4.14: Example of an unsymmetric sandwich beam with honeycomb core

the critical load in the unsymmetric case. In the case of a very high core thickness, the results for the symmetric and the unsymmetric beam coincide, since the critical stress is independent of the face layer thickness in this case (see e.g. eqs. 2.9 and 3.30). This simple example indicates the generality of the new model as compared to other approaches. To the knowledge of the author, the new model is the only analytical approach which is able to calculate wrinkling of this sandwich beam configuration correctly (including the in-plane core stiffness and the unsymmetry).

4.6 Bending

4.6.1 Pure bending

Wrinkling failure can also occur in sandwiches which are loaded by a bending moment only. In this case of pure bending of a sandwich beam it has mostly been assumed up to now, that the face layer which is under tension remains perfectly flat. It is obvious that

this assumption is introducing artificial stiffness into the system which is going to lead to an overestimation of the critical wrinkling load. This assumption has also been used by Stiftinger and Rammerstorfer [1997], whose model is used as reference model in the following. In contrast to this assumption, the new model allows for deformations of the face layer which is under tension.

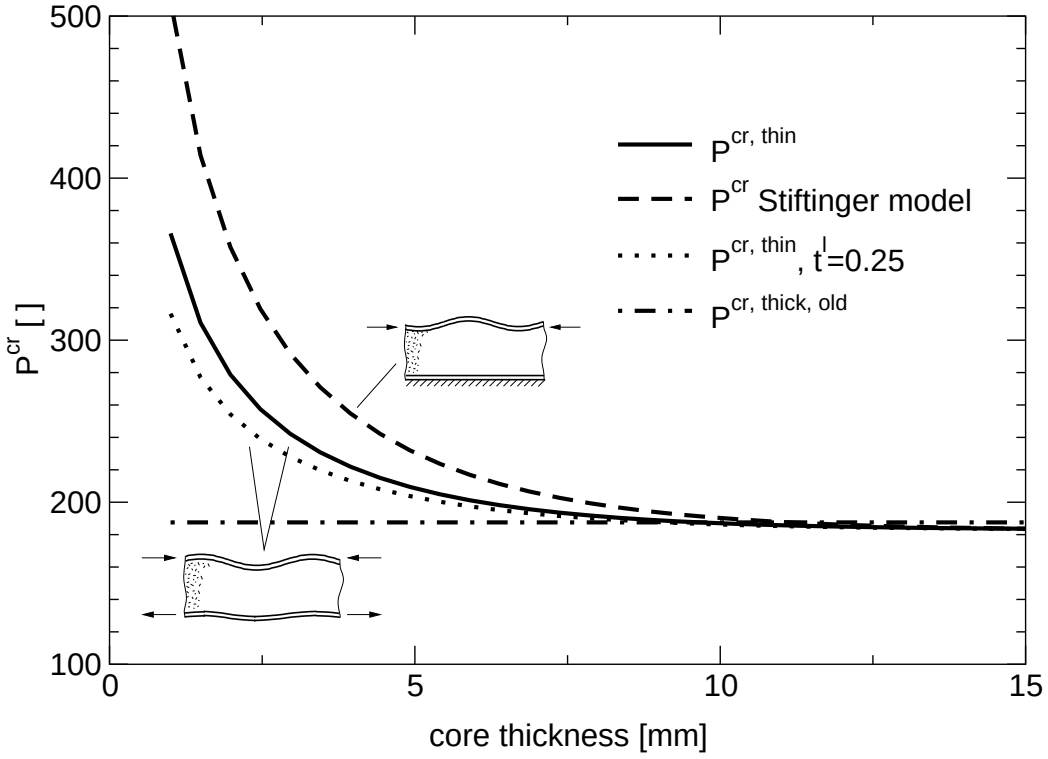

Figure 4.15: Critical load level under pure bending

The basic and conclusive new result for bending is shown in fig. 4.15 which displays the critical load level leading to wrinkling as a function of the core thickness. The sandwich is the same sandwich (aluminium faces, foam core) as used in section 4.3, the only difference is the loading ($\rho^u = 1\text{N/mm}$, $\rho^l = -1\text{N/mm}$).

As long as the core thickness is rather high, the results of the different models coincide, and the classical formula for thick cores is applicable. However, as the core thickness gets smaller, the interaction between the two face layers grows and the face layer which is under tension starts to deform during wrinkling. Therefore, the critical load level $P^{cr,thin}$ is lower than calculated by Stiftinger and Rammerstorfer [1997]. Moreover, it is common practice to use a thinner face layer for the tensile face because local stability problems are

only expected at the compressed face. As shown by the dotted line in fig. 4.15, this has an adverse influence on the critical load level, due to face layer interaction in the case of rather thin cores.

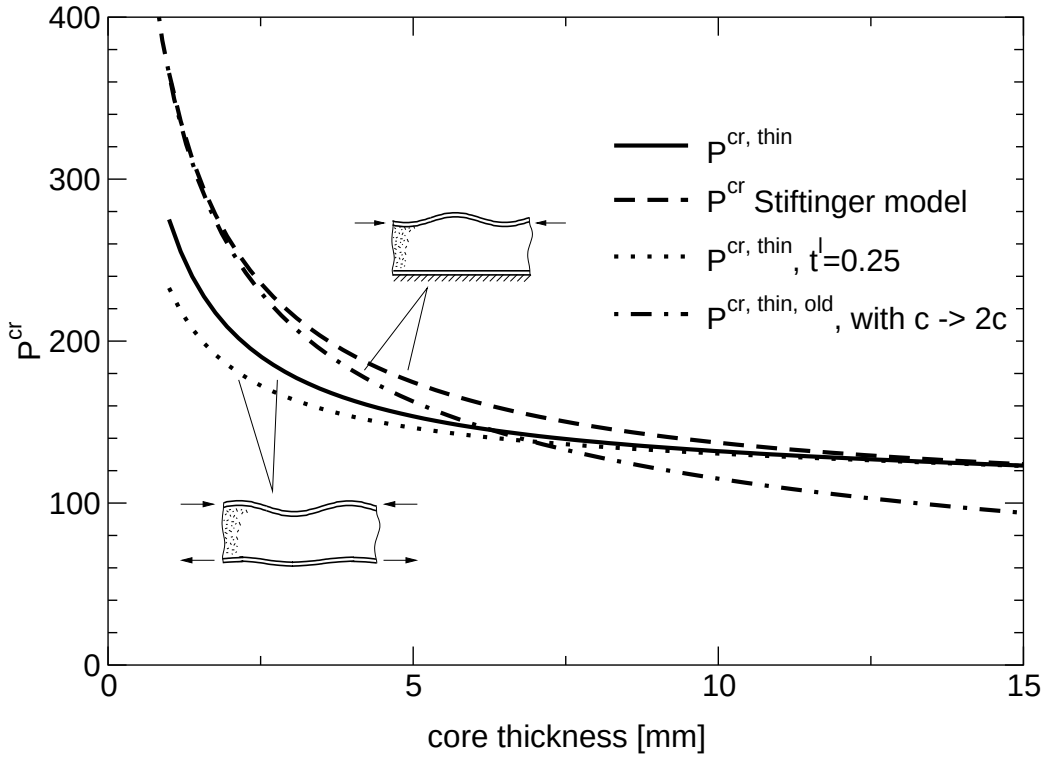

Figure 4.16: Critical load level under pure bending, honeycomb core

The corresponding result for the sandwich beam with honeycomb core (also the same sandwich configuration as used in section 4.3) in fig. 4.16 looks quite similar. The difference between the results from Stiftinger model and the new model diminish for core thickness values above 10mm which corresponds to a c/t value of 20. Additionally, a bending version of the classical model for thin cores is displayed. When using the classical model for thin cores with an imaginary double core thickness (i.e. using $2c$ instead of c in eq. 2.7), it represents a model for bending of thin sandwiches which also precludes deformation of the face layer which is under tensile loading. This simple approximative result is also displayed in fig. 4.15, since it is very easy to obtain. For thin sandwich beams, the result corresponds to the Stiftinger model due to the the very low in-plane core stiffness and the identical assumption of the tensile face layer being rigid. For larger core thickness values, it leads – as in the case of pure compression – to an underestimation of the critical load

and is not very useful. The difficulty in using the classical model for thin cores within wrinkling calculations is – as in the case of pure compression – that one does not know where the applicable parameter range is without employing more advanced models. It is again noticed, that sandwiches with honeycomb cores need a much larger core thickness to reach a constant critical load (i.e. to uncouple the wrinkling problem) than sandwiches with isotropic cores. In fig. 4.15, the stationary value of the critical load is reached at $c = 15$mm, in fig. 4.17 (which merely shows a larger core thickness range of fig. 4.16) at about $c = 100$mm. In the case of honeycomb cores, the classical model for thick cores is leading to rather meaningless results as already explained in the section dealing with sandwich beams under pure compression.

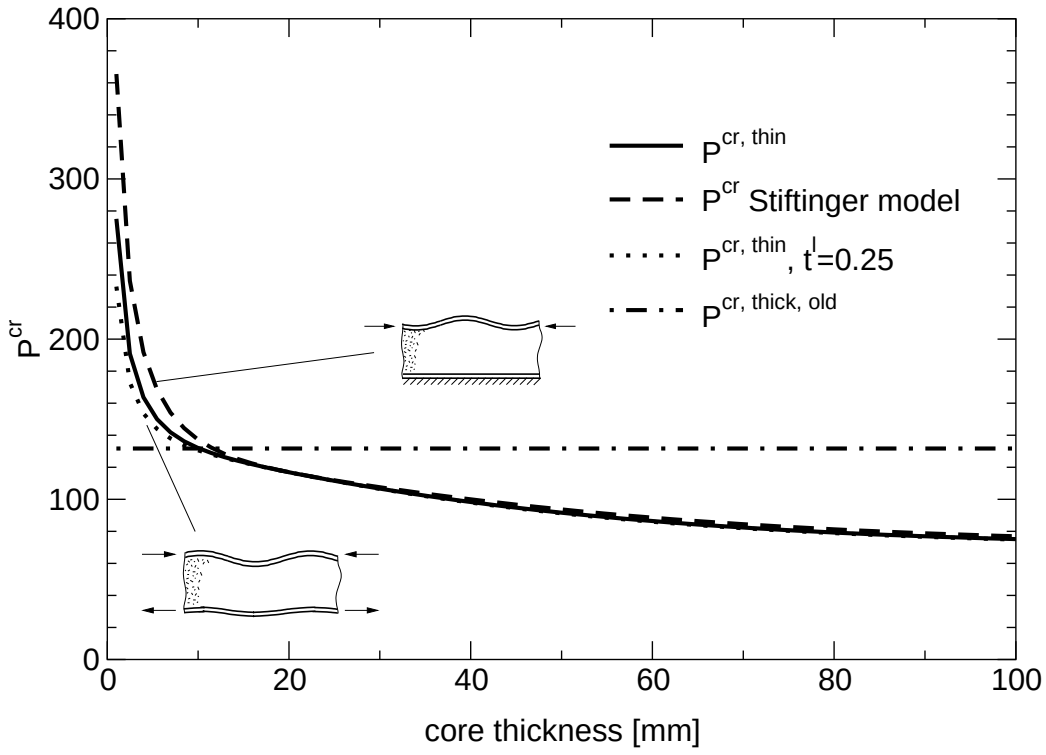

Figure 4.17: Critical load level under pure bending, honeycomb core

4.6.2 Transition bending - compression

Another basic problem that has hardly been investigated up to now is the transition between bending and compression of sandwich beams. In the paper of Stiftinger and

Rammerstorfer [1997], FE calculations are compared to their analytical approach and the agreement is not satisfying. The symmetric sandwich configuration analyzed comprised an isotropic foam core ($E = 28\text{N/mm}^2$, $\nu = 0.17$, $c = 10\text{mm}$) and aluminium face layers ($E = 70000\text{N/mm}^2$, $\nu = 0.3$, $t = 0.5\text{mm}$). Fig. 4.18 shows their results as well as the results of the new model. In the Stiftinger model a foundation stiffness for pure compression and a foundation stiffness for pure bending (with a flat face as explained in the previous section) are calculated. The results in the transition regime between bending and compression are then calculated by interpolating the foundation stiffness between the bending and the compression value [Stamm and Witte, 1974]. However, the FE results as well as the new results indicate that, in the considered example, there is a mode change between the failure under bending load, which is a snake mode wrinkling, and the failure under compressive load, which is shear crimping. Therefore, the interpolation between these two results is not permissible.

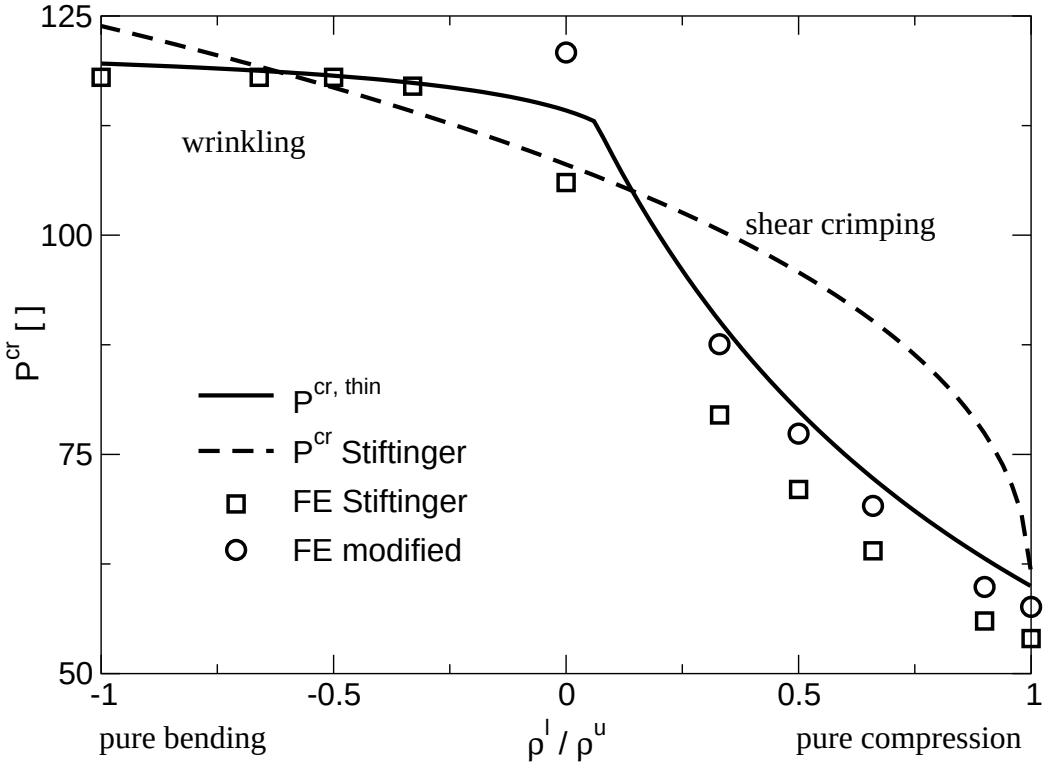

Figure 4.18: Transition bending – compression, [Stiftinger and Rammerstorfer, 1997]

Regarding shear crimping, it has been discussed (section 2.1) that this mode interacts with Euler buckling of the global structure. Using the appropriate interaction formula

(eq. 2.1), the Euler buckling influence can be eliminated from the Stiftinger FE results and these modified FE results correspond to the shear crimping load, which is the local failure load. The agreement between the new model and the FE results in fig. 4.18 is shown to be good. The discrepancy between the FE results and the new model for the case $\rho^{\mathrm{l}}/\rho^{\mathrm{u}} = 0$ is due to the fact that the FE model calculated the critical mode as Euler buckling with shear influence. Therefore, the corresponding modified FE result is on the extension of the shear crimping curve of the new model. However, the local failure mode has already switched to wrinkling.

In cases similar to fig. 4.18 where no mode change takes place, it is also observed that the new model fits FE calculations far better than the Stiftinger model. Thus, the interpolation method proposed by Stamm and Witte leads to considerable errors and should not be applied.

Chapter 5

Results for sandwich plates

Up to this stage, only beam problems have been considered. Therefore, orthotropy of the face layers and in-plane (xy-plane) orthotropy of the core have not been an issue. The direction of wrinkling (r-direction) has been known *a priori* to be the beam direction (x-direction). In the case of sandwich plates made of orthotropic face layers under arbitrary loading conditions, the situation is different in the sense that the direction of wrinkling is a result of the calculation, and depends on the loading conditions and the in-plane material properties of the sandwich materials. Thus, the problem is fully three dimensional and considerably more complex than the beam case. Therefore, it was decided to confine the first part of this chapter to infinitely thick cores (orthotropic plate on an orthotropic foundation) to gain a basic understanding of the effects involved without regarding face layer interaction. In the last section of this chapter a rather general example in the form of a thin unsymmetric orthotropic sandwich plate under combined loading is investigated.

The new model is the first analytical approach to this complex problem. The approach of Stiftinger and Rammerstorfer [1997] also considers orthotropic sandwich plates, but since loading is only permitted in the directions of the material axes and only symmetrical sandwiches are allowed for, there is a very large difference in generality and applicability between these models. However, Stiftinger and Rammerstorfer [1997] report a buckling pattern different from the one used in this approach. This problem is discussed in section 5.2.

Due to the lack of comparable analytical models, the verification of the results is done using the FE models described in the following.

5.1 Verification models

5.1.1 FE unit cell models

FE models simulating wrinkling up to now have been confined to 2D FE models, i.e. sandwich beam models (see e.g. Stiftinger and Rammerstorfer [1997] and Hadi [2001]). In these cases, a sandwich beam is usually discretised over the length of six to ten wrinkling wavelengths to encourage wrinkling at an arbitrary wavelength without too much influence of the boundary conditions. This is easily possible, since the 2D FE models are rather small. The situation is different considering the verification of the new approach: In the case of orthotropic sandwich plates, the problem is fully three dimensional and requires a 3D FE verification model. This leads to large FE models, and the full 3D discretisation of a sandwich plate with the size and meshing to represent about ten waves requires considerable computational resources. Therefore, this has only been done in a special case (section 5.5). In all other cases, small FE "unit cell models" have been used.

The 3D FE models are built up from 3D solid elements (bricks) representing the core and shell elements representing the face layers. All elements are quadratically interpolated, since their performance was observed to be superior compared to linearly interpolated elements.

The FE unit cell models represent a cutout of an infinite periodic problem, by enforcing periodic boundary conditions at the model boundaries. This strategy is commonly used in micro-mechanics and mechanics of materials [Böhm, 1998], however, its application to wrinkling is a novelty. Since the wrinkling problem is periodic in the plane of the sandwich plate (x and y–direction), the 3D model was implemented with two sets of fully periodic boundary conditions, each connecting two parallel boundary planes normal to the face layers. This ensures, that every periodic solution can be found. Examples of the resulting geometry and buckling patterns are given in the following sections and in the Appendix.

The FE models were defined in ABAQUS using the parametric design features which allow for a rather general formulation. Considerable effort had to be put into the correct formulation of the periodic boundary conditions which are formulated as linear constraint equations. The periodicity has been defined in such a way, that the section planes which are connected by the periodicity constraints remain parallel. Therefore, the kinematics of the FE model does not allow for global sandwich plate bending deformations, but only for global compressive deformations. The FE model can, nevertheless, be used in bending due

to the loading formulation which is discussed in the following.

The loading of a unit cell is normally done by the application of concentrated forces or deformations to specified master nodes. The magnitudes of these concentrated forces or deformations which are needed to have certain stresses within the unit cell depends, therefore, on the absolute model dimensions. Since the model dimensions are often varied (as described in the next section), the concentrated forces would have to be altered accordingly. This problem is circumvented by loading the face layers thermally, i.e. assigning appropriate anisotropic thermal expansion coefficients to the face layers and fictitiously heating the model. The thermal expansion coefficients of the core are set to zero in these cases. Therefore, the core does not carry loads as is assumed in the analytical derivation (and generally in sandwich construction).

As indicated above, the major advantage of the fictious thermal loading is that the formulation of the kinematic periodicity constraints is much easier, since even global sandwich plate bending can be simulated on a flat plate. Thus, the two section planes connected by the periodicity boundary conditions can be forced to stay parallel, which is much easier to formulate than global rotation of one of the planes with respect to the other. The bending load is introduced by thermally expanding the one face layer and thermally shrinking the other face layer while forcing the plate to remain flat. This is permitted as long as no geometrically non-linear effects have to be regarded (which is the case).

The resulting ABAQUS input file provides the possibility to simply choose the mesh densities and model dimensions in all directions, and the FE model as well as the periodic boundary conditions are generated appropriately.

This unit cell approach incorporates only one drawback, namely that the overall model dimensions in x and y–direction act as a frequency filter regarding the wavelengths of the periodic patterns that can possibly be found with such a model, compare Suzuki and Yu [1998]. If the model dimension in x and y–direction are denominated by l_x and l_y, respectively, the solution of the FE model *has to be* periodic with the wavelengths a_x and a_y as follows:

$$a_x = \frac{l_x}{n} \qquad a_y = \frac{l_y}{m} \qquad n, m \,\epsilon\, [1, 2, 3, ...] \tag{5.1}$$

where a_x and a_y are connected to the free variables of the analytical model a_r and φ by:

$$\varphi = \arctan\left(\frac{a_x}{a_y}\right), \qquad a_r = a_x \cos\varphi \,. \tag{5.2}$$

This essentially means that within a unit cell model only an integer number of waves can form. Thus, the model size determines which wavelengths of the solution are allowed to

form, and which are not. The maximum number of waves (n and m in eq. 5.1) which can be calculated is naturally limited by the mesh density of the model.

In order to find the lowest buckling eigenvalue and the corresponding wavelength with a certain accuracy, two different strategies were chosen, a small and a large unit cell approach.

5.1.1.1 Small FE unit cell model

A small unit cell model with the dimensions of one wavelength is used, and the model dimensions (l_x and l_y) are varied in order to minimize the calculated eigenvalue. The mesh size is chosen to be able to represent *one* wave across the cell with sufficient accuracy. This leads to a very small FE model requiring only a couple of minutes computing time. Examples of such models are given in figs. 5.1, 5.2, 5.4 and fig. A.1.

This approach requires a minimization scheme, multiple FE calculations and corresponding pre- and postprocessing, all of which was realized within a FORTRAN code that invokes ABAQUS multiple times for the FE calculations. Since the results based on the analytical approach gave very good estimates for the critical wavelengths, this approach proved to be effective because only a small number of evaluations was necessary to reach the minimum eigenvalue. Within this method, the accuracy of the calculated overall minimum eigenvalue can easily be monitored. Generally, all eigenvalues presented here are calculated with an error of less than 0.1% regarding the influence of the model size parameters l_x and l_y.

As explained, the results of the analytical model (a_r, φ) were chosen as starting points of these FE minimizations. From the mathematical point of view, this optimization leads only to a local minimum of the buckling load. One cannot be sure, that this local minimum is also the global one. Essentially, the global minimum could be a solution with a different periodicity (wavelength) which can not be found using these starting values. This problem is addressed with the large FE models.

This method proved to be reliable and quick. The required computing time is very low as compared to the other 3D FE approaches described in the following, the drawback being a somewhat lower generality. The agreement between the small FE unit cell models and the analytical approach is very good. The corresponding charts are given in the following sections.

5.1.1.2 Large FE unit cell models

The results of the small FE unit cell models show, that the wrinkling pattern is sinusoidal. This has been one of the assumptions within the analytical approach. However, since the small FE models enforce a total periodicity with a certain wavelength and wave angle (defined by the FE model dimensions), it is not possible, that the deformation pattern of the upper and the lower face layer differ freely in terms of wavelength and wave angle. Thus an assumption which has been made in the analytical derivation is again enforced in the small FE unit cell models.

In reality, it seems possible, that a wrinkling pattern evolves, which is made up of sinusoidal deflections of the face layers which are *not* oriented in the same wave angle φ and/or do *not* have the same wavelength a_r, while the core is being deformed in a more complicated way to connect the two face layers. This behavior is investigated in section 5.5.

In order to allow for a more general deformation pattern than in the small FE unit cell models, large FE unit cell models are built up. These models are formulated with exactly the same periodic boundary conditions and loading as the small models, but the model size and meshing allows for several waves to form in the unit cell. Thus, step wise different wavelengths and wave angles are allowed for within the unit cell (compare eqs. 5.1 and 5.2). The larger the number of waves within the unit cell, the smaller are the corresponding steps in wavelengths and wave angles. Thus, a large number of waves is desirable.

The periodic boundary conditions lead to rather time consuming FE calculations. This is due to the additional coupling terms which lead to a high bandwidth of the system matrix compared to usual FE calculations. The computing power available limits the maximum dimensions of the large FE unit cells to about 10x10 waves (i.e. the size of 100 small FE unit cells). It is interesting to note, that the new sparse solver is hardly faster in solving this problem than the conventional solver of ABAQUS. This also indicates, that the system matrix is not sparsely filled, but has a high bandwidth.

5.1.2 FE plate models

Additionally to the unit cell FE models, conventional FE models were also used. The models are identical to the large FE unit cell models, except for the boundary conditions. The periodic boundary conditions are not used, but all parts of the sandwich plate are

clamped at the edges of the plate. Thus, the wrinkles can form only in the middle of the plate, and the plate dimensions (10x10 waves) are meant to be large enough so that the boundary conditions at the edges are not of major importance in the middle of the plate. Since no periodic boundary conditions are involved, the formulation of the FE plate model is much easier than in the case of the unit cell models.

5.2 Different analytical and FE mode shape descriptions

As mentioned earlier, Stiftinger and Rammerstorfer [1997] reported that in some parameter regions of biaxial compression (in direction of the material axes) of orthotropic symmetric sandwich plates, the wrinkling pattern is composed of the product of two orthogonal sinus waves. This deformation pattern was also found in FE unit cell calculations conducted by the author:

$$w^{\mathrm{u}} = w^{\mathrm{u}*} \sin\left(\frac{\pi x}{a_x}\right) \sin\left(\frac{\pi y}{a_y}\right) \ . \tag{5.3}$$

In these cases, the critical load calculated by the new model presented here coincides with the results of Stiftinger and Rammerstorfer [1997] and of unit cell FE calculations, but the deformation pattern looks different (corresponding to eq. 3.1). The two deformation patterns are shown in fig. 5.1. For the sake of simplicity, the deformation patterns shown here are derived using very thick cores, i.e. only one face layer buckles on a very thick foundation. The qualitative results can naturally be transfered to thin cores as well. In doing so, it has to be regarded, that the solution of Stiftinger and Rammerstorfer [1997] is only valid for symmetrical sandwiches.

The mathematical explanation of the above differences in the mode shape is given in the following: Bearing in mind that the problem is posed on an infinite plate, shifting of buckling patterns in x and y-direction does not constitute an alteration of the problem and its solution. Therefore, a superposition of a buckling pattern and the same buckling pattern shifted arbitrarily in the $x-y$ plane is also a valid buckling pattern having the same eigenvalue. On this basis, it can be shown that the buckling pattern reported by Stiftinger and Rammerstorfer [1997] (eq. 5.3) is merely a superposition of two buckling patterns used in this work (eq. 3.1), namely the patterns for (a, φ) and $(a, -\varphi)$. This superposition is only permissible if the pair of solutions (a, φ) and $(a, -\varphi)$ belong to a double eigenvalue.

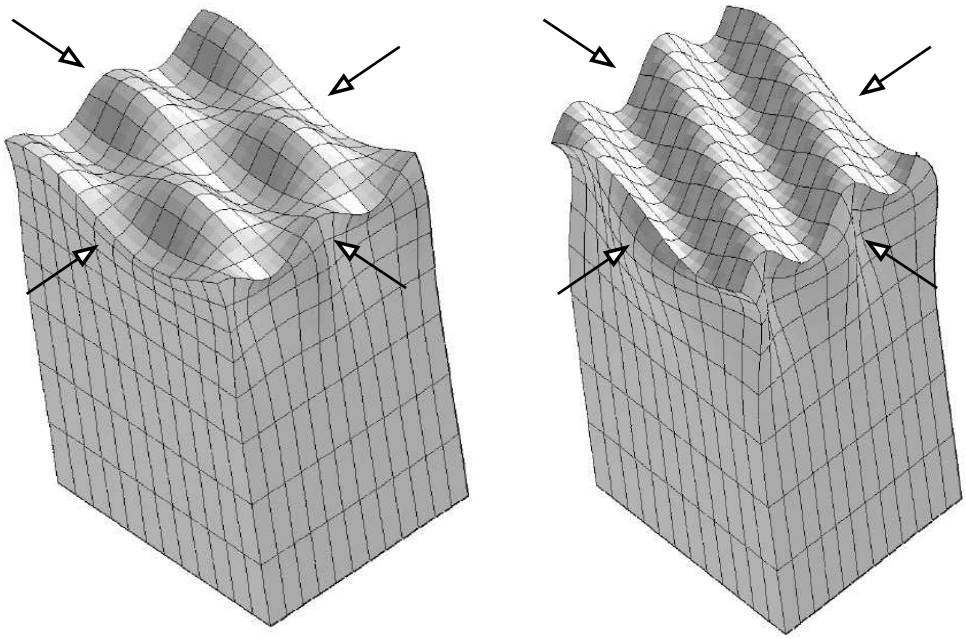

Stiftinger model present model

Figure 5.1: Deformation pattern of the Stiftinger model and the new model

These double eigenvalues exist only if the problem is symmetric with respect to φ (i.e. loading only in the axes of orthotropy). This proves that the approach of Stiftinger and Rammerstorfer [1997] covers only a subset of the buckling patterns of the new approach and in this subset the two approaches are equivalent.

Using the sine theorems and the superposition mentioned above, it can be shown that the two deformation patterns are connected by the following geometric relations:

$$\varphi = \arctan\left(\frac{a_x}{a_y}\right), \qquad a_r = a_x \cos\varphi \,. \tag{5.4}$$

As a result, the wrinkling loads and corresponding wrinkling patterns can be calculated accurately in this special case of biaxial compression in the axes of orthotropy, using either of the analytical models or the FE model. However, the deformation pattern used by Stiftinger and Rammerstorfer [1997] is structurally unstable (if both wavelengths a_x and a_y are finite).

Each of the two analytical deformation patterns is a Ritz ansatz with two free variables. It is clear that the ansatz chosen by the author is superior in terms of generality and

applicability while still having the same number of variables and, therefore, comprising comparable analytical and numerical cost.

Using the FE unit cell model it is easily demonstrated how the eigenvalues split up, by perturbing the model. The unit cell model was loaded exactly in the directions of orthotropy leading to a quadruple eigenvalue of the deformation mode reported by Stiftinger and Rammerstorfer [1997]. By adding a perturbation in form of a very small shear force in the face layers additionally to the compressive forces (which are oriented in the material directions), the quadruple eigenvalue splits up into two double eigenvalues both of which show the deformation mode used in this work. The critical load (eigenvalue) is practically not affected by this perturbation. This behavior again demonstrates the structural instability of the pattern reported by Stiftinger and Rammerstorfer [1997]. The eigenvalues and corresponding modes calculated by these unperturbed and perturbed FE calculations are shown in fig. 5.2. The absolute eigenvalues given are not of any relevance, they are merely included to show that the eigenvalues are hardly affected by the perturbation.

The unit cell FE calculations always lead to (at least) double eigenvalues. This is due to the fact that the phase angle of the sine wave buckling pattern is not determined, because the problem is formulated on an infinite plate. Therefore, two eigenmodes occur at the same eigenvalue and both eigenmodes are sine waves with the same wave angle and wavelength but different phase angles. The deformations caused by the same sine wave at any other phase angle are merely superpositions of the two results already obtained and, therefore, not a valid eigenmode. In other words, a similar sine wave at another phase angle is not orthogonal to the eigenmodes already obtained. Thus, one eigenmode in terms of a_r and φ always corresponds to two FE eigenmodes which occur at the same eigenvalue.

5.3 Face layer orthotropy

In order to capture the influence of face layer orthotropy on wrinkling, a sandwich plate with an unidirectionally glass fiber reinforced face layer (orthotropic, $E_x^{\mathrm{u}} = 58000\mathrm{N/mm}^2$, $E_y^{\mathrm{u}} = 5500\mathrm{N/mm}^2$, $\nu_{xy}^{\mathrm{u}} = 0.3$, $G_{xy}^{\mathrm{u}} = 3000\mathrm{N/mm}^2$, $t^{\mathrm{u}} = 0.1\mathrm{mm}$) and a thick honeycomb core (approximated as transversely isotropic continuum, $E_z^{\mathrm{c}} = 41.3\mathrm{N/mm}^2$, $E_x^{\mathrm{c}} = E_y^{\mathrm{c}} = 1\mathrm{N/mm}^2$, $\nu_{xz}^{\mathrm{c}} = \nu_{yz}^{\mathrm{c}} = 0$, $\nu_{xy}^{\mathrm{c}} = 0.3$, $G_{xz}^{\mathrm{c}} = G_{yz}^{\mathrm{c}} = 10.3\mathrm{N/mm}^2$) is evaluated. The loading of the face layer is assumed to be a uni-axial compressive membrane force P_ψ at an angle ψ to the major axis of orthotropy of the face layer (x-axis). ψ is defined analogously to the definition of the angle φ of the wave pattern (see fig. 3.1). In terms of the plate equation

Unperturbed calculation

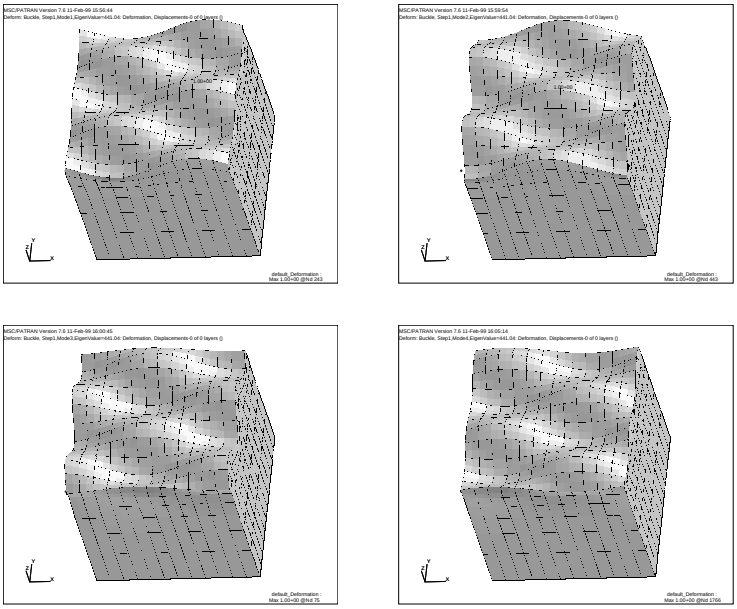

Eigenvalue=441

Perturbed calculation

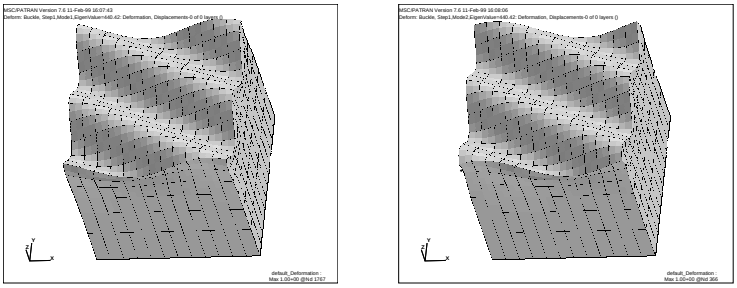

Eigenvalue=440

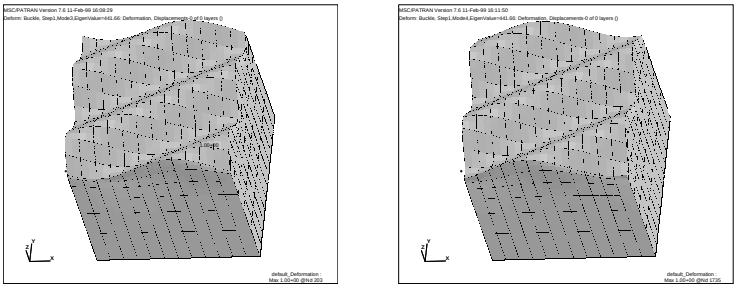

Eigenvalue=442

Figure 5.2: Wrinkling modes calculated by FE

eq. 3.2, this leads to P_x, P_y and P_{xy} being different from zero. Only in the case of $\psi = 0°$ and $\psi = 90°$ (compression in the directions of the material axes), the results of Stiftinger and Rammerstorfer [1997] can be applied, since in these cases the wave direction φ is *a priori* known to be 0° and 90°, respectively. For all other values of ψ, φ is unknown, and the small unit cell FE calculations are used for verification.

The corresponding results presented in fig. 5.3 show the parameters critical membrane force P_ψ^{cr}, angle φ^{cr} and half-wavelength a^{cr} over the angle of the load application ψ. The agreement between the analytical and the numerical results is excellent for all parameters. The difference between φ and ψ due to the orthotropy of the face layer is clearly displayed. The wrinkling angle φ is always larger than the load angle ψ, i.e. the wrinkling pattern does not form in the direction of the largest compressive force, but tends to rotate towards a direction where the stiffness of the face layer is smaller (i.e. towards the y-axis). Imagining isotropic face layers instead, φ and ψ would always be identical, and the wrinkling load and wavelength would be independent of ψ.

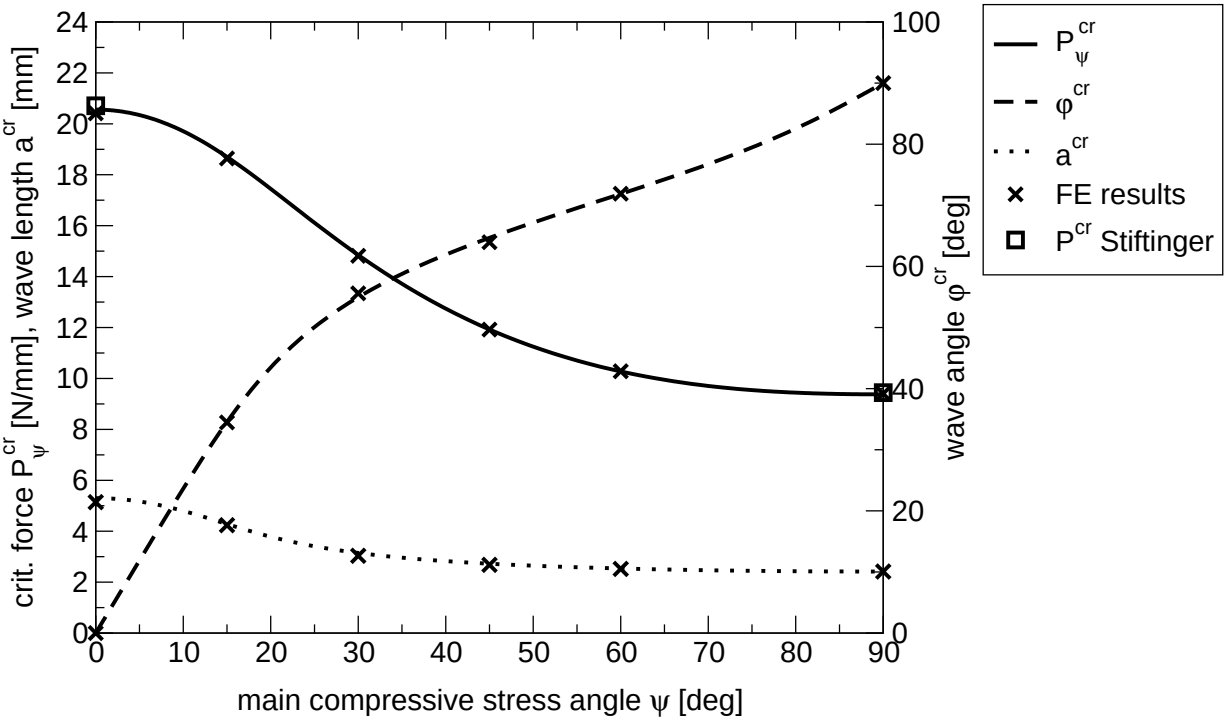

Figure 5.3: Compressive load at variable angle ψ, transversely isotropic core

An example of an FE unit cell result is given in fig. 5.4 which displays the optimized result corresponding to fig. 5.3 at $\psi = 60°$. The FE unit cell model shows considerable

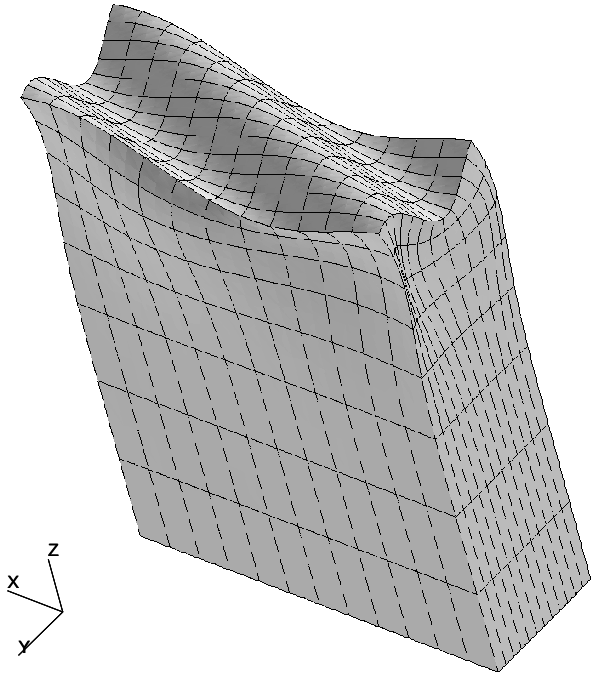

Figure 5.4: FE unit cell result corresponding to fig. 5.3 at $\psi = 60°$

in-plane deformations of the core which form due to the rather low in-plane stiffness of the core.

As second example, a combined loading by compression and shear is shown. In this case, an isotropic foam core material ($E^{\mathrm{c}} = 100\mathrm{N/mm}^2, \nu^{\mathrm{c}} = 0.3$) in combination with a face layer made of the GFRP material defined above and $t^{\mathrm{u}} = 0.24$ is used. The load is a combination of constant compression ($\rho^{\mathrm{u}} = 1\mathrm{N/mm}$) and variable shear ($\zeta^{\mathrm{u}}$) in the material coordinate frame of the face layer. The results are shown in fig. 5.5. On the left border, the shear fraction $\zeta^{\mathrm{u}} = 0$ and, therefore, the case of uniaxial compressive loading is represented. Further to the right an increasing shear force acts additionally to the constant compressive force, and the critical load level P^{cr} is, therefore, decreasing. The agreement between the new model and the reference models is extremely good. To the far right ($\zeta \to \infty$), the solution converges to the case of pure shear load, where the agreement between the new model and the FE results is also excellent. It can already be seen from fig. 5.5, that a pure shear load leads to a wrinkling angle higher than 45° in analogy to the discussion of the wrinkling angle in fig. 5.3.

The two examples above provide a glimpse of the large parameter range where the new model can be used in contrast to other analytical wrinkling approaches.

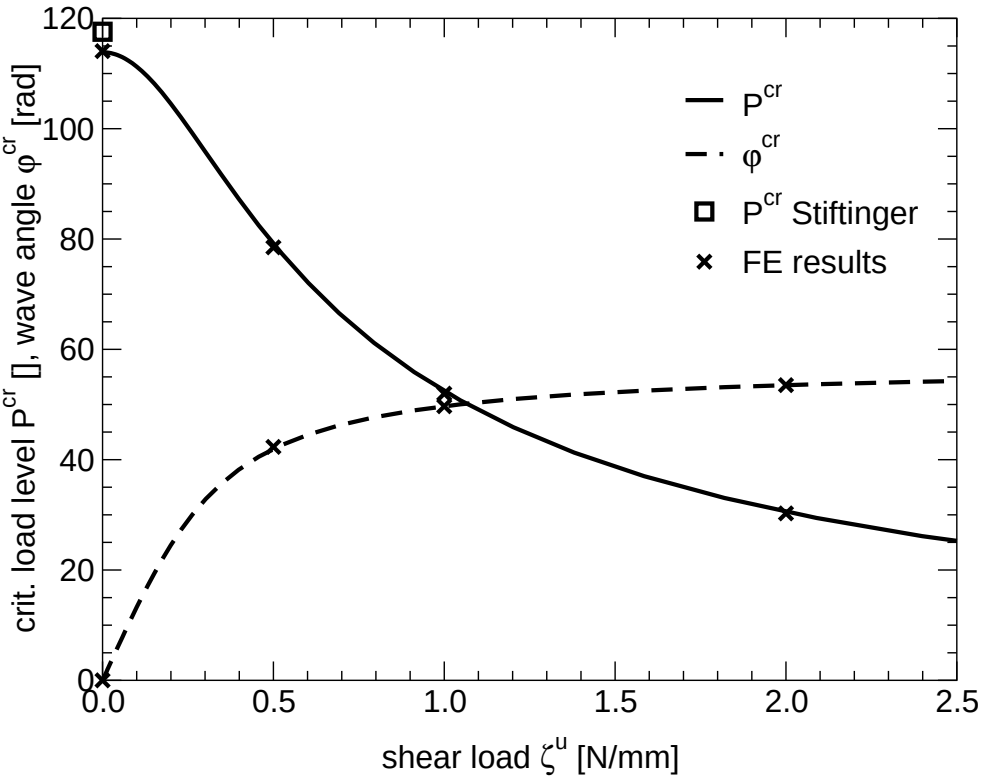

Figure 5.5: Constant compressive load with variable shear load, isotropic core

5.4 In-plane core orthotropy

In the course of the derivation of the new model, a transversely isotropic core material law has been chosen in order to strongly simplify the derivations. Within sandwich construction, the core materials mainly used are foams, honeycombs and balsa. Foams and balsa cores can be quite accurately described using this transversely isotropic material law. The situation is more complex when honeycomb cores are to be considered.

Due to the manufacturing process of real honeycombs, a part of the walls of the honeycomb have double thickness as compared to the others. This leads to a fully orthotropic material behavior [e.g. Gibson and Ashby, 1997] which can not be captured correctly within this new model for wrinkling. Essentially, the in-plane Youngs (E_x^c, E_y^c) and shear moduli (G_{xz}^c, G_{yz}^c) differ by a factor of about 2. It was shown in section 3.2.2 that this leads to coupling terms in the stiffness matrix of the material which have been neglected. In order to estimate the resulting effects on the wrinkling behavior, the following model calculations are performed.

Since the influence of the shear moduli (G^c_{xz}, G^c_{yz}) on the critical load is considered to be much higher than that of the in-plane Youngs moduli (E^c_x, E^c_y), the following special case is taken into account:

$$E^c_x = E^c_y \quad \nu^c_{xz} = \nu^c_{yz} \quad \text{and} \quad G^c_{xz} \neq G^c_{yz} \,. \tag{5.5}$$

As long as the difference between G^c_{xz} and G^c_{yz} is less than a factor of five, the resulting coupling term $C_{rzsz}(\bar{\vartheta})$ (eq. 3.12) will generally be smaller than $G^c_{rz}(\varphi)$ (but not by orders of magnitude!). As explained above, sandwich core materials hardly exceed a factor of 2 in the ratios of in-plane moduli. In order to be on the safe side, the model calculation is performed with a factor of about 3 between G^c_{xz} and G^c_{yz}.

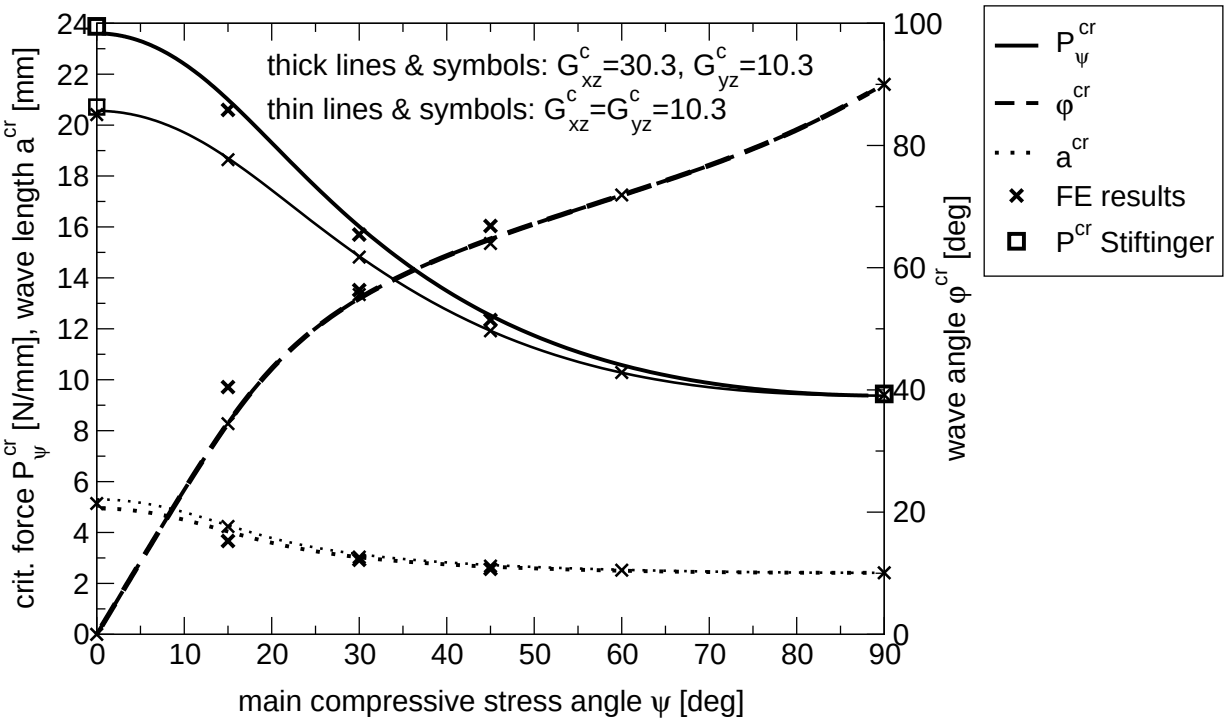

Figure 5.6: Compressive load at variable angle ψ, orthotropic core

The setup of the model is identical to fig. 5.3, only the core shear modulus G^c_{xz} has been altered to a higher value. It is on purpose that a model with a very thick core is used for this evaluation, since it is assumed that the core material law is of higher influence to the wrinkling problem than in the case of a thin core. The results are displayed in fig. 5.6. The thin lines and symbols are the results that were shown in fig. 5.3 and are described

in the previous section. Additionally, the bold lines show the results for the same problem with an increased core shear modulus G^c_{xz}.

Although the coupling terms mentioned above are neglected in the new analytical model, the analytical results still show a reasonable agreement with the FE results, especially concerning the wavelength and critical load. Concerning the wave angle, the FE and the analytical results differ a bit more within a significant range. It is obvious, that the results do not show the same high quality as in the case of $G^c_{xz} = G^c_{yz}$. However, the extension of the new model towards different out-of-plane shear moduli leads to very good results in the parameter region considered. The coupling term seems to be of limited effect as compared to the effect of a varying G^c_{rz} (i.e. $1/C_{rzsz}(\bar{\vartheta})$ in eq. 3.12), which is included in the new model and leads to the differences between the thin and bold lines in fig. 5.6.

It is concluded that the application of the new model to sandwich plates with orthotropic honeycomb cores does not lead to significant errors. Thus, the new model can be used for all common sandwich core materials.

5.5 A complex plate problem

5.5.1 Objectives

So far, the results presented have been confined to rather simple sandwich configurations – mainly to symmetric sandwiches under different loading conditions. The analytical approach derived in this work is capable of dealing with much more complex sandwich plate configurations. Since the new analytical model already includes 28 input parameters (material values, geometrical dimensions and loading parameters), it does not seem to make semse to perform parametric studies concerning all these input parameters. It has, therefore, been decided to conduct a thorough study of a rather complex example problem.

The example problem is chosen in a way that it can be used to investigate the applicability of the main assumption within this approach, namely the deformation pattern used in the Ritz ansatz. In this ansatz (eq. 3.8) it is assumed, that the wave length a_r and the wave angle φ are constant throughout the core thickness. Whether this assumption is met in reality cannot be predicted easily: Regarding an infinitely thick sandwich, where the two face layers do not interact, it is possible that both face layers wrinkle at the same critical load, but at different wave lengths and/or wave angles (i.e. by choosing different materials and loading conditions for the two face layers). If the face layers are really uncoupled,

this problem is solved accurately by the new model presented here and the resulting double eigenvalue is calculated. By reducing the core thickness successively, the interaction between the two face layers gains in influence. It is thought that this interaction might lead to an adaptation of the two wavelengths and wave angles in the sense that they are *not* constant throughout the core thickness. One could expect a wrinkling pattern where the two face layers show a different wrinkling pattern in terms of a_r and φ and the core is deformed in a more complicated way, connecting the two face layers. In this intermediate regime of rather thick cores, it is not obvious which deformation pattern is going to form and whether it corresponds to the Ritz ansatz used. This is to be clarified via the example problem. At very small core thicknesses, it is clear, that the wrinkling wavelength and wave angle have to be identical on both face layers.

5.5.2 Problem description

The setup of the example problem is shown in fig. 5.7. The sandwich plate consists of two identical unidirectional carbon fiber reinforced face layers which are oriented at 90° with respect to each other ($\gamma = 90° \Rightarrow E_x^{\mathrm{u}} = E_y^{\mathrm{l}} = 117000\mathrm{N/mm}^2$, $E_y^{\mathrm{u}} = E_x^{\mathrm{l}} = 8000\mathrm{N/mm}^2$, $G_{xy}^{\mathrm{u}} = G_{xy}^{\mathrm{l}} = 2700\mathrm{N/mm}^2$, $\nu_{xy}^{\mathrm{u}} = \nu_{xy}^{\mathrm{l}} = 0.4$, $t^{\mathrm{u}} = t^{\mathrm{l}} = 1\mathrm{mm}$). The core is chosen to be a honeycomb core ($E_z^{\mathrm{c}} = 55.2\mathrm{N/mm}^2$, $E_x^{\mathrm{c}} = E_y^{\mathrm{c}} = 0.0552\mathrm{N/mm}^2$, $\nu_{xz}^{\mathrm{c}} = \nu_{yz}^{\mathrm{c}} = 0$, $\nu_{xy}^{\mathrm{c}} = 0.3$, $G_{xz}^{\mathrm{c}} = G_{yz}^{\mathrm{c}} = 26.2\mathrm{N/mm}^2$, $G_{xy}^{\mathrm{c}} = 0.0212\mathrm{N/mm}^2$), since the beam problems already have shown that honeycomb cores lead to a more complex behavior regarding interaction and mode changes. The coordinate system of the sandwich plate (xyz - system, defined by the material direction of the upper face layer) is oriented at 45° to a global coordinate reference frame (123 - system) which is used to define the boundary conditions and the deformation based loading. The sandwich plate is fully clamped at edge 3. The edges 1, 2 and 4 are also fully clamped, with the exception of the movement in 1 - direction, which is allowed. The loading is introduced by forcing a movement of edge 1 in direction 1, leading to a prescribed global strain $\bar{\varepsilon}_{11}$ (the notation corresponds to the description of lamination theory in Rammerstorfer [1992]). This configuration leads to a constant strain field (and stress field) throughout the plate. Apart from $\bar{\varepsilon}_{11}$, all other plate strains ($\bar{\varepsilon}_{22}$, $\bar{\varepsilon}_{12}$) and rotations ($\bar{\varphi}'_{11}$, $\bar{\varphi}'_{22}$, $\bar{\varphi}'_{12}$) are zero. Due to the rotations being clamped on all edges of the plate, the deformed plate remains flat, despite its unsymmetry.

Using lamination theory, the plate section forces and moments can be calculated. Due to the unsymmetry of the sandwich plate, the stiffness matrix of the plate contains coupling terms which lead to the bimoment m_{12} being non-zero. The bending moments m_{11} and

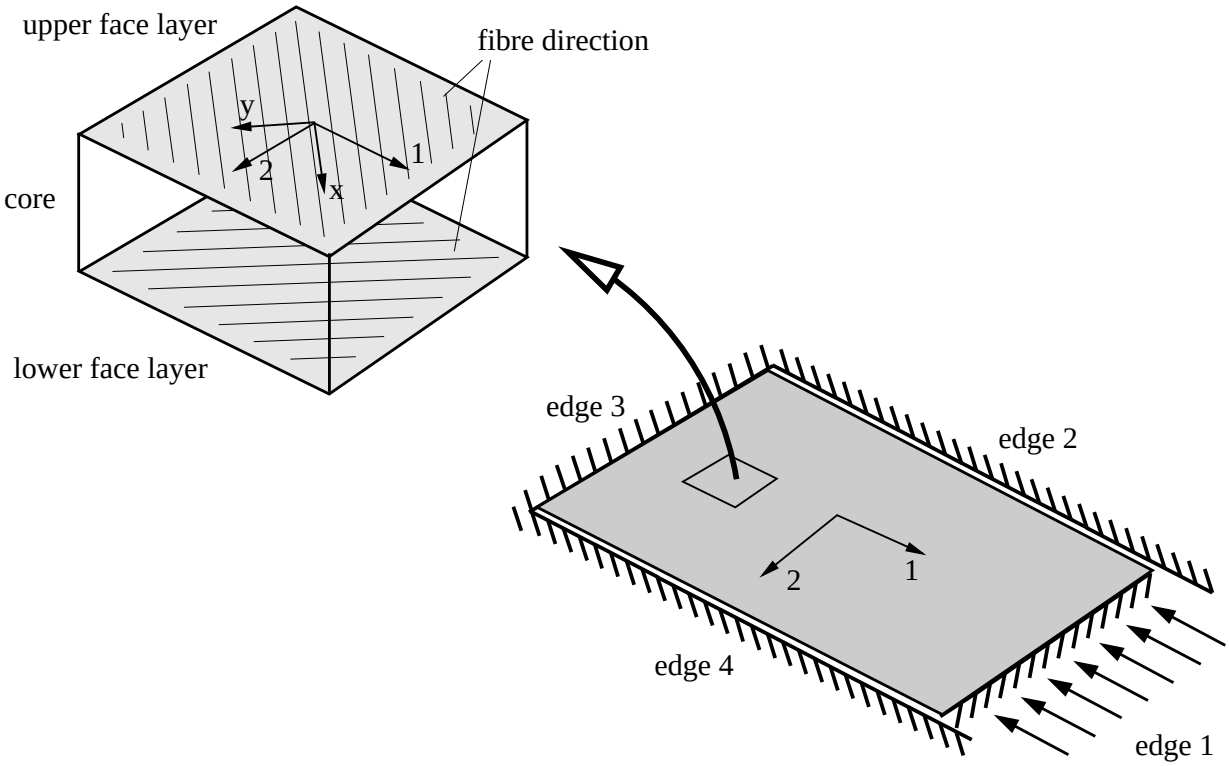

Figure 5.7: Setup of example problem

m_{22} are zero due to the fact that the face layers, despite their different orientations, have the same elastic properties in loading direction. The section forces of the plate (n_{11}, n_{22}, n_{12}) are all non-zero.

Starting from the prescribed strain vector of the sandwich plate with $\bar{\varepsilon}_{11} = 1 \times 10^{-4}$ and using the appropriate coordinate transformations and stiffness matrices of the face layers, the loading of the sandwich can be calculated in terms of the loading parameters for the new model:

$$\begin{aligned} \rho^{\mathrm{u}} &= 6.076\mathrm{N/mm},\ \xi^{\mathrm{u}} = 0.5662\mathrm{N/mm},\ \zeta^{\mathrm{u}} = 0.27\mathrm{N/mm} \\ \rho^{\mathrm{l}} &= 0.5662\mathrm{N/mm},\ \xi^{\mathrm{l}} = 6.076\mathrm{N/mm},\ \zeta^{\mathrm{l}} = 0.27\mathrm{N/mm} \end{aligned} \tag{5.6}$$

Essentially, the high stiffness in fiber direction leads to the face layers taking up load mainly in their fiber direction. Bearing in mind that these loading parameters have been formulated in the coordinate frame of the upper face (xyz system) and that the lower face is oriented at 90° with respect to the upper face, it becomes clear that both faces are loaded equivalently in their own material coordinate frames. In the case of a very thick core, there would be two eigenvalues at the same load level which are based on different

wave directions. The problem is defined such that these directions differ significantly (see fig. 5.8 at high values of c) in order to investigate the above effects associated.

5.5.3 Analytical results

The analytical results for the example problems are shown in fig. 5.8. For small core thickness values ($c \leq 17$mm), shear crimping is again the critical mode. Since shear crimping is a pure core problem, the direction of wrinkling is the loading direction (1-direction) marked by $\varphi^{cr} = 45°$. The corresponding wave length a_r^{cr} is very large as explained in section 3.2.4. As the core thickness reaches about 17mm, the failure mode switches to a snake mode wrinkling. This snake mode wrinkling leads to a double eigenvalue with different values of φ^{cr} which are symmetric with respect to the loading direction. P^{cr} and a_r^{cr} are identical for both modes, as expected. This regime of the core thickness leads to the largest critical load level. At c=22mm the mode switches to the ideal symmetric hourglass wrinkling in loading direction, and the critical load level decreases. As c reaches 164mm the mode type remains an hourglass mode, but a mode jump leads to a double eigenvalue as φ^{cr} differs again from the loading direction. In this regime, the hourglass mode is not ideally symmetric anymore, but the magnitude of the deflections of the upper and lower face layers differ.

Looking closer at the mode jumps described above, these jumps are identified to be structural instabilities of the system, since a small change in a system parameter (in this case the core thickness) leads to qualitatively different results in terms of wave length and wave angle.

Fig. 5.9 shows a detail of fig. 5.8 in the region where the first two mode jumps take place. The new model is capable of calculating secondary eigenvalues as well, which is displayed within the figure. The thick lines correspond to the overall critical values and, the thin lines with the markers correspond to the different mode shapes.

It becomes clear that, although this example still comprises a symmetry about the 1-direction (i.e. $\varphi = 45°$) and bending is eliminated, the results are already quite complex and several mode jumps occur. In the parameter range of the core thickness which has been investigated the critical load level differs by a factor of about two. This shows the need for an accurate wrinkling calculation which is able to deal with such a complex situation correctly when designing sandwich plates.

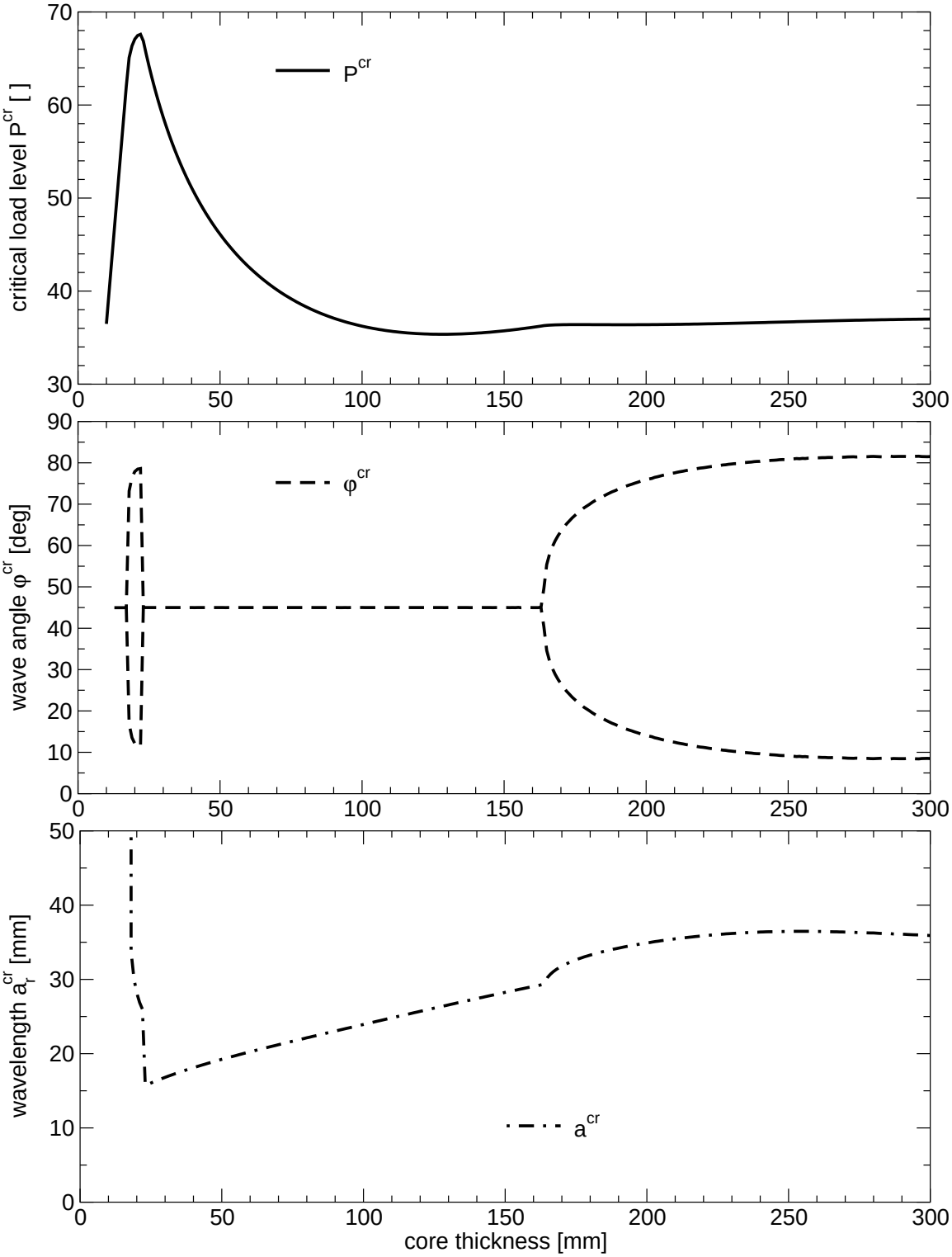

Figure 5.8: Analytical results for the example problem

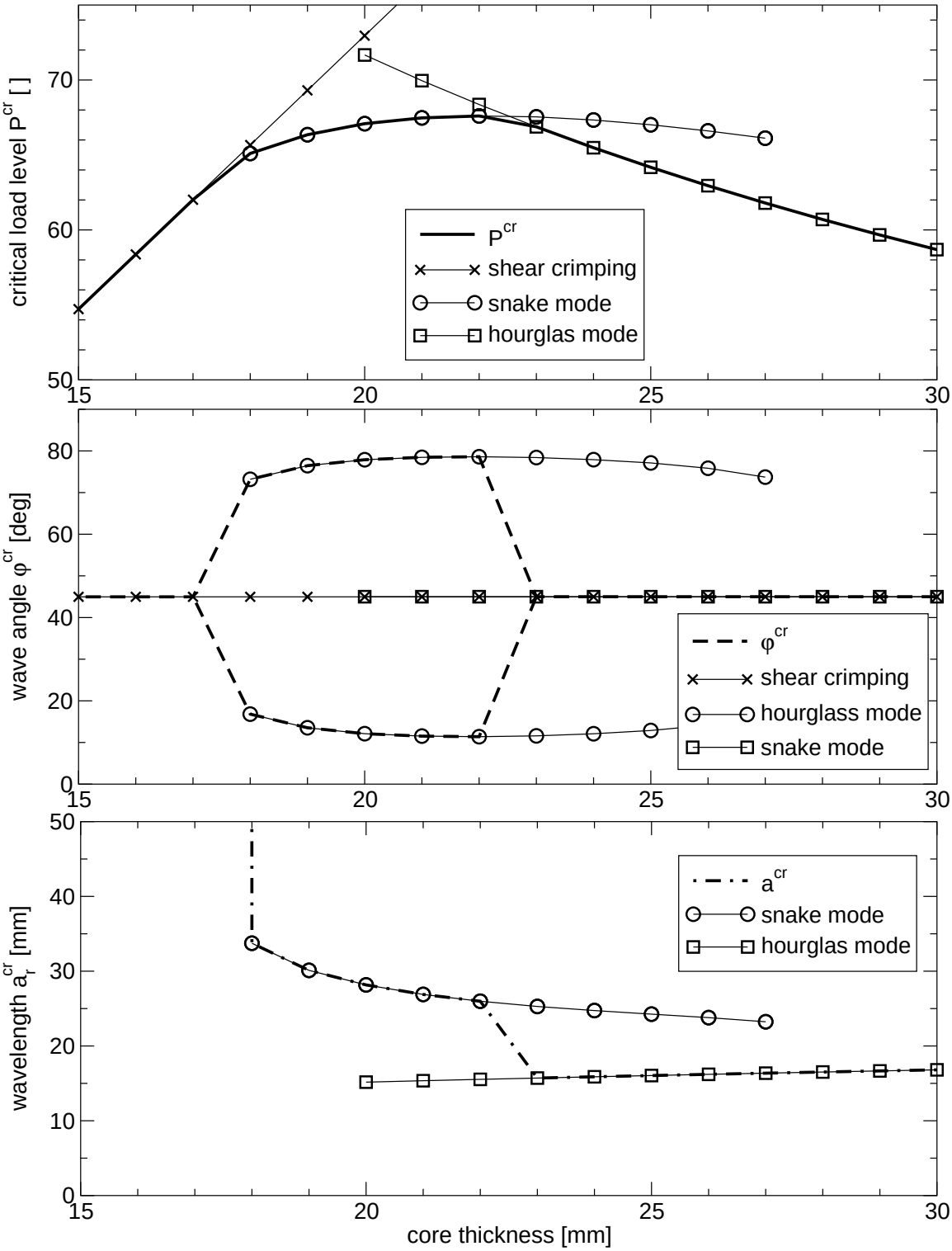

Figure 5.9: Analytical results for the example problem, mode changes

5.5.4 FE results

The results of the new model were verified with the different FE approaches introduced in section 5.1. The parameters eigenvalue, wave length and wave angle were evaluated from the FE results, and fig. 5.10 shows the corresponding results together with the results of the new analytical model. The FE results are in very good agreement with the new model. The FE results show critical loads which are mostly a little bit lower as compared to the analytical approach, a fact which was also observed by Hadi [2001] (concerning 2D FE wrinkling calculations). The results of the large FE unit cell models are shown with error bars which indicate the range of a^{cr} and φ^{cr} which is covered by the deformation pattern which has formed, since the deformation pattern can only change step wise between discrete configurations in these models (as shown in eq. 5.1). The error bars are thus drawn up to to the next possible configuration. The size of the error bars is depending on the aspect ratio of the unit cell and, therefore, varies throughout the calculations. The error bars are meant to give an indication of the step size involved. They are not error bars in the usual sense since the problem is discrete and coupled regarding a_r and φ. Depending on the individual influence of these parameters, it is possible (but not very likely) that errors occur which exceed the error bar size.

Shear crimping itself can generally not be described by FE models due to the large wavelength on the one hand and the interaction effects leading to global buckling on the other hand. As discussed in the literature chapter, shear crimping alone can not be the decisive global failure mode of a sandwich, since the interaction with the Euler buckling load of the sandwich always leads to an even lower critical load (eq. 2.1). These interaction effects are also thought to be the reason for the loss in agreement between the small unit cell FE results and the analytical results as the core thickness gets close to the core thickness leading to shear crimping. In this region the model size of one wavelength seems to be already large enough to lead to these interaction effects. In the case of large FE models, the increased model size (10 waves) leads to the fact that the lowest FE eigenvalues correspond to local eigenvalues only for core thickness values above 25mm. Therefore lower core thickness values could not be investigated with these models. However, the region below c=25mm is not of practical interest regarding wrinkling, since global buckling (and not wrinkling) limits the load carrying capacity of sandwiches in this regime. Moreover, it is clear that this analytical approach should not be used if the global dimensions of the sandwich are only two or three wave lengths as in these cases. In order to investigate failure of sandwiches in this regime, unified models have to be used.

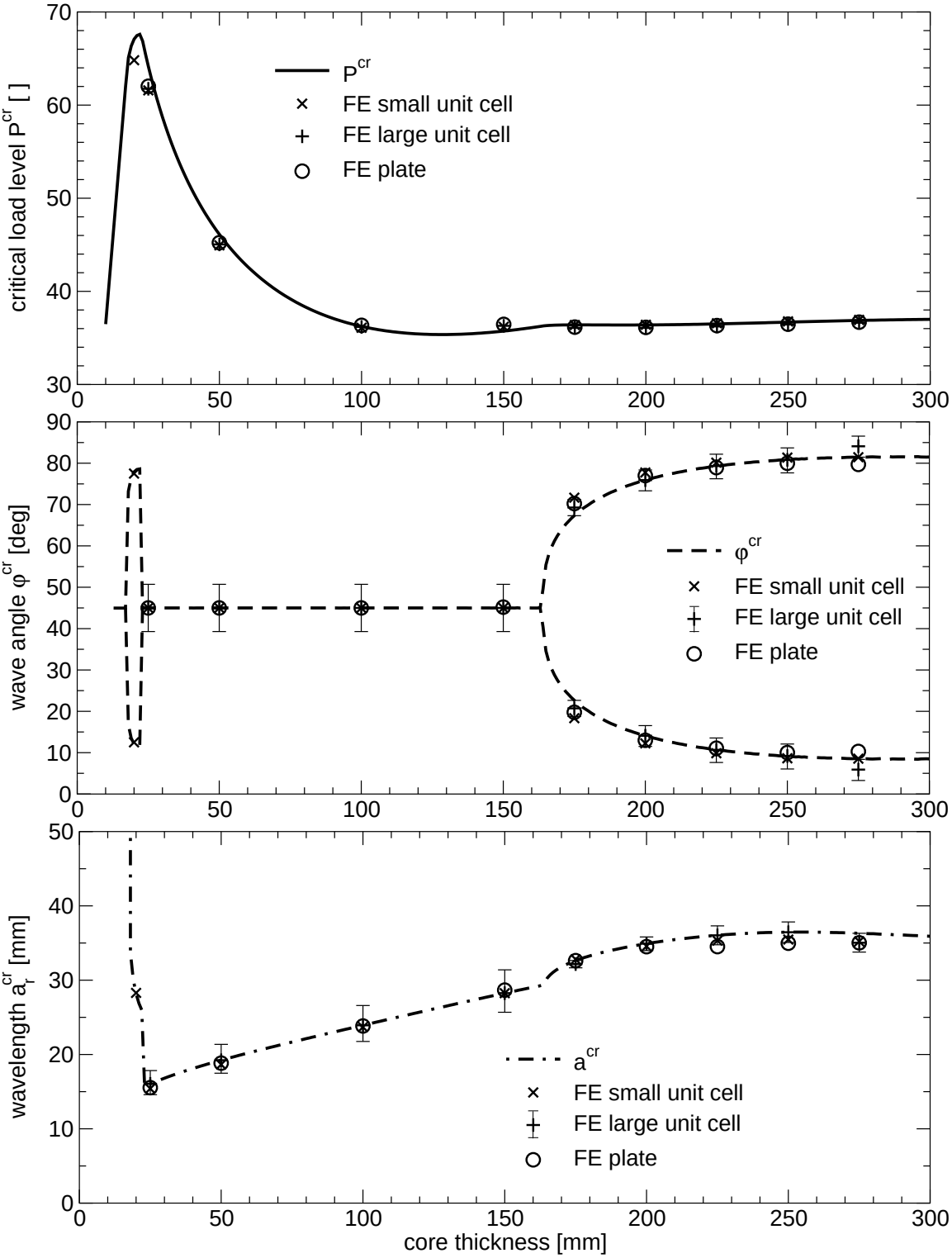

Figure 5.10: Analytical and FE results for the example problem

As explained earlier, one analytical eigenvalue always leads to two FE eigenvalues in the case of unit cell models. This was also the case here. In the region of double analytical eigenvalues, the FE unit cell models lead to quadruple eigenvalues and the corresponding FE mode shapes are different superpositions of the analytically calculated eigenfunctions. Therefore, the visual interpretation of the FE mode shapes is rather difficult. The situation is similar regarding the FE plate models, where numerous very closely spaced eigenvalues occur at the wrinkling load level. The small unit cell models show exact sine patterns (fig. A.1[1)]), whereas the large FE unit cell models sometimes show slightly disturbed or blurred patterns (fig. A.3). This is thought to be due to the fact that the overall dimensions of the large unit cell model always enforce a wave length and a wave angle which is slightly different from the exact values and thus disturbs the deformation pattern. Moreover, numerical inaccuracies may play a role. It is observed that the multiple eigenvalues encountered differ in terms of critical load (around 0.1%) as opposed to the small unit cell models, where the multiple eigenvalues always lead to exactly the same eigenvalue. It can be seen from the deformation plots, that the disturbances encountered are not pronounced and do not seem to be of major influence.

All FE models did *not* show a variation of wave length or wave angle throughout the core thickness. This is clearly visible in the case of a single analytical eigenvalue as shown in fig. A.2. In the case of a double eigenvalue, the superposition of the two modes leads to a more complex pattern which has to be judged carefully (see fig. A.3). By evaluating the deflections w in thickness (z) direction at different values of z throughout the core thickness, it can be shown, that the FE mode shapes consist of a superposition of the two waves which result from the new analytical model (a_r, φ and a_r, $-\varphi$) with a constant wave angle and wave length, similar to the situation encountered in section 5.2. A set of these sections corresponding to the large unit cell model at c=175mm is shown in figs. A.4 and A.5. The fringes mark the vertical deflection of the corresponding section, dark and light grey marking positive and negative displacements respectively. The plots for z=0mm and z=175mm correspond to the face layer deflections shown in fig. A.3. The figures show that the wave angles and wave lengths of the patterns are practically constant throughout the core thickness in both cases of c =150mm and c =175mm (as in all other cases). As explained in the objectives section of this example problem, this result is of high value, since it shows that the Ritz ansatz chosen is valid in this parameter regime of face layer interaction and different possible wrinkling directions, which was not obvious beforehand.

The results of the FE plate model are also in very good agreement with the analytical

[1)] The figures mentioned in the following are located in the Appendix.

results. Regarding the deformation patterns (fig. A.6) it can be seen that the plate model is large enough to incorporate a zone in the middle of the plate which is hardly affected by the boundary conditions. This was also checked numerically by using different plate model sizes. The evaluation of the deformation pattern of the plate model was done as in the case of the large FE unit cell model and the corresponding fringe plots are given in figs. A.7 and A.8. Again, the wave length and the wave angles are constant throughout the core thickness. The results for other values of the core thickness also agree with the new analytical model but are not displayed. The case of c=175mm is displayed extensively within this work because it is thought to be the most critical case since it is close to the bifurcation point and comprises a double eigenvalue.

Comparing the verification methods, FE plate model and large FE unit cell model, it is concluded that the plate model is superior due to the following reasons:

- The plate model has a continuous results space, as opposed to the step wise results space indicated by the error bars in fig. 5.10 which are of considerable size. The model size used in this study (10 waves) proved to be large enough to obtain a region within the FE models where boundary effects have diminished. Thus, the explicit elimination of the boundary effects via the large unit cell approach is not necessary anymore, but the drawback of the large unit cell approach, namely the step wise results space is still of influence.

- The large unit cell model uses a complicated definition of the boundary conditions which has to be programmed individually whereas the plate model is generated most easily.

- The plate model needs shorter computing time at the same model size as compared to the large unit cell model.

The small unit cell model has proven throughout this study to be a reliable verification method which needs only a very small fraction of the computing time required by the large models. However, its drawback is the lower generality and the programming involved.

5.5.5 Conclusions

The new analytical model presented within this work has succeeded in calculating the critical wrinkling loads and mode shapes of this rather complex sandwich plate problem

accurately. The FE calculations did not show deformation patterns which differ significantly from the Ritz ansatz chosen for this work. This example problem was explicitly chosen in order to trigger other deformation patterns. Since this was not the case, it is thought that this analytical approach is quite generally applicable. The calculation of the wrinkling angle φ^{cr} also proved to be reliable. This is of interest regarding possible future developments in the direction of post-wrinkling behavior, since the direction of wrinkling is a very important factor for calculating the structural behavior of a sandwich in the post-wrinkling regime. Generally, the agreement between the new approach and the verification models is better than it was to be expected. The FE verification methods which have been developed within this study show good agreement and their different advantages and disadvantages have been evaluated.

Chapter 6

Conclusions

Within this work, an analytical wrinkling model is presented which is formulated in a very general way in terms of sandwich configuration and loading as compared to other wrinkling approaches in the literature. Besides, the use of a Ritz ansatz leads to a numerically efficient calculation scheme. The deformation field used for the Ritz ansatz is rather simple and comprises only two free variables. Nevertheless, it proved to be able to describe the correct deformation fields even in the case of complex sandwich configurations. In contrast to practically all other wrinkling approaches to the wrinkling problem, the new model uses a complete continuum description of the core instead of the usual 'anti-plane' core simplifications.

This new model was compared to different analytical and FE verification models. The agreement in terms of critical load and buckling pattern is very good in all cases investigated. The results indicate that the new model is very generally applicable and covers most sandwich configurations which are currently used.

The results presented within this work show a number of new and important effects which govern the occurrence of wrinkling. The influence of the in-plane core stiffness on the wrinkling behavior is the most basic and most important effect discovered. This issue is, therefore, investigated in much detail in this work. It is shown, that the analytical models used in the sandwich literature are based on different assumptions regarding the in-plane core stiffness and that this difference is very important and may lead to substantial errors, both qualitatively and quantitatively. This problem is pronounced due to the fact that the in-plane core stiffness is extremely low in the case of honeycomb cores, leading to unexpected effects. The new model takes the in-plane core stiffness correctly into account

and can be used, in contrast to practically all other approaches, with both foam and honeycomb cores. Regarding the classical design formulas, it is observed that they have rather limited ranges of applicability which cannot always be defined in a straightforward way and which are given incorrectly in the literature. Essentially, the wrinkling models used up to now are either only applicable to honeycomb cores (highly orthotropic), or only to foam cores (isotropic) and can only be used for a limited range of core thickness values. Closely connected to this finding, it is shown that the widespread rule of a c/t ratio above 50 ensuring a 'thick' sandwich core is valid only in the case of isotropic cores. In the case of honeycomb cores, the situation is much more complex.

Since the new model is not limited to symmetric sandwiches or symmetric loading it can also be applied to the wrinkling of thin sandwiches due to bending loads. This has, for the first time, been subject to a thorough investigation, and the results show that the usual assumption of a "rigid"tensile face layer in bending (i.e. no buckling deformations in this layer) may lead to a severe overestimation of the critical load. This effect was anticipated, but has not been quantified before.

The new model is able to calculate the wrinkling loads and patterns in the wide range of unsymmetric orthotropic sandwiches under general loading conditions. Due to the lack of such general solutions, these sandwich configurations have not been the subject of investigation up to now. A number of example problems were studied in this parameter regime and the corresponding results are conclusive and give a valuable insight into wrinkling of such sandwiches. The examples were verified by different three dimensional FE models and the agreement of the results is more than satisfactory. The FE verification models partly use a periodic unit-cell formulation which seems to be a novelty in stability calculations such as wrinkling. The different FE verification models are compared in terms of efficiency and generality and it is observed that the small unit-cell formulation in conjunction with an optimization scheme leads to a rather general and very efficient FE wrinkling calculation. However, large but basic FE models are the most general verification method, the drawback being the substantial numerical effort which is drastically limiting the applicability of this method.

Appendix A

Deformation plots for section 5.5

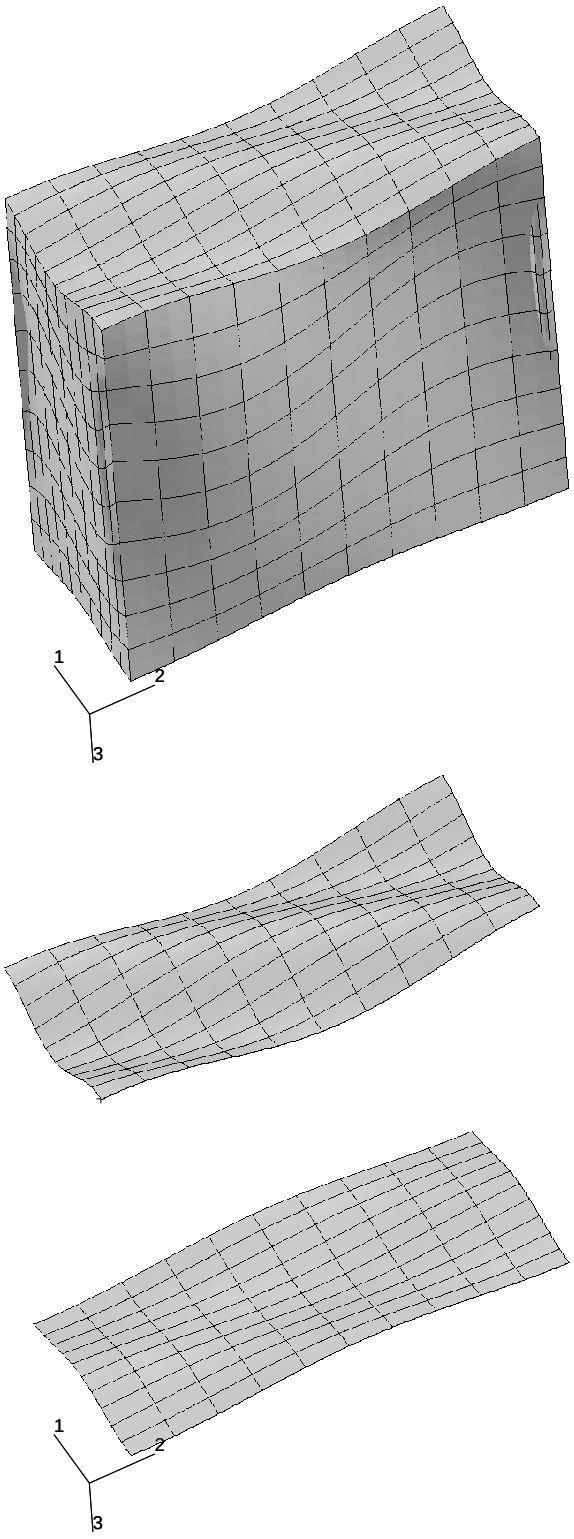

Figure A.1: FE buckling pattern, small unit cell, c=175mm, bottom: transparent core

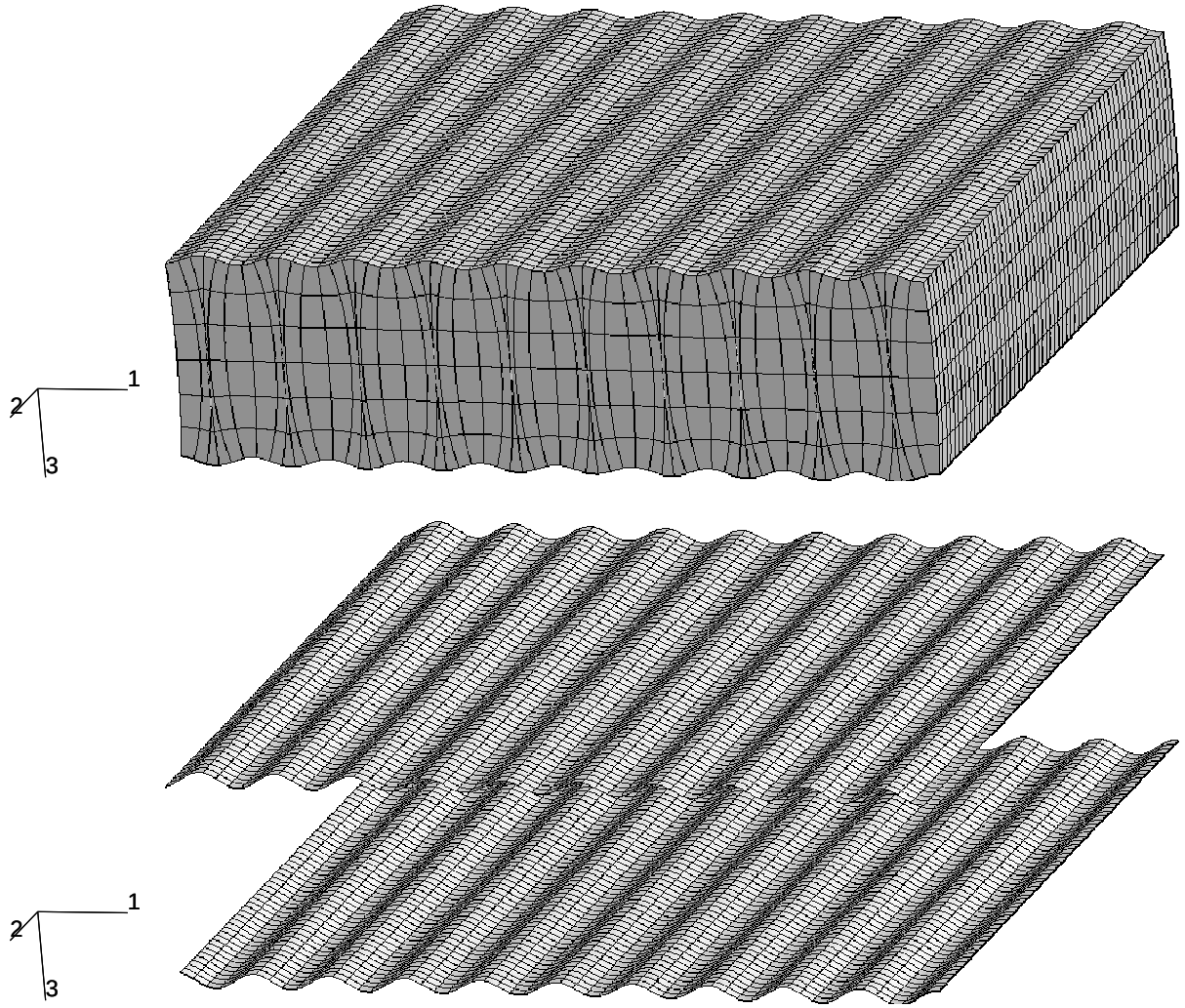

Figure A.2: FE buckling pattern, large unit cell, c=150mm, bottom: transparent core

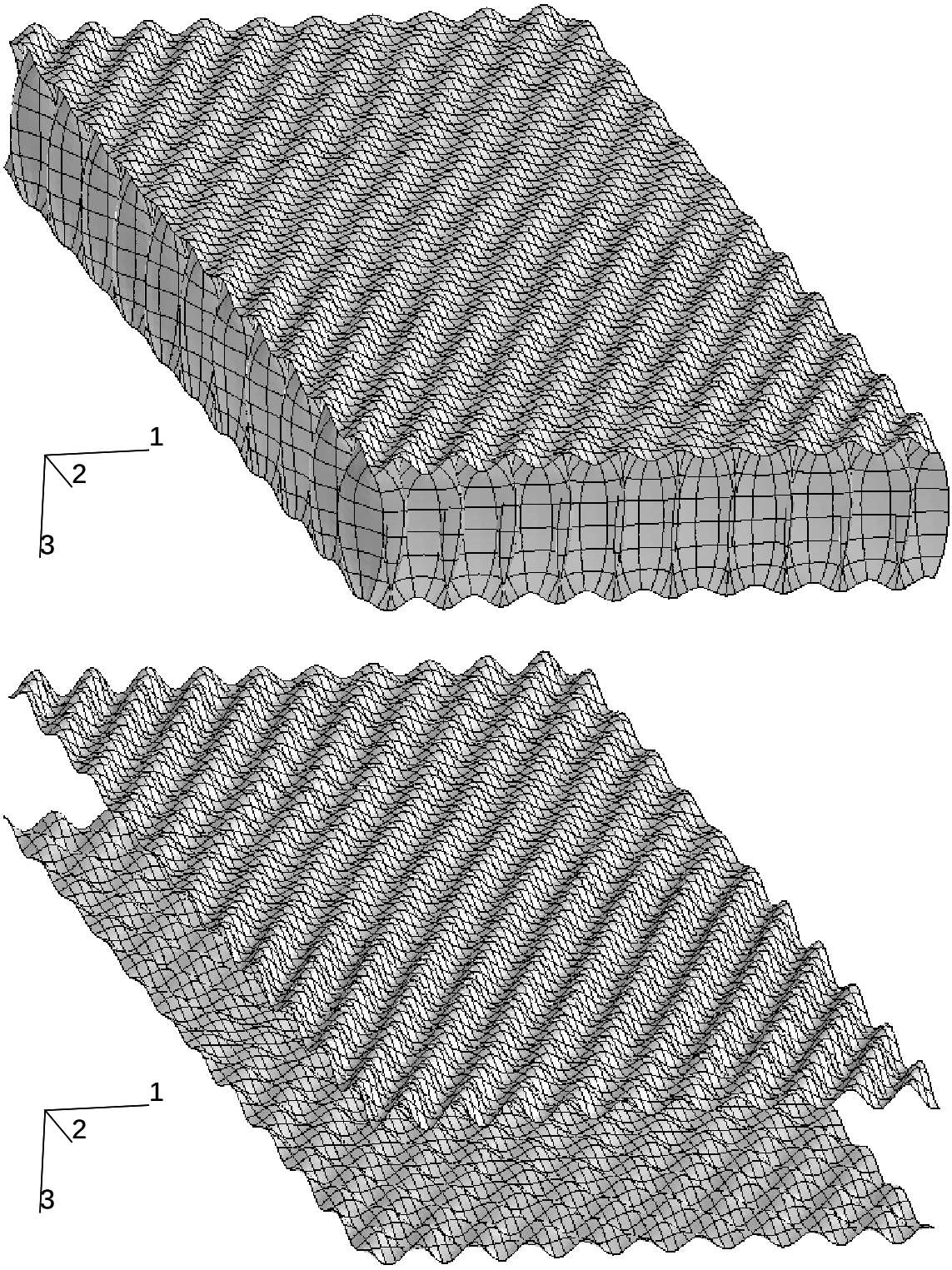

Figure A.3: FE buckling pattern, large unit cell, c=175mm, bottom: transparent core

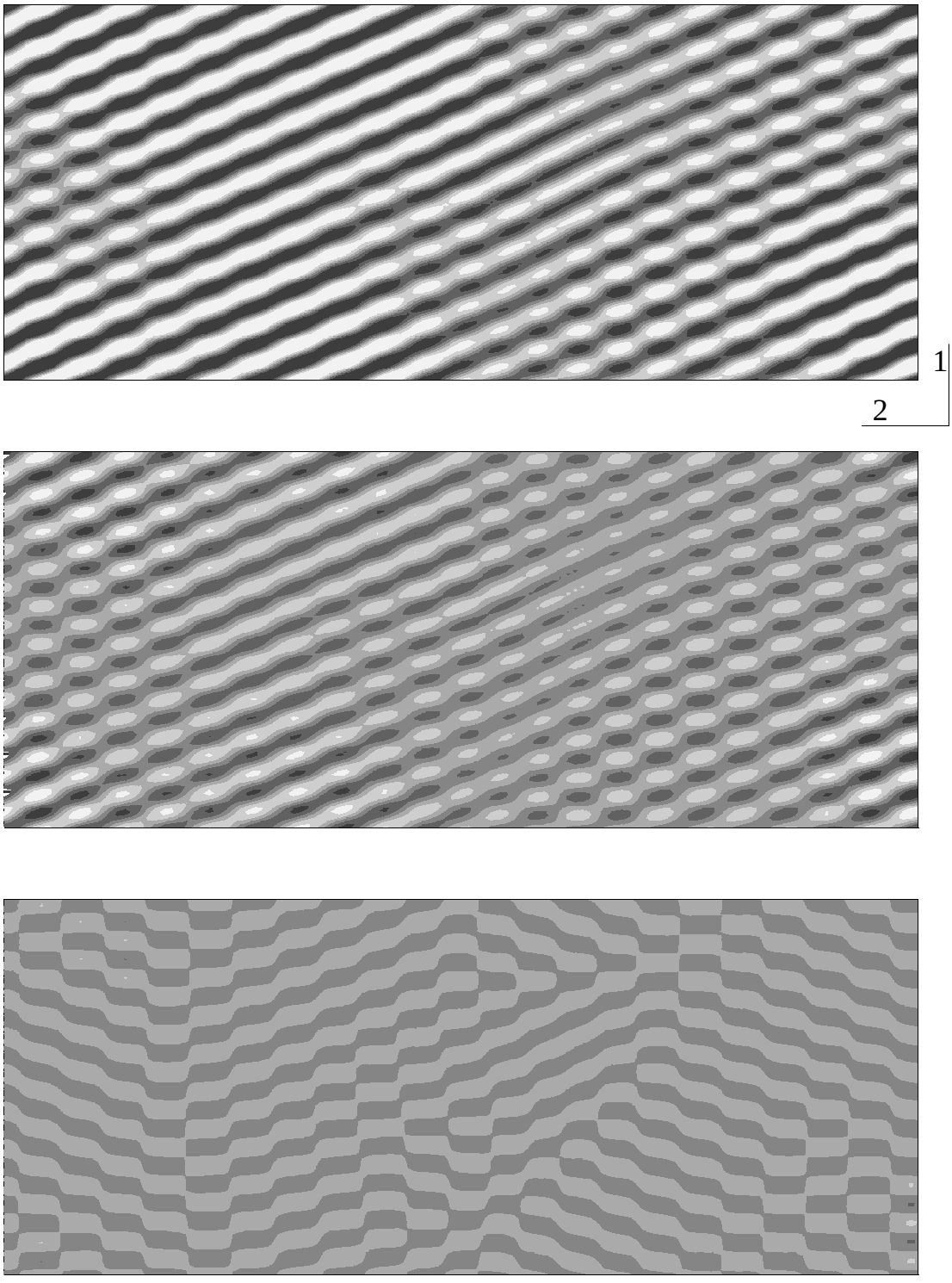

Figure A.4: Displacement w (compare fig. 3.1), FE large unit cell model, c=175mm
top: z=0mm (surface), middle: z=27mm (section), bottom: z=56mm (section)

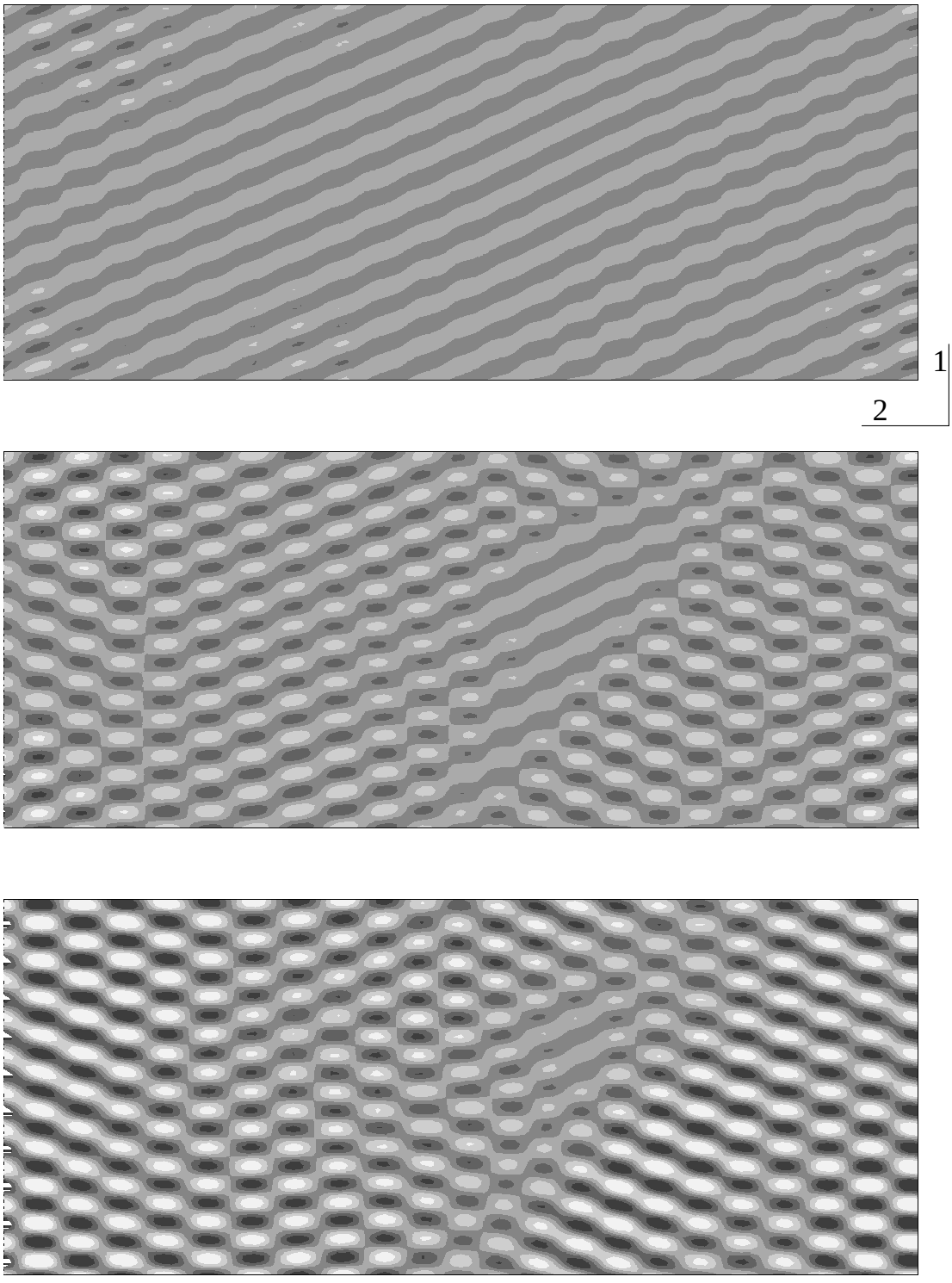

Figure A.5: Displacement w (compare fig. 3.1), FE large unit cell model, c=175mm
top: z=118mm (section), middle: z=148mm (section), bottom: z=175mm (surface)

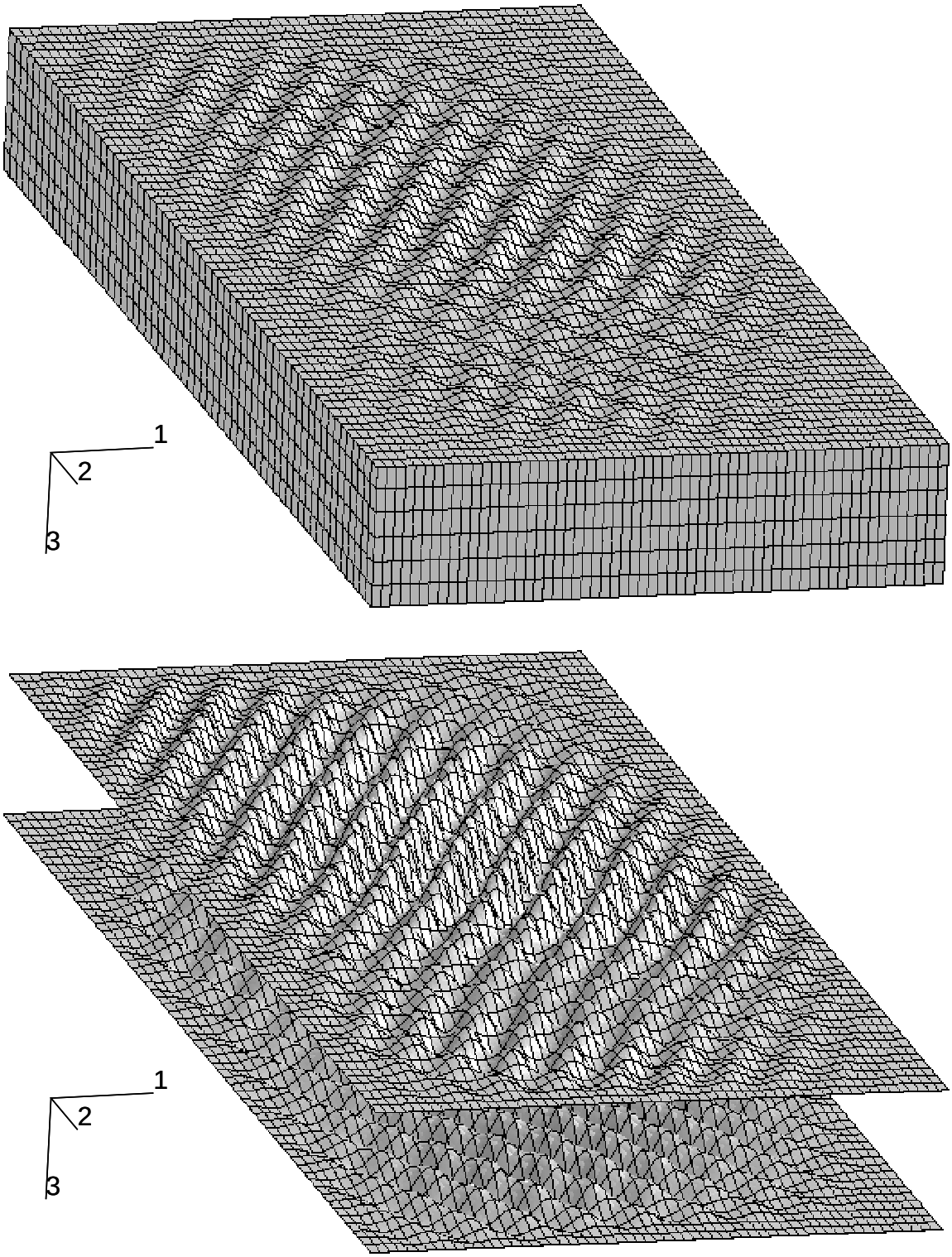

Figure A.6: FE buckling pattern, plate model, c=175mm, bottom: transparent core

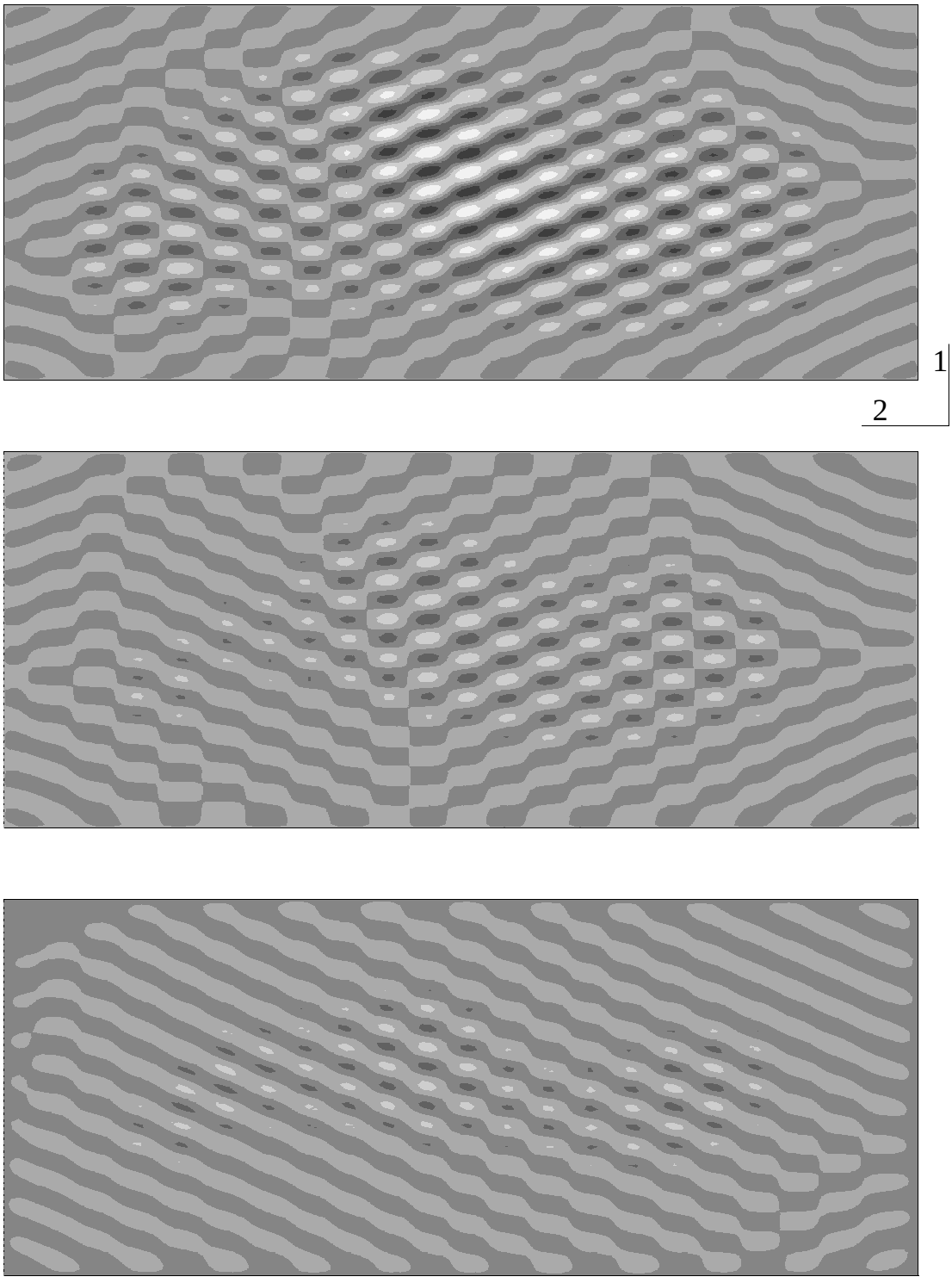

Figure A.7: Displacement w (compare fig. 3.1), FE plate model, c=175mm
top: z=0mm (surface), middle: z=27mm (section), bottom: z=56mm (section)

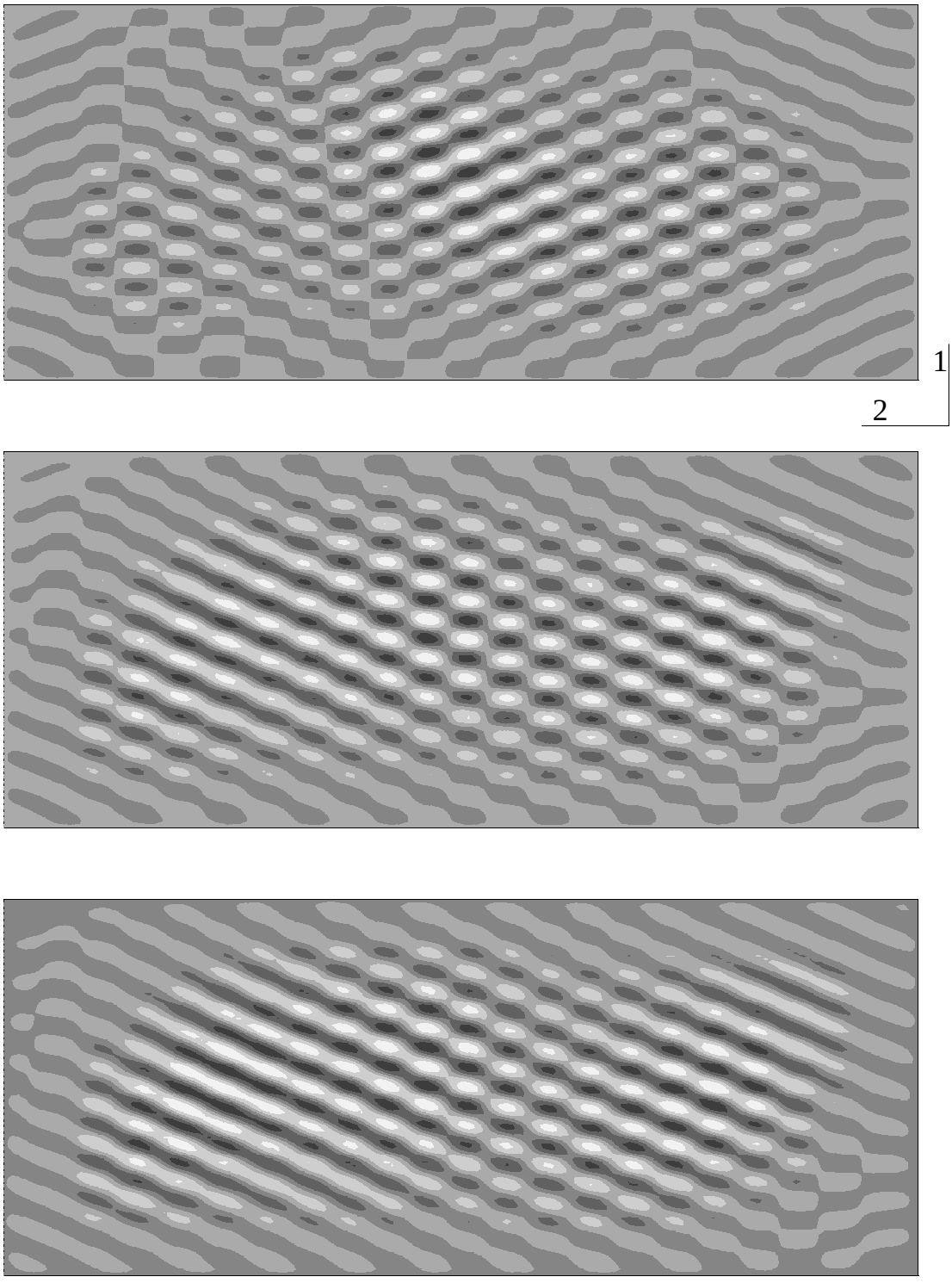

Figure A.8: Displacement w (compare fig. 3.1), FE plate model, c=175mm
top: z=118mm (section), middle: z=148mm (section), bottom: z=175mm (surface)

Bibliography

Allen, H. G. (1969). *Analysis and Design of Structural Sandwich Panels.* Pergamon Press, Oxford.

Benson, A. S. and Mayers, J. (1967). General instability and face wrinkling of sandwich plates - unified theory and applications. *AIAA Journal* 5(4), pp. 729–739.

Boender, C. G. E., Rinnoy Kan, A. H. G., Timmer, G. T. and Stougie, L. (1982). A stochastic method for global optimization. *Mathematical Programming* 22, pp. 125–140.

Böhm, H. (1998). A short introduction to basic aspects of continuum micromechanics. Technical report, CDL-FMD Report 3-1998, Institute of Lightweight Structures and Aerospace Engineering, Vienna University of Technology.

Bufler, H. and Kennerknecht, H. (1983). Prestrained elastic laminates: deformations, stability and vibrations. *Acta Mech.* 48(1-2), pp. 1–30.

Csendes, T. (1988). Nonlinear parameter estimation by global optimization. *Acta Cybernetica* 8, pp. 361–370.

Frostig, Y. (1998). Buckling of sandwich panels with a transversely flexible core - high order theory. *Int. J. Sol. Struct.* 35(3-4), pp. 183–204.

Frostig, Y. and Baruch, M. (1993). High-order buckling analysis of sandwich beams with transversely flexible core. *J. Eng. Mech. ASCE* 119(1), pp. 476–495.

Gibson, L. J. and Ashby, M. F. (1997). *Cellular Solids - Structure and properties.* Cambridge University Press, Cambridge, 2nd edition.

Gough, G. S., Elam, C. F. and de Bruyne, N. A. (1940). The stabilisation of a thin sheet by a continuous supporting medium. *J. R. Aeronaut. Soc.* 44(349), pp. 12–43.

Gutierrez, A. J. and Webber, J. P. H. (1980). Flexural wrinkling of honeycomb sandwich beams with laminated faces. *Int. J. Sol. Struct.* 16, pp. 645–651.

Hadi, B. K. (2001). Wrinkling of sandwich column: comparison between finite element analysis and analytical solutions. *Composite Structures* in print.

Hadi, B. K. and Matthews, F. L. (2000). Development of Benson–Mayers theory on the wrinkling of anisotropic sandwich panels. *Composite Structures* 49, pp. 425–434.

Hegedüs, I. and Kollàr, L. P. (1989). Wrinkling of faces of compressed and bent sandwich bars and its interaction with overall instability. *Acta Technica Acad. Sci. Hung.* 102(1-2), pp. 49–63.

Hertel, H. (1960). *Leichtbau.* Springer Verlag, Berlin.

Hoff, N. J. and Mautner, S. E. (1945). The buckling of sandwich type panels. *J. Aeronaut. Sci.* 12(3), pp. 285–297.

Horgan, C. O. (1998). Saint–Venant end effects for sandwich structures. In: D. Weissman-Berman and K.-A. Olsson (eds.), *Sandwich Constructions 2*, volume 1, pp. 196 – 205. EMAS.

Hunt, G. W., Da Silva, L. S. and Manzocchi, G. M. E. (1988). Interactive buckling in sandwich structures. *Proc. R. Soc. Lond. A* 417, pp. 155–177.

Hwang, S. F. (1998). The buckling of an orthotropic layer on a half space. *Int. J. Mech. Sci.* 40(7), pp. 711–721.

Kühhorn (1991). *Geometrisch nichtlineare Theorie für Sandwichschalen unter Einbeziehung des Knitterphänomens.* Number 100 in 18. VDI Verlag, Düsseldorf.

Leotoing, L., Drapier, S. and Vautrin, A. (2000). Closed form solution for local–global buckling in sandwich structures. In: H.-R. Meyer-Piening and D. Zenkert (eds.), *Sandwich Construction 5*, volume 1, pp. 25–36. EMAS.

Martikainen, L. and Hassinen, P. (1996). Load-bearing capacity of continuous sandwich panels. Dept. of Structural Engineering, Report 135, Helsinki University of Technology.

Niu, K. and Talreja, R. (1999). Modeling of wrinkling in sandwich panels under compression. *J. of Eng. Mech., ASCE* 125(8), pp. 875–883.

Patzelt, O. (1973). *Wachsen und Bauen. Konstruktionen in Natur und Technik.* Vincentz-Verlag, Hannover.

Plantema, F. J. (1966). *Sandwich Construction.* John Wiley & Sons, New York.

Rammerstorfer, F. G. (1992). *Repetitorium Leichtbau.* Oldenbourg Verlag, Wien.

Stamm, K. and Witte, H. (1974). *Sandwichkonstruktionen - Berechnung, Fertigung, Ausführung.* Springer–Verlag, Wien.

Starlinger, A. and Rammerstorfer, F. G. (1992). A finite element formulation for sandwich shells accounting for local failure phenomena. In: D. Weissman-Berman and K.-A. Olsson (eds.), *Sandwich Constructions 2*, pp. 161–178. EMAS.

Stiftinger, M. A. and Rammerstorfer, F. G. (1997). On face layer wrinkling in sandwich shells – theoretical and experimental investigations. *Thin-Walled Structures* 29(1-4), pp. 113–127.

Stockinger, T. (1996). *Analytische, numerische und experimentelle Untersuchungen des Knitterns der Deckschichten von Schaumkern-Sandwichplatten unter Biegung und Druck.* Diploma Thesis, Institute of Lightweight Structures and Aerospace Engineering, Vienna University of Technology. ILFB DA Nr. 84.

Stronge, W. J. and Kashtalyan, M. (1997). Saint-Venant's principle for two-dimensional anisotropic elasticity. *Acta Mech.* 124, pp. 213–218.

Suzuki, T. and Yu, P. (1998). Complex elastic wave band structures in three-dimensional periopdic elstic media. *J. Mech. Phys. Solids* 46(1), pp. 115–138.

Timoshenko, S. P. and Goodier, J. N. (1988). *Theory of Elasticity.* McGraw-Hill, Singapore.

Vinson, J. R. (1999). *The Behavior of Sandwich Structures of Isotropic and Composite Materials.* Technomic Publishing Company, Inc., Lancaster, PA.

Vonach, W. K. and Rammerstorfer, F. G. (2000a). The effects of in-plane core stiffness on the wrinkling behavior of thick sandwiches. *Acta Mech.* 141, pp. 1–10.

Vonach, W. K. and Rammerstorfer, F. G. (2000b). Wrinkling of thick orthotropic sandwich plates under general loading conditions. *Arch. Appl. Mech.* 70, pp. 338–348.

Vonach, W. K. and Rammerstorfer, F. G. (2001). A general approach to the wrinkling instability of sandwich plates. *Struct. Eng. and Mech.* Under review.

Wadee, M. A. and Hunt, G. W. (1998). Interactively induced localized buckling in sandwich structures with core orthotropy. *J. Appl. Mech.* 65(2), pp. 523–528.

Webber, J. P. H., Kyriakides, S. and Lee, C. T. (1976). On the wrinkling of honeycomb sandwich columns with laminated cross-ply facings. *Aeronautical Journal* pp. 264–272.

Wiedemann, J. (1986). *Leichtbau.* Springer Verlag, Berlin.

Yusuff, S. (1955). Theory of wrinkling in sandwich construction. *J. R. Aeronaut. Soc.* 59(529), pp. 30–36.

Yusuff, S. (1960). Face wrinkling and core strength in sandwich construction. *J. R. Aeronaut. Soc.* 64, pp. 164–167.

Zenkert, D. (1995). *An Introduction to Sandwich Construction.* EMAS, Solihull, UK.